

Structure Formation in Isoporous Block Copolymer Membranes by Controlled Evaporation-Induced Self-Assembly



Universität Hamburg

DER FORSCHUNG | DER LEHRE | DER BILDUNG

Dissertation with the aim of achieving a doctoral degree (Dr. rer. nat.)

Institute of Physical Chemistry, Department of Chemistry

University of Hamburg

Submitted by

Kirti Sankhala

Hamburg, 2019

This study was conducted between April 2015 and September 2018 at the Institute of Polymer Research, Helmholtz-Zentrum Geesthacht (HZG), Geesthacht, Germany under the supervision of Prof. Dr. Volker Abetz.

Reviewers of the thesis: Prof. Dr. Volker Abetz

Prof. Dr. Horst Weller

Date of defense and approval for publication: 26.07.2019

*In Memory of my grandfather Shri Jagdish Sigh Ji Arya ...
Who personified 'only a life lived for others is worth living'*

I. Publications

The following list contains chronologically ordered peer-reviewed journal articles, patent applications, oral and poster presentations in conferences, and awards within the framework of this research project.

Journal Articles

1. **Kirti Sankhala**, Joachim Koll, Maryam Radjabian, Ulrich A. Handge, Volker Abetz, “A Pathway to Fabricate Hollow Fiber Membranes with Isoporous Inner Surface”, *Advanced Materials Interfaces* 4 (7), 1600991, 2017
2. **Kirti Sankhala**, Joachim Koll, Volker Abetz, “Setting the Stage for Fabrication of Self-Assembled Structures in Compact Geometries: Inside-Out Isoporous Hollow Fiber Membranes”, *ACS Macro Letters* 7 (7), 840-845, 2018
Cover Picture: *ACS Macro Letters* 7 (7), 2018
3. **Kirti Sankhala**, D. C. Florian Wieland, Joachim Koll, Maryam Radjabian, Clarissa Abetz, Volker Abetz, “Self-Assembly of Block Copolymers during Hollow Fiber Spinning: An *In Situ* Small-Angle X-Ray Scattering Study”, *Nanoscale* 11, 7634-7647, 2019
Cover Picture: *Nanoscale* 11, 8049, 2019

Patent Applications

1. Volker Abetz, **Kirti Sankhala**, Joachim Koll, Ulrich A. Handge, “Structure of Hollow-Fiber Polymer Membrane”, EP 3147024 (A1), (filed: 2015)
2. **Kirti Sankhala**, Volker Abetz, Joachim Koll, “Method for Preparing Isoporous Hollow Fiber Composite Membranes”, EP 3434357 (A1), (filed: 2017)

Oral Presentations

1. **Kirti Sankhala**, Joachim Koll, Maryam Radjabian, Volker Abetz, “A Pathway for Fabrication of Inside Selective Isoporous Hollow Fiber Membranes”, International Conference on Soft Materials, *ICSM 2016*, Jaipur, India
2. **Kirti Sankhala**, Joachim Koll, Maryam Radjabian, Ulrich A. Handge, Volker Abetz, “Fabrication of Inside-Out Isoporous Hollow Fiber Membranes”, International Congress on Membranes and Membrane Processes, *ICOM 2017*, San Francisco, CA, USA
3. **Kirti Sankhala**, Joachim Koll, Maryam Radjabian, Clarissa Abetz, Volker Abetz, “Progressing from Outside to Inner Side: Inside-Out Isoporous Hollow Fiber Membranes”, North American Membrane Society, *NAMS 2018*, Lexington, KY, USA
4. **Kirti Sankhala**, Joachim Koll, D. C. Florian Wieland, Maryam Radjabian, Clarissa Abetz, Volker Abetz, “Structure Formation in Isoporous Hollow Fiber Membranes”, *ICSM 2018*, Jaipur, India

Poster Presentation

- **Kirti Sankhala**, Joachim Koll, D. C. Florian Wieland, Maryam Radjabian, Clarissa Abetz, Volker Abetz, “Self-Assembly of Block Copolymers in Isoporous Hollow Fiber Membranes”, Dead Sea Water 2019 Workshop, Ein Gedi, Israel

Awards

- *Student presentation award* by ICSM 2016
- *Travel award* by European Membrane Society (EMS) for participation in Dead Sea Water 2019 Workshop at Ein Gedi, Israel
- *Nature Nanotechnology Poster Prize* in Dead Sea Water 2019 Workshop, Ein Gedi, Israel
- Got selected among 580 young scientist from around the globe to participate in prestigious *Lindau Nobel Laureate meeting 2019, dedicated to Physics* (as a *MARS fellow*)

II. Contents

I . PUBLICATIONS	I
II . CONTENTS	III
III . SYMBOLS AND ABBREVIATIONS	VII
ZUSAMMENFASSUNG.....	XI
ABSTRACT	XIII
A. Graphical Abstract	xiv
1. INTRODUCTION	1
1.1. MOTIVATION	1
1.2. OVERVIEW OF MEMBRANES FOR LIQUID SEPARATIONS	4
1.2.1. <i>Membranes and materials</i>	4
1.2.2. <i>Polymeric membranes and their structures</i>	5
A. Porous membranes	5
B. Nonporous membranes.....	6
C. Symmetric membranes	6
D. Asymmetric membranes	6
1.2.3. <i>Fabrication of polymeric membranes via phase inversion process</i>	7
A. Precipitation from the vapor phase	7
B. Precipitation by controlled evaporation.....	7
C. Thermally induced phase separation	7
D. Immersion precipitation	8
1.2.4. <i>Pressure-driven membranes for liquid filtration processes</i>	9
A. Microfiltration	9
B. Ultrafiltration.....	10
C. Nanofiltration	10
D. Reverse Osmosis.....	11
1.2.5. <i>Fundamental transport mechanism in pressure-driven liquid separation membranes</i>	11
1.2.6. <i>Membrane operations</i>	14
A. Dead-end filtration	14
B. Cross-flow filtration.....	15
1.2.7. <i>Membrane geometries, module configurations and processes</i>	16
A. Plate-and-frame module	16
B. Spiral wound module	16
C. Tubular modules.....	17
D. Hollow fiber membrane modules.....	17
a. Inside-out hollow fiber membranes	18
b. Outside-in hollow fiber membranes	18
1.3. BLOCK COPOLYMERS, SELF-ASSEMBLY AND ISOPOROUS MEMBRANES	20
1.3.1. <i>Block copolymers</i>	20
1.3.2. <i>Self-assembly of amphiphilic diblock copolymers</i>	21
A. Self-assembly in bulk	23
B. Self-assembly in (dilute) solutions.....	24
C. Self-assembly in fabrication	25
1.3.3. <i>Isoporous membranes</i>	26
1.3.4. <i>Fabrication of isoporous block copolymer membranes via SNIPS process</i>	27
1.3.5. <i>Mechanism of structure formation in isoporous block copolymer membranes</i>	28
1.3.6. <i>Factors influencing the structure formation in isoporous membranes</i>	31
A. Phase-selective chemistry of block copolymers	31
B. Controlling pore size and functionality.....	32
C. Influence of additives and solution composition	33

D.	Influence of directional fields	33
1.3.7.	<i>Outside-in isoporous hollow fiber membrane fabrication by spinning</i>	34
1.3.8.	<i>Fabrication of isoporous composite membranes</i>	36
A.	Isoporous composite flat sheet membranes	37
a.	Spray coating	37
b.	Dip coating	37
c.	Roll-to-roll coating	37
B.	Isoporous composite hollow fiber membranes	37
a.	Dual-layer hollow fiber membranes by spinning	38
b.	Composite isoporous hollow fiber membranes by coating	38
1.3.9.	<i>Characterization techniques to investigate self-assembly and membrane fabrication</i>	39
1.3.10.	<i>Performance characterization of isoporous membranes</i>	39
A.	Water flux	40
B.	pH-responsive flux behavior	40
C.	Retention (<i>R</i> %)	41
2.	AIM OF THE WORK	43
2.1.	STRATEGY OF THE RESEARCH	43
2.2.	OUTLINE OF THESIS	44
3.	INFLUENCE OF ADDITIVE IN BLOCK COPOLYMER SOLUTION AND ON STRUCTURE FORMATION IN FLAT SHEET MEMBRANES	49
3.1.	PREPARATION OF BULK FILMS AND THEIR CHARACTERIZATION	51
3.2.	WEAKLY SEGREGATED BLOCK COPOLYMER SOLUTIONS AND FLAT SHEET MEMBRANE FABRICATION	52
3.3.	ORDERED BLOCK COPOLYMER SOLUTIONS AND FLAT SHEET MEMBRANE FABRICATION	54
3.4.	ADDITION OF MgAC ₂ IN DILUTE BLOCK COPOLYMER SOLUTIONS	58
3.5.	CONCLUSION	59
4.	STUDY OF STRUCTURE FORMATION IN OUTSIDE-IN ISOPOROUS HOLLOW FIBER MEMBRANES BY <i>IN SITU</i> SMALL ANGLE X-RAY SCATTERING	61
4.1.	OUTSIDE-IN HOLLOW FIBER MEMBRANE FABRICATION AND EXPERIMENTAL SET-UP FOR <i>IN SITU</i> SAXS	63
4.2.	INFLUENCE OF SPINNING PARAMETERS ON STRUCTURE FORMATION IN HOLLOW FIBER MEMBRANES	64
A.	Influence of polymer flow rate	65
B.	Influence of evaporation time given by the air gap distance	71
4.3.	INFLUENCE OF ADDITIVE MgAC ₂ IN THE BLOCK COPOLYMER SOLUTION IN ISOPOROUS HOLLOW FIBER MEMBRANE FABRICATION	73
4.4.	CONCLUSION	80
5.	FABRICATION OF INSIDE-OUT ISOPOROUS BLOCK COPOLYMER HOLLOW FIBER MEMBRANES	81
5.1.	MEMBRANE FABRICATION VIA DRY-JET WET SPINNING TECHNIQUE	82
5.2.	STRUCTURE FORMATION ON THE INNER SURFACE	83
5.3.	INFLUENCE OF SPINNING PARAMETERS ON HOLLOW FIBER MEMBRANE MORPHOLOGY	84
A.	Influence on the morphology of inner surface	85
B.	Influence on the morphology of outer surface	87
C.	Optimized parameters	88
D.	Other polymer solutions for isoporous hollow fiber membrane fabrication	89
5.4.	MEMBRANE CHARACTERIZATION	91
5.5.	CONCLUSION	91
6.	FABRICATION OF INSIDE-OUT ISOPOROUS COMPOSITE HOLLOW FIBER MEMBRANES	93
6.1.	INFLUENCE OF SUBSTRATE HOLLOW FIBER MEMBRANE	96
6.2.	FABRICATION OF INSIDE-OUT COMPOSITE HOLLOW FIBER MEMBRANE	98
6.3.	SELECTION OF POLYMER SOLUTION AND THE STRUCTURE FORMATION	100
6.4.	COATING PARAMETERS INFLUENCING THE FABRICATION OF COMPOSITE ISOPOROUS HOLLOW FIBER MEMBRANES	105
6.5.	MEMBRANE PERFORMANCE	107
A.	Membrane water flux	107
B.	Membrane water flux from the block copolymer layer	107
C.	Membrane water flux from the active layer predicted by Hagen-Poiseuille Equation	108
6.6.	CONCLUSION	109

7. INFLUENCE OF CONTROLLED EVAPORATION BY GAS FLOW ON THE EVAPORATION-INDUCED SELF-ASSEMBLY OF BLOCK COPOLYMERS	111
A. Difference from the conventional evaporation-induced self-assembly	118
B. Influence of the gas flow rate.....	118
C. Benefits over conventional evaporation under environmental conditions.....	119
8. SUMMARY AND OUTLOOK	121
9. EXPERIMENTAL SECTION	125
9.1. MATERIALS	125
9.2. PREPARATION OF PS- <i>b</i> -P4VP POLYMER SOLUTION	126
9.3. PREPARATION OF BULK FILMS.....	126
9.4. FLAT SHEET MEMBRANE FABRICATION.....	126
9.5. OUTSIDE-IN HOLLOW FIBER MEMBRANE FABRICATION VIA SPINNING	127
9.6. SMALL-ANGLE X-RAY SCATTERING	128
A. SAXS from bulk films.....	128
B. SAXS from Solutions	128
C. <i>In situ</i> synchrotron SAXS during hollow fiber spinning.....	128
9.7. INSIDE-OUT HOLLOW FIBER MEMBRANE FABRICATION VIA SPINNING	130
9.8. MODULE DESIGN FOR COATING EXPERIMENTS	130
9.9. MORPHOLOGICAL CHARACTERIZATION	131
A. Scanning electron microscopy.....	131
a. Analysis of SEM micrographs using ImagiC.....	131
b. Analysis of SEM micrographs using analysis.....	132
c. Analysis of SEM micrographs by DigitalMicrograph.....	133
B. Transmission electron microscopy	133
9.10. MEMBRANE CHARACTERIZATIONS	134
A. Water flux measurements.....	134
B. Retention experiments.....	135
SAFETY HAZARDS.....	136
REFERENCES.....	137
ACKNOWLEDGMENT.....	147
DECLARATION ON OATH.....	149
AFFIDAVIT.....	149
CURRICULUM VITAE.....	150

III. Symbols and Abbreviations

Symbols

\mathcal{D}	Dispersity index
η	Viscosity
μ_i	Chemical potential of component i
τ	Tortuosity
Δf_m	Free energy of mixing
Δp	Transmembrane pressure
Δt	Change in time
ΔV	Change in volume
χ	Flory-Huggins-Staverman interaction parameter
A	Active surface area of membrane
<i>-b-</i>	<i>-block-</i>
C_p	Concentration of solute in permeate
C_f	Concentration of solute in feed
J	Water flux
J_v	Volumetric water flux
d	Domain spacing
d_{c-c}	Average center-to-center distance between pores
D	Diameter of hollow fiber
D_h	Hydrolic pore diameter
D_p	Average pore diameter
F	Volume fractions of the different polymer blocks
L	Length of cylindrical pore
L	Thickness of membrane
L_a	Air gap distance between spinneret and precipitation bath
M_n	Number average molecular weight
N	Degree of polymerization
N_p	Number of pores

P	Pressure
q	Scattering vector
q^*	Principle scattering vector
Q_{N_2}	Nitrogen flow rate
Q_p	Polymer flow rate
Q_s	Solvent flow rate
Q_w	Water flow rate
$R\%$	Retention
T	Temperature
t	Time
t_{N_2}	Time of nitrogen flow
t_p	Time of polymer flow
t_s	Time of solvent flow
t_w	Time of water flow

Abbreviations

bcc	Body centered cubic
BSE	Back-scattered electron (contrast)
$CdCl_2$	Cadmium(II) chloride
CS	Cross-section
CS_{is}	Cross-section near inner surface
CS_{os}	Cross-section near outer surface
DMF	<i>N,N</i> -dimethylformamide
DOX	<i>1,4</i> -dioxane
$FeCl_3$	Iron(III) chloride
GISAXS	Grazing incidence small-angle X-ray scattering
GPC	Gel permeation chromatography
H_2O_2	Hydrogen peroxide
hcp	2D hexagonally-packed cylinder
HFM	Hollow fiber membrane
$MgAc_2$	Magnesium acetate
MWCO	Molecular weight cut-off

NIPS	Non-solvent induced phase separation
NMR	Nuclear magnetic resonance spectroscopy
P2VP	Poly(2-vinylpyridine)
P4VP	Poly(4-vinylpyridine)
PAA	Poly(acrylic acid)
PAN	Polyacrylonitrile
PDMA	<i>N,N</i> -dimethylacrylamide
PEG	Poly(ethylene glycol)
PEI	Poly(ether imide)
PEO	Poly(ethylene oxide)
PES	Poly(ether sulfone)
PI	Polyisoprene
PLA	Poly(lactic acid)
PPS	Poly(propylene sulfide)
PVDF	Poly(vinylidenedifluoride)
PS	Polystyrene
SAXS	Small-angle X-ray scattering
SE	Secondary electrons (contrast)
SEM	Scanning electron microscopy
SNIPS	Self-assembly of block copolymer and non-solvent induced phase separation
TEM	Transmission electron microscopy
THF	Tetrahydrofuran
TIPS	Thermally induced phase separation

Zusammenfassung

Nanoskalige Strukturen, die einen selektiven Transport und einen hohen Durchfluss ermöglichen, haben ein enormes Potenzial für eine Vielzahl von Trennanwendungen. Die Selbstorganisation von Blockcopolymeren ermöglicht die Gestaltung maßgeschneiderter isoporöser selektiver Oberflächen für vielversprechende energieeffiziente Trennungen. Das Ziel dieser Dissertation ist es, die Kinetik, der durch Verdampfung induzierten Selbstorganisation von Blockcopolymeren und die Nicht-Lösungsmittel induzierte Phasentrennung (*engl.* SNIPS) zur Herstellung von isoporösen Membranen, zu verstehen, hauptsächlich um neuartige isoporöse Hohlfasermembranen (HFM) zu entwickeln.

In dieser Dissertation wurden sowohl reine Polystyrol-*block*-poly(4-vinylpyridin) (PS-*b*-P4VP) - Diblockcopolymerlösungen als auch Lösungen mit Zusatz von Magnesiumacetat (MgAc_2) verwendet, um die Strukturbildung in Flach- und Hohlfadenmembranen zu untersuchen. Die Kleinwinkel-Röntgenstreuung (SAXS) zeigt, dass die Zugabe von MgAc_2 bereits bei niedrigeren Polymerkonzentrationen zur Bildung von Mizellen in den Blockcopolymerlösungen führt und diese Mizellen einem erhöhten Domänenabstand im Vergleich zu der reinen Lösung aufzeigen. In *in situ* SAXS-Experimenten wurden sowohl die geordneten als auch die schwach getrennten Lösungen verwendet, um den Einfluss der Extrusion und der Spinnparameter auf die Selbstorganisation von Blockcopolymeren während des Spinnens von HFM zu untersuchen. Die erhaltenen Strukturmerkmale korrelieren mit den Strukturen in den Blockcopolymerlösungen ohne Scherung und mit den Morphologien von Flach- und Hohlfadenmembranen, die aus rasterelektronischen Aufnahmen stammen.

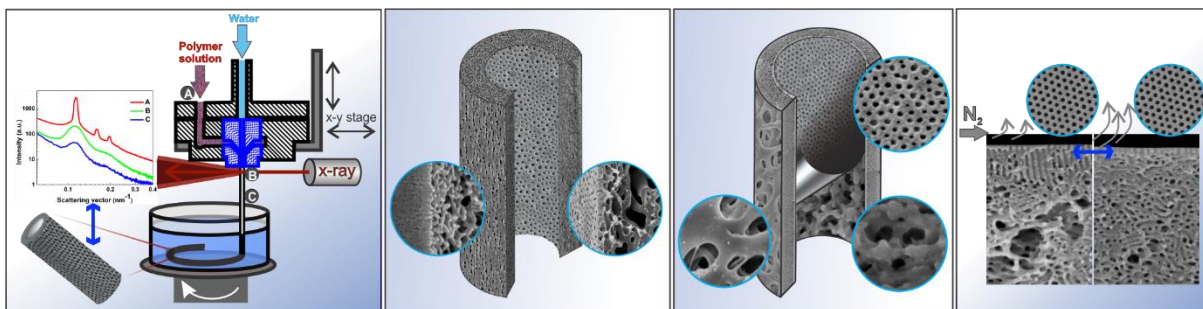
Ein gängiger Ansatz um regelmäßige selbstorganisierte Strukturen zu erhalten ist eine Mikrophasentrennung, welche durch Verdampfen des Lösungsmittels unter normalen Umgebungsbedingungen erreicht wird. In dieser Dissertation wird ein neuer Ansatz zur Steuerung der Kinetik der Mikrophasentrennung vorgestellt: eine kontrollierte Gasströmung anstelle der Verdampfung unter Umgebungsbedingungen. Dieses Konzept erlaubt es die Bildung selbstorganisierter Strukturen in kompakten Geometrien zu erreichen, wie z.B. auf der Innenseite einer HFM.

Die Studie konzentriert sich auf das Verständnis der durch Gasströmung induzierten gesteuerten Selbstorganisation auf der inneren Oberfläche von HFM für die Herstellung von integral asymmetrischen und von innen nach außen gerichteten isoporösen HFM durch Spinn- bzw. Beschichtungsverfahren. Die Strukturbildung unterscheidet sich in beiden Verfahren. Für das Spinnen von HFM werden viskosere Polymerlösungen verwendet im Gegensatz zum Beschichtungsverfahren.

Die hohe Viskosität der Lösung verlangsamt die Selbstorganisation, die durch die scherinduzierte Orientierung oder die Ausrichtung der Mikrodomänen bei der Extrusion beeinflusst wird. Auf der anderen Seite verkomplizieren die hohen Polymerrelaxationsraten, die verringerten thermodynamischen Triebkräfte, sowie die hohen kapillaren Saugwirkungen in dem porösen Substrat die Selbstorganisation des Blockcopolymer, die Herstellung einer gleichmäßigen Beschichtung bei der Verwendung von verdünnenden Lösungen. In dieser Arbeit wurden die benötigten Bedingungen für eine isoporöse Trennschicht auf der Lumenseite der HF mit einem Durchmesser von ≤ 1 mm in beiden SNIPS Verfahren erreicht.

Die Untersuchung der Selbstorganisation von Blockcopolymeren unter kontrollierten Verdampfungsbedingungen wurde in einem weniger komplexen System an Flachmembranen fortgesetzt. Um eine kontrollierte Gasströmungsrate und Verdampfungszeit auf eine gegossene Membran einwirken zu lassen, wurde für diesen Zweck eine spezielle Abdeckung entwickelt. Die Gießparameter und die Blockcopolymerlösung wurden in einem großen Bereich variiert. Das Konzept der Nutzung eines Gasstroms kann im Vergleich zu normalen Verdampfungsbedingungen eine isoporöse Strukturbildung in einem größeren Parameterfenster ermöglichen und ist der einzige praktikable Weg, um durch verdampfungsinduzierte mikrophasengetrennte Strukturen in kompakten Geometrien zu erreichen.

Grafische Zusammenfassung



Abstract

Nanoscale structures providing selective transport and fast flow have a huge potential in a wide range of separation applications. The self-assembly of block copolymers enables to design tailorable isoporous selective surfaces for promising energy-efficient separations. The objective of this dissertation is to understand the kinetics of evaporation-induced self-assembly of block copolymers and non-solvent induced phase separation (SNIPS) for the fabrication of isoporous membranes, mainly to develop novel isoporous hollow fiber membranes (HFM).

In this dissertation, polystyrene-*block*-poly(4-vinylpyridine) (PS-*b*-P4VP) diblock copolymer solutions as pristine and with additive magnesium acetate (MgAc_2) were used to study the structure formation in flat sheet and HF membranes. Small-angle X-ray scattering (SAXS) characterization shows that the addition of MgAc_2 leads to ordering of micelles in the block copolymer solutions already at lower polymer concentrations and shows more prominent micelles with increased domain spacing as compared to the pristine solution. Both the ordered and the weakly segregated solutions were used to investigate the influence of extrusion and the spinning parameters on the self-assembly of block copolymers during HF spinning by conducting *in situ* SAXS experiments. The obtained structural features are correlated with the structure in the block copolymer solutions in absence of shear and with the morphologies obtained from flat sheet and the HF membranes by *ex situ* SEM.

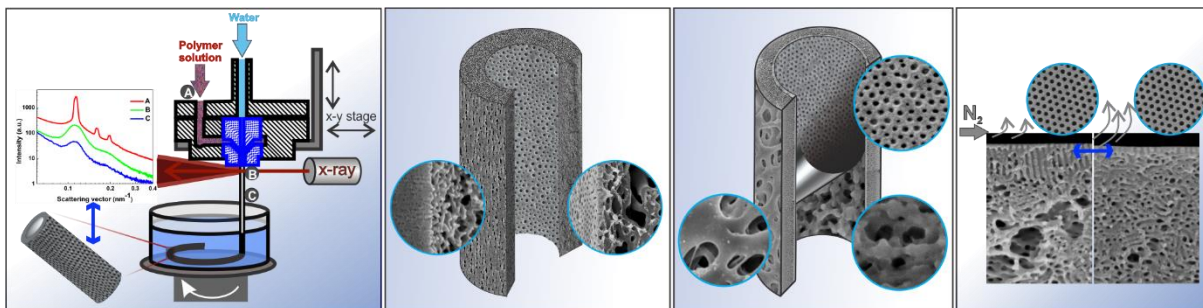
So far, evaporation under normal environmental conditions has been a common approach to achieve evaporation-induced microphase separation providing lateral order of self-assembled structures. This dissertation introduces a novel approach of controlling the kinetics of microphase separation of block copolymers by using gas flow instead of commonly used environmental conditions. By this concept, the self-assembled structures could be developed in compact geometries such as the lumen of a HFM.

The study focuses on the understanding of gas-flow induced controlled self-assembly on the inner surface of HFM for fabrication of integral asymmetric and composite inside-out isoporous HFM by spinning and coating processes, respectively. The requirement of viscous and dilute polymer solutions for spinning and coating, respectively, completely differentiates the structure formation in both the methods. The viscous solution challenges the self-assembly due

to shear-induced orientation or alignment of microdomains during extrusion while the high polymer relaxation rates and decreased thermodynamic driving forces, as well as high capillary suction in the porous substrates complicates the block copolymer self-assembly and fabrication of uniform coated layers using dilute solutions in the coating process. In this study, the conditions required for SNIPS were achieved on the lumen side of the HF having a diameter ≤ 1 mm in both the processes.

In order to explicitly understand the influence of gas flow on the self-assembly of block copolymers, the study was further continued in a comparatively less complex system of flat sheet membranes. To provide controlled gas flow rate and evaporation time to as-cast membrane, a casting envelope was designed; the casting parameters and the block copolymer solution were varied in a large range. The concept of using gas flow can provide isoporous structure formation in a larger window as compared to normal evaporation conditions and is the only feasible way to achieve evaporation-induced microphase separated structures in compact geometries.

Graphical Abstract



1. Introduction

1.1. Motivation

“The future depends on what you do today.”

- Mahatma Gandhi

Potable water is one of the most important factors for healthy lives. Safe and easy access to water can lift-up the lifestyle by strengthening the health of people that increases their efficiency. This can contribute greatly to poverty reduction by boosting countries' economic growth. Moreover, everyone has the right to safe, sufficient, physically accessible, and affordable water for day-to-day use. Absent, insufficient, or inappropriately-managed water and sanitation services expose individuals to preventable health issues. Water scarcity enforces the use of contaminated water and leads to the transmission of diseases such as cholera, diarrhoea, dysentery, hepatitis A, typhoid, and polio. According to the fact sheet, 'Drinking-water' (February 2018), provided by World Health Organization (WHO)¹, 844 million people still lack an essential drinking water service and by 2025, half of the world's population will be living in water-stressed areas. Some 8,42,000 people are estimated to die each year from diarrhoea because of inadequate and unsafe drinking water. Almost 240 million people are affected by

¹ <http://www.who.int/en/news-room/fact-sheets/detail/drinking-water>

schistosomiasis or snail fever caused by parasitic worms contracted through exposure to infested water.

Moreover, deforestation, demographic changes, climate change, urbanization, population growth, and increasing fresh water shortage already pose challenges for water supply systems. The requirement of fresh water sources for drinking water and irrigation are continuously growing with an increasing reliance on groundwater and alternative sources, including wastewater.

Most of the above-mentioned issues can be prevented and solved by improving purification efficiency and availability, which is largely covered by pressure-driven ultrafiltration membranes. Re-use of wastewater to recover water for irrigation, nutrients, or energy is becoming an important strategy, thus requiring safe and efficient management of wastewater around the world, which increases the importance and urgency of effectual membrane filtration processes. Membrane filtration offers high efficiency and filtration performance for reclamation and reuse of water and in the general filtration processes of liquids and gases as compared to the conventional methods such as distillation and adsorption. The main advantage of membrane technology is the transport selectivity of the membrane without requiring additional stimulating fields like temperature. So, both upscaling and downscaling of membrane processes, as well as their integration into other separation or reaction processes, are easy. Membranes are widely used in different separation processes such as gas separation, dialysis, reverse osmosis, nanofiltration, ultrafiltration, and microfiltration. Especially, ultrafiltration and often in conjunction with microfiltration are increasing in importance to filter contaminated water. For example, they remove particles, microbes, and parasites. The other important roles of membrane technology for artificial organs, mainly in dialysis, blood oxygenator and controlled drug delivery, has become a major life-saving procedure. The increasing demand for efficient separations enforces vast research in the field of synthetic membrane science and technology. In this, polymeric membranes dominate a very broad range of industrial membrane applications due to their cost-effective industrial scale production *via* robust manufacturing methods and versatility of polymeric materials, membrane geometries, and module configurations.

These widely known facts showing the importance and impressive success of membrane technology in dialysis and desalination, growing large-scale separation demands not only in water treatment but also in the food and pharmaceutical industries and chemical industry, require innovative research and development toward improved membrane materials and processes. In addition, being someone who grew up in the Thar desert facing shortage of water in everyday

life has been a strong driving force to learn about the membrane fabrication and designing novel membranes for efficient separation. The desire to share my responsibility in solving such problems gave me the determination to learn with passion and commitment.

1.2. Overview of membranes for liquid separations

1.2.1. Membranes and materials

A membrane is a selective interphase between two adjacent phases that allows something(s) to pass through while stops others in a specific manner.¹ This separation principle is a vital part of the living cells and is well-known from biology.² Biological membranes inspire membranologists to achieve similar perfection in morphology, design and separation efficiency in synthetic membranes. In recent decades, the knowledge from biological membranes is being transformed into industrial processes with synthetic membranes, making them applicable in myriad applications.³⁻⁵ A synthetic membrane can be porous or dense, solid or liquid, neutral or charged, polar or non-polar, symmetric or asymmetric, thin (less than 100 nm) or thick (up to several mm), and can be made from organic or inorganic materials in different geometries.⁶ Membrane selection depends on a variety of factors, including application type, separation goals, composition of the feed solution, and operating parameters.^{5, 7, 8} The state-of-the-art membranes are applicable for separation of molecular mixtures, controlled release of active agents, chemical and biochemical synthesis, and energy storage and conversion.^{1, 9-18}

A majority of industrial membranes consist of synthetic or natural polymers and known as organic membranes.¹⁹ Artificial polymers are synthesized by the polymerization of a monomer or co-polymerization of two or more monomers for different polymer configurations such as linear, branched and cross-linked structures, and natural polymers like rubber, wool and cellulose.^{20, 21} Polymer selection depends on compatibility with membrane fabrication technology and intended applications.^{3, 22} *E.g.*, a polymer may require a low affinity towards the permeate for particular separations, while other times it may need to withstand harsh cleaning conditions due to membrane fouling.²³ Polymer characteristics include interactions and rigidity of polymer chains, functional group polarity, and stereoisomerism.²⁴ Linear-chained thermoplastic polymers are more soluble in organic solvents and become soft or malleable with increasing temperature while cross-linked thermosetting polymers are almost infusible and insoluble in organic solvents and do not soften with increasing temperature.²⁴

Other types of artificial membranes are made from inorganic materials. This mainly includes metallic, ceramic and zeolite membranes.¹⁷ Metallic membranes are made from sintering metal powders such as tungsten, palladium or stainless steel and then depositing them onto a porous substrate. These are mainly used for hydrogen separation. Ceramic membranes consist of metal (*e.g.* aluminum or titanium) and non-metals (*e.g.* oxygen, nitrogen, or carbon leading to the corresponding oxides, nitrides, or carbides, respectively). They are generally used for highly acidic or basic environments due to inertness but the high sensitivity to temperature gradient leads to membrane cracking.²⁵⁻²⁹ Zeolite membranes are used in highly selective gas separation due to uniform pore size while a thick layer is required to prevent cracks and pinholes, which provides relatively low gas flux; this material is beneficial for catalytic membrane reactor applications.^{30, 31}

Some advantages of inorganic over organic membranes are high thermal and chemical stability, inertness to microbiological degradation, and ease of cleaning after fouling.³² However, inorganic membranes tend to have higher capital costs and one of the reasons is requirement of specific thickness to withstand pressure drop differences.³³

1.2.2. Polymeric membranes and their structures

Most commercially utilized synthetic membranes in separation industry are made of polymeric materials due to the commercial availability of various types of polymeric materials and selective barriers.⁶ Polymeric membranes can be porous, nonporous, or charged, and are capable of offering consistent quality in industrial-scale production at a reasonable cost. The transport rate of permeate flux through these membranes not only depends on the top surface but also depends on the complete membrane structure.¹⁴ Membrane thickness increases the resistance to mass transfer.³⁴ The barrier structure of membranes and their function can be classified according to their structural features as porous, nonporous, symmetric/isotropic and asymmetric/anisotropic membranes. The structure of membrane depends on the preparation techniques.³⁵

A. Porous membranes

Most industrial membranes are either porous or at least contain porous parts or components that are essential for their performance.^{20, 36} Entirely porous membranes are mainly used for

microfiltration and ultrafiltration. In order to achieve high selectivity, pores in the membrane need to be relatively smaller than the particles in the feed.¹⁶ In addition, chemical and thermal stability are significant factors to consider when selecting porous materials because temperature and concentration affect selectivity and flux of the membranes.³⁵

A. Nonporous membranes

Nonporous membranes are mainly used for reverse osmosis, nanofiltration, or molecular separation in the gas phase.⁶ The membrane is a homogeneous dense film where permeate diffuses through by partial pressure, concentration, or electrical potential gradient.³⁷ One disadvantage of nonporous membranes is low flux; therefore, the dense film is usually made extremely thin and is deposited on top of a porous membrane, which might also affect the performance of the membrane.¹⁴

B. Symmetric membranes

Symmetric membranes have a uniform composition and structure throughout the membrane cross-section, which can be porous or dense. Since the flux is inversely proportional to the membrane thickness, a thinner membrane is prioritized.⁷ For the defect-free fabrication of thin membranes, the membrane thickness is kept greater than 20 μm in the conventional film fabrication. In porous symmetric membranes for liquid separation, mainly in microfiltration, fouling within membrane causes flux decline over time.^{38, 39}

C. Asymmetric membranes

A typical asymmetric membrane comprises of a relatively dense and extremely thin selective surface layer, known as permselective layer, supported by a much thicker porous substructure.⁴⁰ The membrane can be integrally asymmetric or consist of a number of layers each with different structures and permeability such as a thin-film composite or a mixed matrix composite membrane.⁶ The selective layer is always on the feed side of the membrane. The skin layer determines the separation properties like permeation rates or resistance to mass transfer; and the substructure functions as mechanical support, with virtually no separating function.⁴⁰ Such separation from the top surface provides high transport rates, which is desired in commercial processes for efficiency and economic reasons.

1.2.3. Fabrication of polymeric membranes *via* phase inversion process

Phase inversion is a common method to fabricate polymeric separation membranes using artificial polymers.⁴¹ In this phenomenon, a controlled transformation of polymers from a liquid phase of solvent(s)-(non-solvent)-polymer mixture (polymer solution) to a solid phase as polymeric membrane takes place by removing the solvent(s) (and non-solvent).^{41, 42} Generally, this transformation occurs if there is a change in stability of the polymer solution. This, consequently, minimizes the free energy of the mixture, which causes the solution to separate into two phases.⁴¹ The change in the stability of the polymer solution is accomplished by temperature variation, solvent evaporation, or by mass exchange with non-solvent/coagulant bath. The phase inversion process is highly dependent on the type of polymer used and the solvent used to dissolve the polymer, which can significantly differ with the addition of non-solvent or other additives.^{15, 43} There are four basic techniques to create phase inversion membranes.

A. Precipitation from the vapor phase

In this process, the cast polymer film is placed in a vapor atmosphere that contains a non-solvent saturated with the same solvent that is used in the polymer solution. Due to the high concentration of solvent in the vapor atmosphere, the solvent from the cast film stays within while diffusion of non-solvent into the cast film leads to the phase inversion and results in a porous membrane.^{44, 45}

B. Precipitation by controlled evaporation

The polymer in this case is dissolved in a mixture of solvent(s) and non-solvent. The controlled evaporation of the solvent due to high volatility changes the composition to have a higher non-solvent and polymer content.^{38, 46} The polymer eventually precipitates and forms a skinned membrane.

C. Thermally induced phase separation

In this method, the polymer membrane is prepared by mixing the polymer with solvent(s) and non-solvent that act as a solution at high temperature for casting or spinning the solution, and

solidifies upon cooling. Since the transformation of the polymer solution into a membrane or the phase separation takes place due to a change in temperature of the polymer solution, the process is called as thermally induced phase separation (TIPS).⁴⁷ A mixed or single solvent polymer solution can be used for membrane formation by TIPS, which happens due to solvent evaporation.⁴⁸ This method is often used to prepare microfiltration membranes.⁴⁸

D. Immersion precipitation

A polymer solution is either cast on a proper support or spun as a hollow fiber (HF); afterwards, the as-cast or as-spun polymer film or fiber is immersed in a coagulation bath. Here, the precipitation or solidification of polymer solution takes place due to the solvent and non-solvent exchange, thus the process is called as non-solvent induced phase separation (NIPS).^{43, 49} The rate of phase inversion and the characteristics of the final membrane primarily depend on solubility of the solvent in the non-solvent, insolubility of the polymer in the non-solvent, and temperature of the non-solvent, which controls the mass transfer driven by the kinetics and thermodynamics of the process.⁵⁰

Out of these four processes, immersion precipitation has been the most widely used technique for preparing polymeric membranes since its introduction in membrane technology in the 1960's. The reverse osmosis membrane developed by Loeb and Sourirajan was a milestone in membrane technology, which provided high salt rejections and high fluxes at moderate hydrostatic pressures.⁵¹ This invention of asymmetric membranes with a dense skin lead to the large-scale industrial use of membranes that began in 1970's with water desalination and purification to produce potable and high quality industrial water.⁵² The membranes prepared *via* combination of NIPS and TIPS have also been widely studied and applied in the fields of microfiltration and ultrafiltration. The combined process of non-solvent-thermally induced phase separation is known as N-TIPS.^{53, 54}

The use of commercially available green solvents, such as PolarClean[®] and acetyl tributyl citrate (Citroflex[®] A4), as an alternative of commonly used toxic solvents is the new trend in preparation of membranes *via* phase inversion processes, however, this may apply in specific cases only.⁵⁵

1.2.4. Pressure-driven membranes for liquid filtration processes

Membrane separation processes and their applications are as diverse as membrane structures, which are defined by the chemical and physical properties of synthetic membranes and separated particles as well as the choice of driving force.⁵⁶ In contrast to biological membranes, synthetic membranes have only passive transport properties. The most commonly used driving forces of a membrane process in industry are pressure and concentration gradients.

The main application of membranes today is in the separation of molecular and particulate mixtures. The separations are largely covered by hydrostatic pressure-driven filtration processes. This includes micro-, ultra- and nano-filtrations, and reverse osmosis, in the order of decreasing pore size.⁵⁷ Conceptually, these pressure-driven separation processes are similar because of the hydrostatic pressure gradient as the driving force for mass transport. However, the selective pore size makes a big difference in the operating conditions and mass-transport mechanism.¹²

Membranes can also be categorized based on their application and separation regime.⁵⁸ The range of application of these pressure-driven membranes for water separation processes are illustrated in Figure 1.1.

A. Microfiltration

In microfiltration, the particles and dissolved macromolecules larger than 0.1 μm are rejected.⁵⁹ The membranes are applied in pharmaceutical, chemical and semiconductor industries for separation of catalysts, enzymes, yeasts, purifying extraction fluids, and separation of glass cutting and metal particles from oil/fluid, respectively. Microfiltration membranes are also used as a pre-filtration in the process of water treatment by ultrafiltration, nanofiltration and reverse osmosis. The pre-filtration is applied for the removal of large particulates, colloids and bacteria from feed streams, mainly for wastewater treatment in the food & beverage industry.^{57, 60} The membranes are characterized by performing bubble point test and retention tests of bacteria, latex or other micrometer-sized particles.

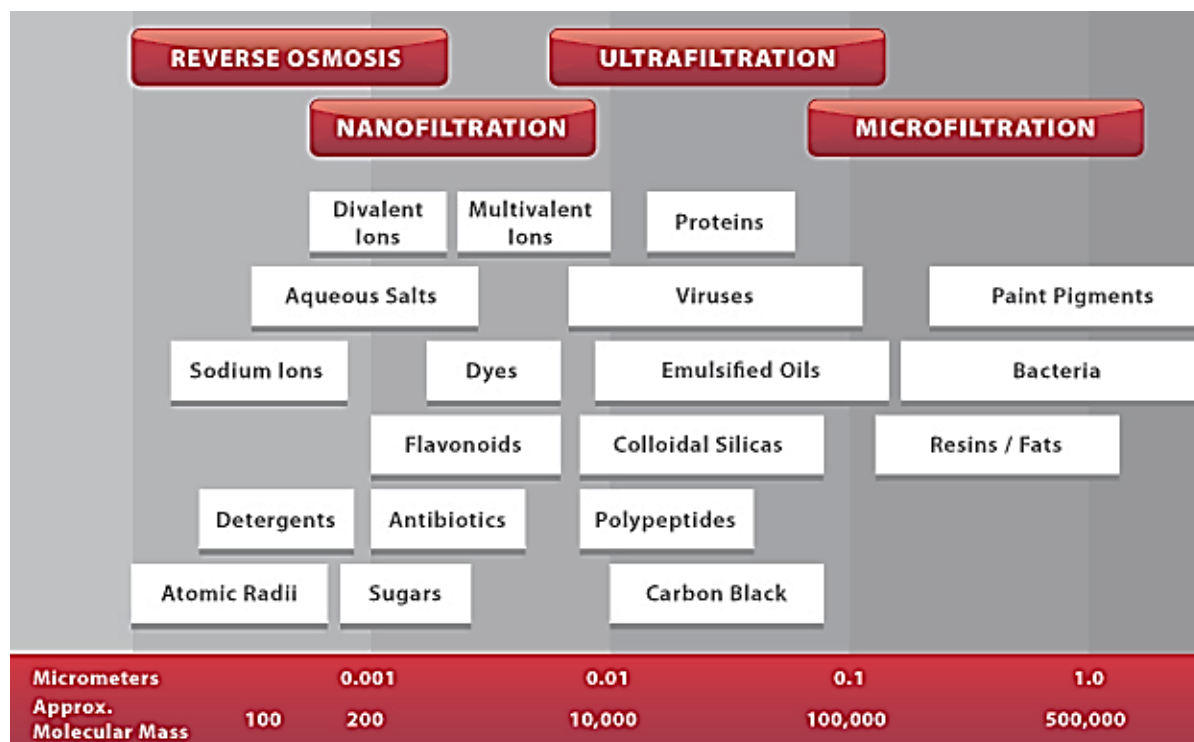


Figure 1.1. Description of the pressure-driven membrane separation processes and their applications. Copied with permission from Synder Filtration, © 2019 Synder Filtration, Inc.²

B. Ultrafiltration

Ultrafiltration is a process that is similar to microfiltration in which the particles and dissolved macromolecules smaller than $0.1 \mu\text{m}$ and larger than about 2 nm are rejected.⁵⁹ The membranes used for ultrafiltration comprises a molecular weight cut-off range of $1\text{-}500 \text{ kDa}$. These membranes are used in rejecting bacteria, viruses, colloids and polypeptides, and are widely used in wastewater treatment and concentration of proteins, enzymes *etc.*⁵⁷ Ultrafiltration membranes are commonly characterized by solute rejection tests by passing molecules with a known molecular weight through the membrane such as globular proteins or linear water soluble molecules like polydextran, poly(ethylene glycol) (PEG) and poly(vinyl pyrrolidone).^{20, 60, 61}

C. Nanofiltration

The pressure-driven membrane based separation process provides rejection of the particles and solutes smaller than 2 nm .⁵⁹ These membranes are able to reject multivalent salts and uncharged solutes, while allowing some monovalent salts to pass through. Nanofiltration membranes are

² <http://synderfiltration.com/learning-center/articles/introduction-to-membranes/pressure-driven-membrane-filtration-processes/>

similar to reverse osmosis membranes in that they contain a selective thin-film composite layer (<1 μm) on top of a porous layer (50 to 150 μm) for small ion selectivity. The membranes can also function at lower pressures than reverse osmosis membranes, which make them ideal for achieving an optimal combination of flux and rejection.^{9, 56}

D. Reverse Osmosis

Reverse osmosis membranes are tighter than nanofiltration membranes, and are able to reject all monovalent ions while allowing water molecules to pass through in aqueous solutions. The pores in these membranes are so small, from 3 to 5 \AA in diameter, that they are within the range of thermal motion of the polymer chains that form the membrane. In these membranes, separation occurs because of the difference in solubility and mobility of different solutes in the membrane, as explained by the solution-diffusion model.⁶ Common applications for reverse osmosis filtration include desalination of brackish ground water or seawater and industrial water treatment. The membranes are operated at much higher pressure as compared to micro- and ultrafiltration membranes.^{62, 63}

1.2.5. Fundamental transport mechanism in pressure-driven liquid separation membranes

The most general description of flux is ‘the amount of a property passing through a unit area per unit time under a given driving force’. That is:

$$J = -L \cdot \frac{dX}{dx} \quad (1)$$

Where J is a flux of a property, X is a driving force, x is the directional coordinate perpendicular to the membrane surface, and L is a phenomenological coefficient.⁶⁴

The properties transporting through the membranes can be mass, volume, energy, electrical charge, *etc.* Here, we consider hydrostatic pressure as main cause of the flux of water.

In case of volumetric flux caused by a hydrostatic pressure gradient, Darcy’s law expresses the flux of a certain volume (of water) through a porous medium or a membrane in the direction perpendicular to the membrane surface, such as:

$$J_v = -L_p \cdot \frac{dp}{dz} \quad (2)$$

Where J_v is the volumetric flux, L_p is the hydrodynamic permeability, and dp/dz is a driving force of pressure gradient in the z-direction.⁶⁵

Thus, the volumetric water flux (J) in pressure driven membrane processes is calculated as follows:

$$J_v = \frac{\Delta V}{A \cdot \Delta t \cdot \Delta p} \quad (3)$$

Where, ΔV is the volume of collected water between two mass measurements, A is the active surface area of membrane, Δt is the time between two measurements, and Δp is the transmembrane pressure.

While this expression is the general description of flux, for a comprehensive description of the mass transport through membranes, the properties of membranes, the coupling of fluxes and deviation from the ideal behavior of molecular mixtures need to be taken into account. In this context, the fluxes through the membranes can either be by viscous flow through defined permanent pores or by diffusion through a dense layer or both viscous flow and diffusion in the mixture passing the membrane by viscous flow.

Viscous liquid flow through a cylindrical capillary pore driven by the pressure gradient across the membrane is described by the Hagen-Poiseuille equation, given as:

$$J_v = -\frac{\pi D_p^4}{128 \eta l} \cdot \Delta p \quad (4)$$

Where, J_v is the flux, D_p diameter of the pore; Δp is the pressure difference across the pore; η is the viscosity of liquid (in case of water, 8.94×10^{-4} Pa s at 24 °C)⁶⁴; l is the length of a straight cylindrical pore.^{66, 67}

Assuming that all pores on the membrane surface have the same geometry, the flux from the active layer of the membrane consisting of a series of N_p number of cylindrical capillary pores is the sum of all the laminar liquid flows through the individual pores and is given as:

$$J_v = -N_p \cdot \frac{\pi D_p^4}{128 \eta l} \cdot \Delta p \quad (5)$$

Where, N_p is the average number of pores per unit area on the membrane surface.

The Hagen-Poiseuille equation considers that the fluid must be incompressible and the flow in the pores must be laminar, which is valid in membrane filtration.⁶⁶ The equation defining the flow from an individual pore helps to understand the difference in the above-mentioned four pressure-driven water separation methods. According to the equation, the flux through the capillary pores is proportional to the power four of pore diameter and the pressure difference across the pore (equation 5). Since the typical pore diameter of a microfiltration membrane is 100-times larger than the average ultrafiltration pore and 1000-times larger than the (nominal) diameter of pores in reverse osmosis membranes, the permeance (flux per unit pressure difference), from microfiltration is considerably higher as compared to reverse osmosis membrane. In addition, the operating pressure and the used conditions define the flux in all the four processes.

However, there is a significant influence of tortuosity and shape of pores, and flow resistance of membrane substructure on the permeability and the selectivity of membranes. Accounting the tortuosity of the pores, the sum of all the laminar liquid flows through the individual pores is given as:

$$J_v = -N_p \cdot \frac{\pi D_p^4}{128 \eta l \tau} \cdot \Delta p \quad (6)$$

Where, τ is the pore tortuosity; $\tau = 1$ for a capillary with a circular cross section.⁶⁸

Several studies have contributed to estimate the permeability of porous media and modified the classical Hagen-Poiseuille equation for tortuous and noncircular channels. For example, Pickard proposed a slightly different form of the Hagen-Poiseuille equation:

$$J_v = -k \cdot \frac{\pi D_h^4}{128 \eta l} \cdot \Delta p \quad (7)$$

Where, D_h is hydraulic diameter, k is a geometry correction factor dependent on the shape of the capillary and its eccentricity with $k = 1$ for a capillary with a circular cross section, $k = 1.43$ for a square, and $k = 1.98$ for an equilateral triangle.⁶⁹ The detailed calculations of these values and insightful studies are available in the referenced literatures.⁷⁰⁻⁷³

1.2.6. Membrane operations

The pressure-driven membranes can be operated in two ways, dead-end and cross-flow modes, as schematized in Figure 1.2.⁵⁹

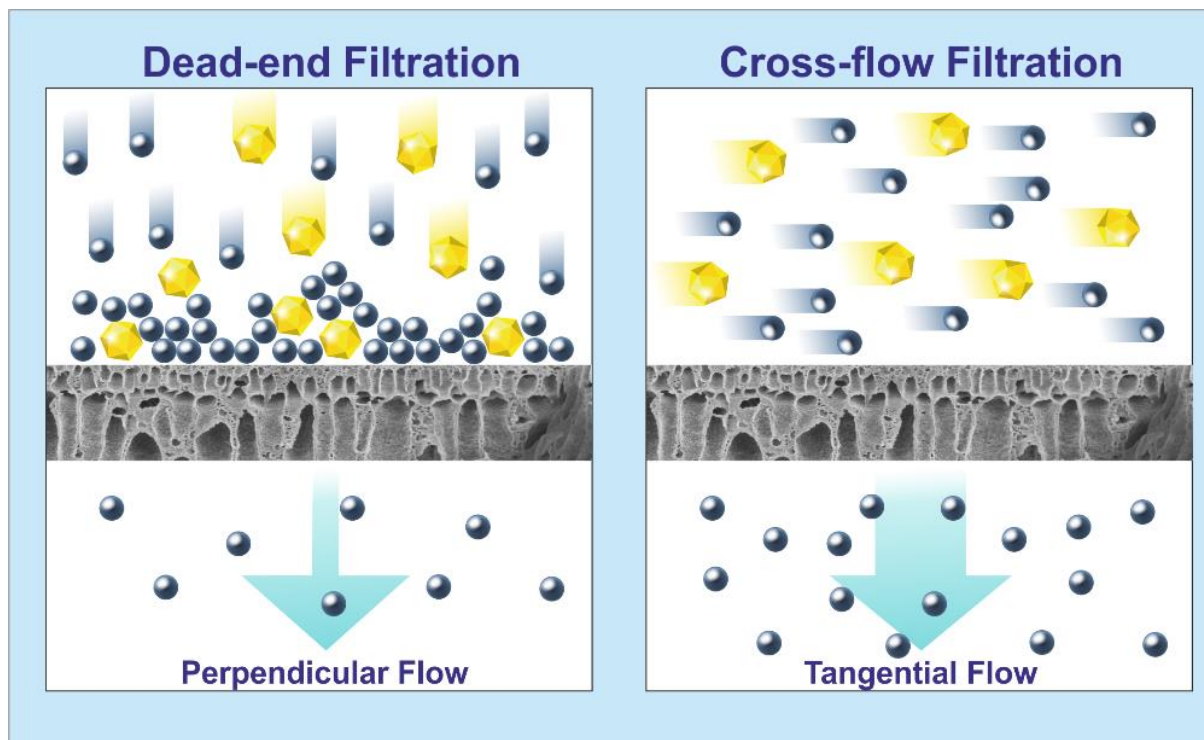


Figure 1.2. Schematic diagram of pressure-driven separations operated in dead-end and cross-flow modes.

A. Dead-end filtration

In the dead-end filtration, the feed flow is applied perpendicular to the membrane surface. This provides a permeate through the membranes and retentate on the membrane surface. The separation works through cake filtration process, which starts when the feed solution passes through the filter plates and creates a build-up of solids on the filter surface. The cake layer reduces the effective pore size and the flux with time.

B. Cross-flow filtration

In cross-flow filtration the feed flow is applied tangentially across the membrane surface. As feed flows across the membrane surface, permeate passes through while retentate accumulates at the opposite end of the membrane.

Advantages of cross-flow versus dead-end

There are several advantages of using cross-flow over dead-end membrane filtration process. The build-up of cake layer in dead-end filtration leads to an increase in the resistance with increase in the thickness of the cake formed on the membrane. Whereas in cross-flow processes, the foulants deposit until the forces of the binding cake to the membrane surface are balanced by the shear-forces of the feed stream. As a consequence, the permeability and the flux rapidly decrease in the dead-end separation, proportionally to the concentration of retentate and, thus, requires a periodic cleaning. While for cross-flow processes, the tangential flow of feed limits build-up of retentate on the surface of the membrane and the permeate flux does not drop as fast when compared to dead-end filtration.⁶

Therefore, the lesser demand of periodic cleaning in cross-flow configuration improves production efficiency and quality control as compared to dead-end, and improves membrane lifespan by helping to prevent irreversible fouling, which in turn can cut down the operating cost.

It should be noted that the cross-flow filtration is preferred for the filtration of fluid having low solute concentrations or solids while for filtration of viscous fluids, dead-end filtration works better, in which the cake layer can be removed after a span of time.

1.2.7. Membrane geometries, module configurations and processes

Advanced and reliable manufacturing processes offer membranes, membrane modules in various shapes and formats, and of respective flow configuration as required for particular applications. The major breakthrough in membrane technology came with the membranes developed by Loeb and Sourirajan; the membranes were developed in flat sheet geometry for reverse osmosis application.⁵² Later a different approach, spinning of polymer solution with a bore fluid, lead to a self-supporting hollow fiber membrane geometry.⁷⁴ To date, membranes are mainly produced in three different configurations: flat sheets, capillary or HF, and tubular devices. Other type of the processes, such as membrane (micro)capsules may have significant potential for controlled drug release but do not play a large role in industrial applications yet.⁷

Soon after the development of efficient membranes, the appropriate membrane housing devices, called modules, were established. ‘Module’ describes a complete unit, composed of the membranes, the pressure support structure, the feed inlet, the outlet for permeate and retentate streams, and an overall support structure.⁵⁹ The principal types of membrane modules include plate-and-frame, spiral wound, tubular and HFM modules.

A. Plate-and-frame module

In a plate-and-frame module, the flat sheet membranes are bolted together with a frame around the perimeter; the feed passes between the membranes of two adjacent membrane assemblies.⁷⁵ Common applications for plate-and-frame configurations include cosmetics production, membrane bioreactor, and specialty high solids food and beverage applications.

B. Spiral wound module

Spiral wound modules comprise of a flexible permeate spacer placed between two flat membranes, forming a membrane sandwich, which is then rolled into a circular configuration. Spiral membrane elements offer the best value per membrane area, a very high packing density, surpassing the packing density of plate-and-frame, tubular, and capillary configurations, smallest footprint, robust design that prevents membrane breakage (compared to HFM) and has relatively low capital and operating costs. However, spiral element fouling is greater, cannot handle

mechanical cleaning like tubular elements, and spiral wound modules have a lower packing density than HF.

C. Tubular modules

Tubular modules consist of a minimum of two tubes; the inner tube, called the membrane tube, and the outer tube, which is the shell. Tubular modules in cross-flow configuration are primarily used in micro- and ultrafiltration applications and are generally used to process difficult feed streams such as oily wastewater treatment, membrane bioreactor and other high solids processes. Tubular systems get less fouling compared to plate-and-frame systems, and a similar amount of fouling when compared to spiral and capillary. The membranes allow robust cleaning using harsh chemicals, backwash, and even mechanical or physical cleaning with sponge balls. They have low packing density as compared to capillary, HF, and spiral wound elements; thus, the larger size is a disadvantage of tubular modules.

D. Hollow fiber membrane modules

HF filtration utilizes thousands of long, porous HF ranging from 1-3.5 mm in diameter, which are potted in a polymeric or metallic shell. The HF configuration works in a similar way to tubular configuration but the filaments having narrow diameter are flexible. Due to the small strand diameter, a bundle of hundreds to thousands of HF can be inserted into a pressure vessel for module fabrication. Often the main criterion for selection is the required membrane area; modules with capillary or HF membranes can contain a much higher membrane area per volume than those equipped with flat-sheet membranes.⁶ The flexibility of the fiber strands allows certain filter configurations that cannot be achieved in other filtration configurations. HFM can also be back-flushed from the permeate side and air scoured, and can process feed streams with high total suspended solids, mainly in outside-in configuration.

HFM can find usages in all types of filtration, ranging from microfiltration to reverse osmosis. Widely applied separations by HFM include dialysis, membrane bioreactor, reverse osmosis pretreatment, industrial/domestic wastewater treatment, juice processing, and biotech applications. HFM can carry out the filtration in two ways, either “inside-out” or “outside-in”.^{76,77}

a. Inside-out hollow fiber membranes

As the name describes, in the inside-out HFM, the direction of separation is from inner side towards outer side, as shown in Figure 1.3. The feed flows across the inside of the fiber and travels through the pores in the membranes, exiting through the top of the shell as permeate. As the feed travels down the fiber length, it exits at the other side as permeate (concentrate).⁷⁸
⁷⁹ The inside-out configuration provides better control over hydrodynamics of feed flow.

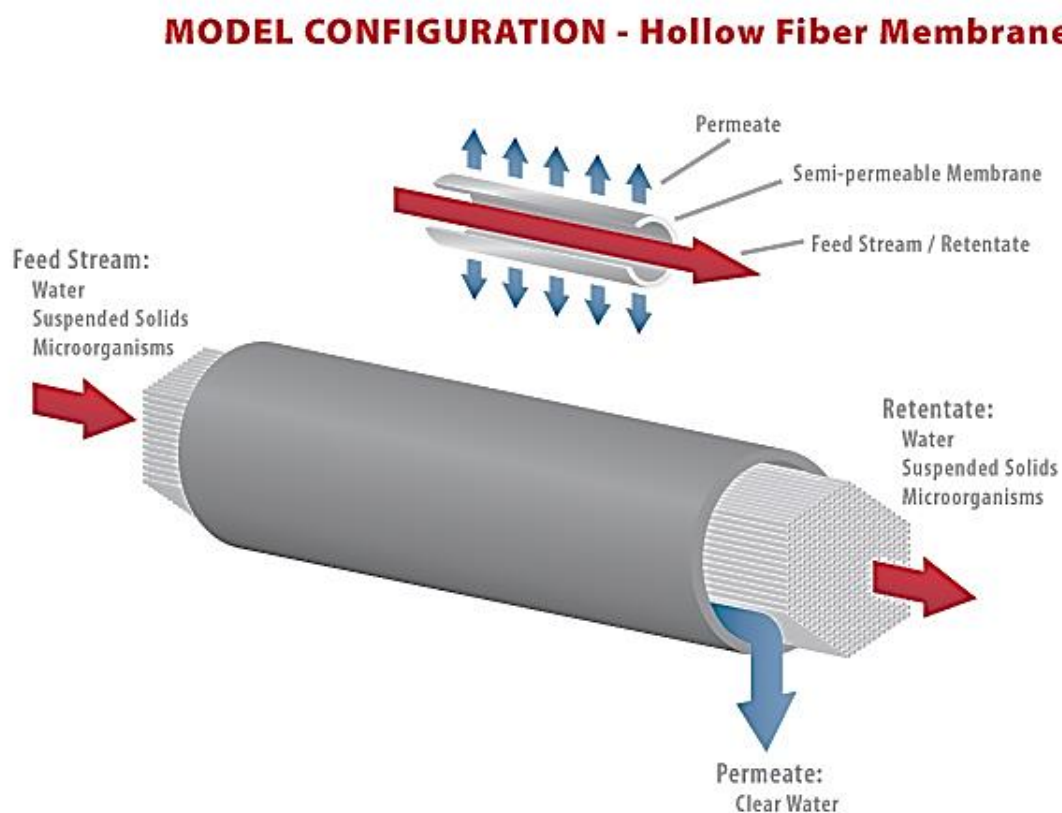


Figure 1.3. Schematic diagram of a HFM module in inside-out filtration configuration. Copied with permission from Synder Filtration, © 2019 Synder Filtration, Inc.³

b. Outside-in hollow fiber membranes

The feed is applied to the outside of the fiber and the permeate is collected from the lumen side. The outside-in configuration provides a higher surface area as compared to the inside-out

³ <http://synderfiltration.com/learning-center/articles/module-configurations-process/hollow-fiber-membranes/>

configuration, while the active surface area can be different due to the sticking of fibers to each other or due to fouling.⁷

Flexibility of the fibers make them easy to break under high strain as compared to other methods of filtration such as tubular or spiral wound elements. HFM tend to have moderate capital costs, but high operating costs compared to other configurations. Rigidity and strength are not high in HF as compared to tubular filtration units. However, the robust single layer having a thickness of few hundred micrometers or dual-layer HFM are easily applicable in normal processes like ultra- and microfiltration, which do not require high transmembrane pressures.⁷⁶

1.3 Block copolymers, self-assembly and isoporous membranes

1.3.1. Block copolymers

A block copolymer consists of different continuous series of identical repeating units or random copolymers connected into one macromolecule. The enormous range of possible molecular architectures of block configurations is basically classified based on two parameters: the number of chemically distinct blocks and linear, branched, or cyclic sequencing of the blocks.⁸⁰⁻⁸³ With advanced polymer synthetic strategies and techniques, *e.g.*, controlled polymerization techniques along with facile post-functionalization, block copolymers with precisely controlled molecular weights and defined macromolecular architectures can be prepared.⁸⁴ The designed macromolecules combine the properties of constituting blocks but may display new properties, depending on the way the different blocks are combined into one macromolecule, the strength of incompatibility between different blocks and their respective molecular weights. The advances in synthetic techniques allow almost complete freedom in selecting the polymer for each block. This, in turn, allows each block to have properties tailored for ultimate applications.^{85, 86} Stunning block configurations can be constructed by using two or more types of repeating units during polymer synthesis, which may lead to AB diblock, ABC triblock, ABA triblock, ABABA pentablock, $(AB)_nX$ star diblocks, $(AB)_n$ multiblock, or segmented copolymers, *etc.*^{87, 88} A further modification in the polymer is possible *via* a large number of well-defined post modification roots such as click-chemistry.⁸⁹⁻⁹²

Diblock copolymers

The simplest and most studied architecture is the linear AB or A-*b*-B diblock copolymer, which consists of a series of identical repeating units of type A that is covalently bonded to another chemically different long sequence of type B repeating units, *e.g.*, polystyrene-*block*-poly(4-vinylpyridine) (PS-*b*-P4VP) diblock copolymer, as shown in Figure 1.4.

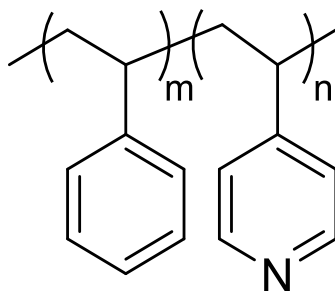


Figure 1.4. Structure of PS-*b*-P4VP diblock copolymer.

1.3.2. Self-assembly of amphiphilic diblock copolymers

The growing demand of miniaturization in today's materials science enforces more research in “bottom-up” fabrication methods. The immiscibility of chemically incompatible blocks drives the macromolecules to self-assemble into exquisite nanostructures, just like their small molecule analogues, lipids and surfactants. This provides an avenue for Prof. Richard Feynman's vision of bottom-up fabrication approach. In the last decades, various block copolymers have been studied as molecular building blocks for fabrication of large-scale prescribed structures generated by the “bottom-up” approach of self-assembly.⁹³⁻⁹⁶ The ability to precisely control the length scale of microstructures in the range of 5-100 nm through the simple expedients of changing molecular weight, structure of repeating unit, temperature, dilution with other polymers or solvents *etc.* make block copolymers the pre-eminent self-assembling materials.⁹⁷⁻⁹⁹

In the thermodynamically driven process of self-assembly, the incompatible block segments of a copolymer prefer to stretch out as individual polymer chains in an effort to get as far away from each other as possible but are unable to because of the chemical linkage holding them together. The formation of the various morphologies is attributed to two competing factors: interfacial energy between the two blocks (an enthalpic contribution) and chain stretching (an entropic contribution). The degree of chain stretching depends on the volume fraction of one block and the degree of polymerization of the diblock copolymer, as shown in Figure 1.5. As microphase separation occurs, the two blocks separate from each other in such a way as to minimize interfacial area in order to lower the total interfacial energy. *E.g.*, when the diblock copolymer is highly asymmetric, *i.e.*, the volume fraction of one block such as A block is small, the A blocks prefer to aggregate into spherical microdomains, leaving the B blocks to surround

them as ‘coronas’. This way, the system gets the lowest interfacial area and increased conformational entropy relative to other morphologies, and thus is energetically favorable. As volume fraction of A increases at a fixed temperature and the effective volume fraction of block B decreases, the polymer chains have to adopt new arrangements to reduce their stretching, leading to a morphological transition from spheres to cylinders and to lamellae for a symmetric diblock copolymer.

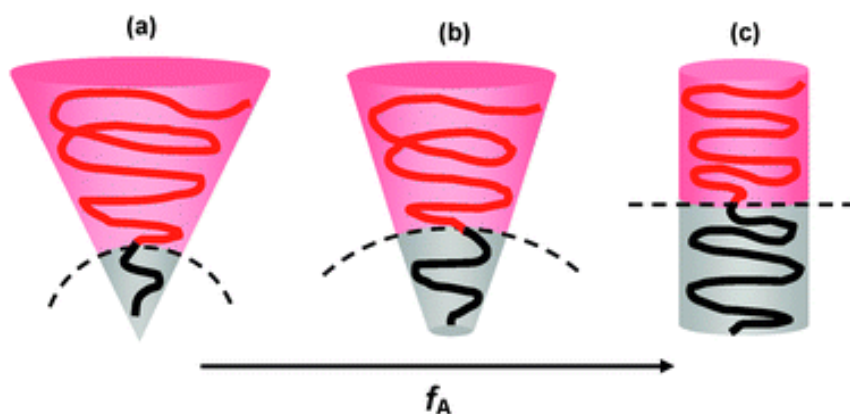


Figure 1.5. Schematic illustration of the possible polymer chain arrangements in different morphologies of AB diblocks changing from sphere (a) to cylinder (b) and to lamella (c), as the volume fraction (f_A) of the A block (black) increases to ~ 0.5 . The dash curve in each morphology represents a part of the interface between A and B domains.¹⁰⁰

The system balances the energetic factors; an unfavorable mixing enthalpy coupled with a small mixing entropy, to achieve a microphase-separated structure and can produce lateral order of astonishingly complex self-assembled nanostructures on the macromolecular scale.^{80, 83, 87, 102-106} This lateral order of a particular morphology depends on the volume fractions of the different polymer blocks (f), the total degree of polymerization (N), and the degree of incompatibility between the block segments, which is determined by the Flory-Huggins-Staverman interaction parameter (χ). An increase in the number of blocks and components leads to a rapid increase of possible structures and an increased level of complexity for self-assembly.^{87, 103, 107} χ measures the thermodynamic incompatibility between the two blocks, which depends on the temperature of the system as well. At high temperatures, entropic contributions dominate and the system forms a homogeneous disordered phase. As the temperature decreases, repulsive interactions between the two polymer blocks become more important, which leads to microphase separation into ordered morphologies. Therefore, by manipulating these molecular parameters, various morphologies including spherical, cylindrical, lamellar, and others have

been revealed both experimentally and theoretically. The self-consistent mean-field theory provides the calculations of free energies and composition profiles for the various ordered states for weak thermodynamic interactions ($\chi \ll 1$) combined with the large number of interchain contacts ($\approx N$).^{108, 109} The equilibrium morphologies of narrow disperse diblock copolymers are shown schematically in Figure 1.6.

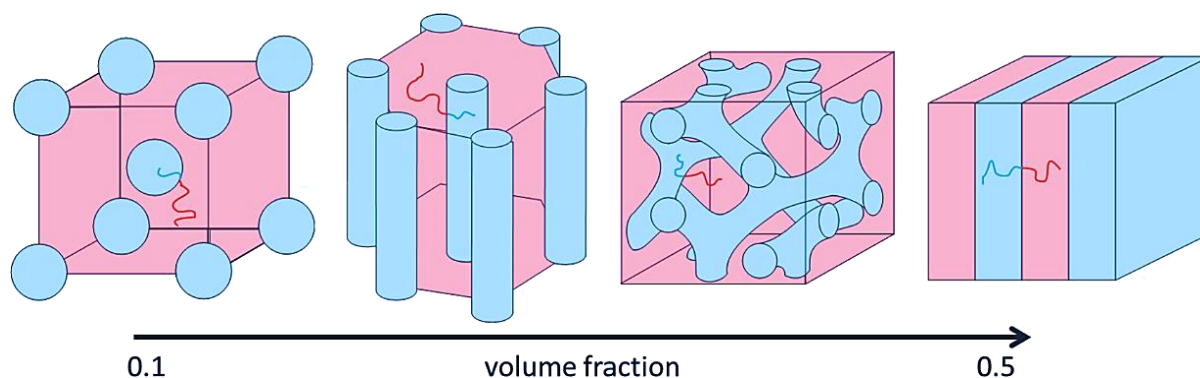


Figure 1.6. Morphologies of diblock copolymers. From left to right the volume fraction of the blue component increases: spheres, cylinders, double gyroid, and lamellae. Copied with permission; © 2014, John Wiley and Sons; license number: 4552980528271.¹¹⁰

In particular, the cylindrical^{36, 103, 112, 113} and gyroidal^{114, 115} morphologies fascinate membrane scientists. Segregation of the blocks on the molecular scale can produce astonishingly complex nanostructures, such as the striking "knitting pattern" using a triblock terpolymer, discovered by Prof. Reimund Stadler's group.^{102, 116, 117} This reflected a delicate control over kinetics of macromolecular system. Therefore, the ability to precisely control morphology, the length scale of microstructures, domain functionality and properties, retention of the traditional advantages of polymeric material, quantitative prediction of equilibrium structures, *etc.*, makes block copolymers the pre-eminent self-assembling materials.

A. Self-assembly in bulk

Self-assembly of block copolymers in bulk has been studied extensively for over 50 years. In conventional bulk self-assembly studies, the films were prepared under such conditions that the block copolymers are segregated in the state of thermodynamic equilibrium. The process is governed by an unfavorable mixing enthalpy coupled with entropic losses due to macromolecular junctions and chain stretching. The bulk film fabrication is commonly done by dissolving the block copolymer in a solvent and allowing the slow evaporation of this solution after

pouring in a mold.^{103, 118-121} Afterwards, the temperature is slowly raised above the glass transition temperature of all the blocks in the block copolymer for their segregation in the melt state.^{80-83, 102} In the bulk state the selection of morphology is dictated primarily by composition but temperature, diluents, and changes in architecture can also be used to modulate the equilibrium structure. The bulk assembly of traditional A-B diblock copolymers is well-researched both theoretically and experimentally.¹⁰³

The bulk morphologies (diblock and multiblock) got wide attention as precisely nanostructured templating materials for applications ranging from catalysis, photovoltaic¹²² and optics¹²³ to fuel cells and lithography^{124, 125}. The double gyroid morphology is a triply periodic minimal surface and attracts special attention as precursor in hybrid materials design¹²⁶ for applications requiring high surface area and symmetry like solar cells¹²⁷ or nanofoams^{128,18} Current commercial applications of bulk block copolymers include thermoplastic elastomers, such as gaskets, cable insulation, footwear, blending, adhesives, automotive bumpers, snowmobile treads; thermoplastics for medical devices, protective headgear, and piping systems. The facile and low-cost generation of a myriad of application-specific recyclable, flexible, thermoformed (or blow-moldable), creep-resistant, and durable thermoplastic elastomer materials as compared to conventional thermosets is primarily due to the prescribed nanoscale phase separation.⁹⁷

B. Self-assembly in (dilute) solutions

When block copolymers are dispersed in solvents that are selective and in particular if the solvent (or solvent mixture) is near or below the theta temperature for one of the blocks, micelles will form, as shown in Figure 1.6.¹²¹ By this self-assembly in solutions, a myriad of tailor-made micellar morphologies are accessible that can meet the demands of precisely tunable micro- and nanostructures.^{3, 129} Spherical, cylindrical and helical micelles as well as vesicles can be obtained by the use of selective solvent(s). More complex preparation steps involving cross-linking or guided hierarchical self-assembly protocols enable the formation of Janus, patchy and multicompartment micelles such as clover-, hamburger-, raspberry- and football-like particles.⁹⁴

Such self-assembly of block copolymers in a solution paves the way for the construction of excellent templates for the selective incorporation and stabilization of nanoparticles, giving rise to highly relevant applications in the field of catalysis, sensing, optoelectronic devices, *etc.*^{95, 130-133} Moreover, the block copolymer micelles in aqueous solutions hold promise for the delivery

of a large array of chemically diverse therapeutic compounds.^{121, 134-138} Typically, the fabricated self-assembled block copolymer structures are obtained from solutions, which leads to a possible influence of the solvent on the finally obtained structure or in a kinetically trapped state of the micro-phase separation.¹³⁹

C. Self-assembly in fabrication

Particular morphologies using block copolymers in bulk, solutions, melts, *etc.*, can be achieved either by reaching the thermodynamic equilibrium state or by quenching the morphologies at a particular segregation strength. In context of this thesis, one of the most common studies on fabrication techniques using block copolymers includes film fabrication like thin films by spin coating, spraying, electro-spraying or dip coating or thick films by dip coating or casting of block copolymer solutions.¹⁴⁰⁻¹⁴³ The surface topology or nanostructure formation of block copolymers in various fabrication processes is more complex as compared to the bulk and in-solutions due to a number of additional driving forces such as surface fields, film thickness, substrate polarity, environmental conditions, or sample preparation history.¹⁴⁴⁻¹⁴⁷

The thin film morphologies have been operated for media storage, photonics, nanolithography for patterning next-generation semiconductor devices, nanotemplating for dense bit-patterned media, and membranes for nano- and ultrafiltration applications. However, the hurdles of cost-effective and scalable approaches, understanding the influence of nanostructure formation kinetics and processing protocols on morphology and orientation, elimination (or significant reduction) of defects, and translation of nanopatterning techniques to various substrates such as flexible substrates, porous scaffolds, graphene, metals limit the wide-spread usage of block copolymer thin films in emerging technologies¹⁴⁸⁻¹⁵¹

1.3.3. Isoporous membranes

The common understanding from the term “iso” is “equal or identical” so an isoporous membrane means the membrane having pores of equal diameter on the top surface. In this category, for nanometer-sized pores, track-etched membranes are commercially available and claim to provide accurate fractionation of particulates because of their precise pore size with uniform capillary pore structure. However, the surface porosity of these membranes is very low. Likewise, the commonly used polymeric membranes are well-established systems but lacks high surface porosity on top. The other type of isoporous membranes is anodic aluminum oxide membrane, which provides a self-organized hexagonal closed pack nanostructure. The membranes are produced *via* an electrochemical process, in which an oxide layer is slowly developed on the aluminum surface. However, the straight uniform pores do not provide good flux as compared to the membrane having a selective surface on an asymmetric and more porous substructure. Since the key property of membrane-based separation is subject to permeability-selectivity trade-offs, that decide its overall efficacy, it is required to have high surface porosity providing high permeability along with uniform pore size providing specific retentions. In this context, the self-assembled isoporous block copolymer membranes are preferred due to their capability of providing high density of evenly sized pores on top of a spongy substructure..¹⁵² A membrane may be considered an isoporous membrane if the ratio of the diameter of the largest pore to the diameter of the smallest pore is less than three.¹⁵³

As discussed in Section 1.3.2, the segregation between blocks of a block copolymer leads to microphase-separated domains. These self-assembled porous structures can be used as separation tools. The initial block copolymer based self-assembled structures were developed in thin or thick films, by providing controlled evaporation rate after coating or casting of block copolymer solutions onto solid substrates.^{142, 154-156} Afterwards, the selective etching of one block led to desired porous structures, *e.g.*, in the thin films prepared from polystyrene-*b*-poly(ethylene oxide) PS-*b*-PEO, selective etching of the PEO block leaves the porous PS monoliths. However, after etching there is typically some functionality remaining from where the two blocks were covalently connected but this is not high enough to impact the surface properties of the pores. Consecutively, the concept was used for triblock terpolymers with a central sacrificial block to facilitate etching. Moreover, the triblock terpolymers provide a scope to tailor

the surface chemistry as well, by introducing functionality into the pores of monolithic materials. *E.g.*, an A-B-C triblock terpolymer, comprising of blocks A as the matrix component, B as a nondegradable midblock for pore functionality, and C as the sacrificial block that is eventually etched.¹⁵⁷ Using this approach on polystyrene-*b*-poly(*N,N*-dimethylacrylamide)-*b*-polylactic acid (PS-*b*-PDMA-*b*-PLA), porous PS monoliths with hydrophilic PDMA lining on the pore walls can be prepared¹⁵⁸. In addition, the PDMA can be hydrolyzed to give poly(acrylic acid) (PAA), and these acids can be functionalized by various amines using standard diimide coupling chemistry.^{159, 160} Later on, the thin films were also studied using various di and tri block copolymers, by incorporation of ionic additives¹⁶¹, homopolymers^{156, 162}, nanoparticles¹⁶³, in presence of various directional fields, *etc.*^{36, 87, 104, 147, 154, 155, 157, 163-167}

The formation of such isoporous monolithic films by selective etching of at least one block requires a substrate, either porous or a dense material from which the cast polymer film has to be removed. In this case, the polymer film should have sufficient mechanical strength to be used as a free-standing membrane, which is hard in the case of thin polymer films, thus requires a mechanical stabilization, and therefore needs to be transferred onto a porous substrate support showing a negligible resistivity towards the permeating flux. Such composite membranes showed good fluxes and good selectivity.^{155, 168} However, the main drawbacks of thin films are the requirement of selective etching of one block for fabrication of porous structures, the removal of the polymer film from the substrate and the mechanical stability of the membrane. This increases the time, costs and complexity of membrane fabrication. Therefore, an alternative method was desired to reduce the number of steps in the fabrication process.

1.3.4. Fabrication of isoporous block copolymer membranes *via* SNIPS process

In 2007, “one-step” method for fabrication of integrally asymmetric isoporous block copolymer flat sheet membranes was introduced. The isoporous membranes were fabricated by a comparatively straightforward approach, *via* self-assembly of block copolymers in combination with non-solvent induced phase separation (SNIPS) process, as shown in Figures 1.7 and 1.8. A solution of PS-*b*-P4VP diblock copolymer in a solvent mixture of *N,N*-dimethylformamide (DMF) and tetrahydrofuran (THF) was cast on a glass plate and the as-cast film was

immersed in the precipitation bath after providing a short evaporation time. This way, the evaporation-induced self-assembly of block copolymers on the top surface of cast block copolymer film was trapped by non-solvent induced phase separation.¹³⁹ The more volatile solvent THF is selective for PS while DMF is selective for the pore forming minority block P4VP.^{139, 169} A key feature of the SNIPS process is that it can lead to a rather thin selective isoporous surface on top of a sponge like support structure of the same material, thus leading to a membrane with high selectivity and high permeance at the same time, which enforces more research in the field.

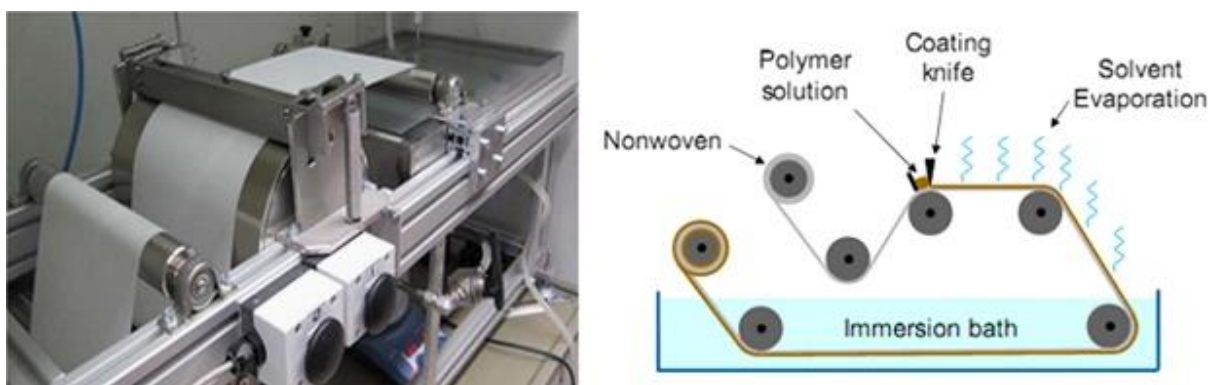


Figure 1.7. Flat sheet membrane fabrication by doctor blade casting. Laboratory-size casting machine and the schematic representation of the operation principle. Copied with permission; © 2013 Elsevier B.V.; license number: 4553090148149.¹⁶⁹

1.3.5. Mechanism of structure formation in isoporous block copolymer membranes

For fabrication of isoporous membranes, homogeneous block copolymer solutions are required. The polymer solution may remain homogeneous upon standing for a very long time, despite the possibility to reduce the Gibbs energy that is mainly possible because of evaporation of solvent(s) causing phase separation. The membrane fabrication process begins with the casting of the homogeneous polymer solution on a substrate glass plate or a non-woven or any other support. After casting, the evaporation of volatile solvents inevitably right away lead to a reduction in the Gibbs energy with fluctuation in concentration. This initiates the microphase separation and the demixing process takes place *via* nucleation and growth, which means that the individual microdomains of the minor phase (P4VP block) formed in the early state of the

process grow slowly. The minor microdomains are dispersed in the matrix of the corresponding coexisting microphase (PS) and can become rather large on micro scale depending upon the thermodynamics driving their growth. During the short evaporation time, mainly THF evaporates from the film surface leading to a high polymer concentration and self-assembly of the block copolymer in the top layer. Due to the evaporation, the PS matrix starts to solidify while P4VP domains remain swollen in DMF (P4VP phase in blue, PS in orange), see Figure 1.8. With increase in evaporation time, the concentration gradient from the top surface increases and the P4VP domains align perpendicular to the surface as cylinders. For fabrication of isoporous membranes, the hexagonally-packed pores are achieved by quenching the kinetic process of self-assembly or demixing after a certain time by immersing the film in a non-solvent (water) bath. The non-solvent induced phase separation leads to spinodal decomposition of the polymer solution underneath the microphase separated skin layer and forms the porous sublayer. For spinodal decomposition, the morphology is co-continuous, *i.e.* for each phase it is possible to find paths through the entire system without the necessity of penetrating into the other coexisting phase.

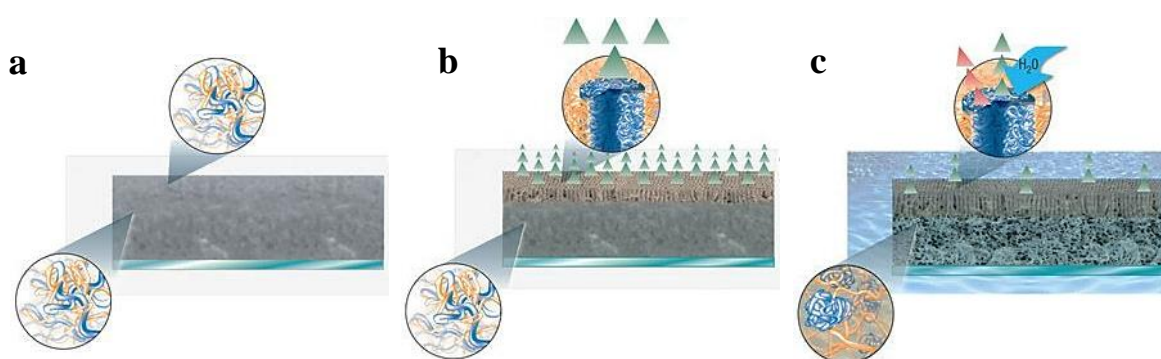


Figure 1.8. Schematic diagram of structure formation in PS-*b*-P4VP isoporous membranes (P4VP phase in blue, PS in orange). (a) Casting of the polymer solution. (b) the formation and alignment of cylinders start within the first ten seconds. (c) Immersion of the film in a water bath leads to a non-solvent-induced phase separation and the formation of the porous sublayer. Reused with permission; © 2007, Springer Nature; license number: 4552990315850.¹³⁹

In this fabrication process two factors are of high importance: (1) The evaporation of volatile solvent from the block copolymer solution where the incompatible blocks lead to the self-assembled structure by microphase separation. (2) The immersion in the coagulation bath where the precipitation traps this ordered structure on the surface and generates the sponge-like substructure by the exchange of solvent by non-solvent.^{110, 169, 170} The influence of rate of evaporation on the self-assembly of block copolymers in thin films is explained by Phillip *et. al.*¹¹²

The conclusive remarks highlight the requirement of a certain evaporation rate to direct the orientation of pore forming block perpendicular to the surface, while an evaporation rate lower than under the atmospheric conditions leads to the growth of pore forming domains parallel to the surface and results in cylinders lying on the surface. Further, Abetz explained the mechanism of the isoporous membrane fabrication by providing the ternary phase diagram of a polymer, solvent, and non-solvent, as shown in Figure 1.9.

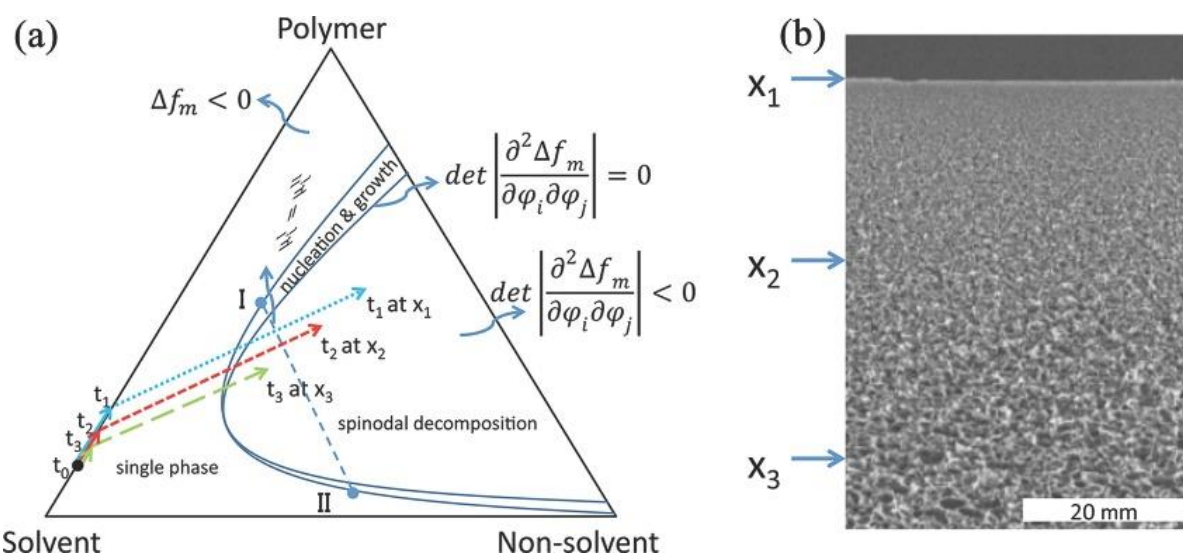


Figure 1.9. (a) Schematic of a ternary phase diagram of a polymer, solvent, and non-solvent. The condition for the single phase region is a negative free energy of mixing ($\Delta f_m < 0$), for phase separation by nucleation & growth in the metastable region the condition for the coexisting equilibrium phases is the equality of the chemical potential μ_i of component i in the two coexisting phases I and II, respectively. Spinodal decomposition is observed in the region of a negative determinant of the second derivatives of the free energy of mixing with respect to the volume fractions ϕ_i and ϕ_j , which vanishes at the spinodal. The composition of the casting solution is given at time t_0 when the solution is cast (by doctor blade or spinneret). t_1 is the time of immersion into the precipitant (non-solvent). During the time interval $t_1 - t_0$ the polymer concentration increases due to partial evaporation of the solvent. If the evaporation rate is large enough, a concentration gradient is built up perpendicular to the film surface. At the time t_1 after quasi instantaneous quench into the precipitation bath (indicated by the dashed blue arrow), the surface of the cast solution film x_1 has a certain composition in the spinodal region. Due to the retarded exchange of solvent by non-solvent across the surface x_1 at later times (for example t_2 and t_3), the compositions at x_2 and x_3 also change quasi instantaneously from a pure polymer–solvent mixture with certain compositions (depending on the initially built up concentration gradient in the cast solution film and the temporary re-equilibration of concentration at the times t_2 and t_3) to compositions in the spinodal region, which are closer to the single phase region than for the surface at x_1 (indicated by the red and green arrows). (b) A typical example of a cross sectional view of an integral asymmetric polymer membrane, as observed by SEM. A rather dense polymer layer occurs at x_1 , while at lower positions of the membrane the structure coarsens (increasing porosity) as observed, for example, at x_2 and x_3 . Copied with permission; © 2014, John Wiley and Sons; license number: 4552980528271.¹¹⁰

So far, the amphiphilic PS-*b*-P4VP diblock copolymer is the most studied diblock copolymer for the formation of isoporous membranes.^{139, 169, 171-173} In subsequent works, suitable conditions for isoporous membrane fabrication *via* SNIPS were also reported using other diblock copolymers, namely polystyrene-*b*-poly(2-vinylpyridine) (PS-*b*-P2VP)¹⁷⁴, poly(*tert*-butylstyrene)-*b*-poly(4-vinylpyridine) (PtBS-*b*-P4VP)¹⁷⁵, poly(4-trimethylsilylstyrene)-*b*-poly(4-vinylpyridine) (PTMSS-*b*-P4VP)¹⁷⁵, polystyrene-*b*-poly(solketal methacrylate) (PS-*b*-PSMA)¹⁷⁶, polystyrene-*b*-poly(glyceryl methacrylate) (PS-*b*-PGMA),¹⁷⁶ polystyrene-*b*-poly(iso-propylglycidyl methacrylate)¹⁴³, PS-*b*-PEO¹⁷⁷, polystyrene-*b*-poly(methyl methacrylate) (PS-*b*-PMMA)¹⁷⁸, polystyrene-*b*-poly(2-hydroxyethyl methacrylate) (PS-*b*-PHEMA)^{179, 180} *etc.* In addition, some triblock copolymers were also used for fabrication of the functional isoporous membranes. The used triblock copolymers include PS-*b*-P2VP-*b*-PEO¹⁸¹, PI-*b*-PS-*b*-P4VP^{182, 183}, PI-*b*-PS-*b*-PAA¹⁸⁴, and PI-*b*-PS-*b*-PDMA¹⁸⁵. All these works tried to elaborate the mechanism of isoporous structure formation.¹⁶⁹⁻¹⁷²

1.3.6. Factors influencing the structure formation in isoporous membranes

Besides expanding the number of block copolymer membranes obtained by SNIPS, several efforts have been made to understand the block copolymer membrane formation mechanism. Investigations were focused on the block copolymer structure formation in dependence of solvent selectivity¹⁸⁶, solvent composition¹⁷⁴, addition of non-solvent^{171, 187}, influence of additives helping to assemble the pore forming blocks by hydrogen bonds¹⁸⁸ or complex formation^{189, 190}, the influence of the casting conditions like solvent evaporation rate^{110, 112, 164}, temperature or humidity¹⁹¹.

A. Phase-selective chemistry of block copolymers

Since the important energies in the formation of interfaces in block copolymers are the entropic chain-conformational energy and the enthalpic interaction energy. This strength required for the thermodynamically driven morphologies can be tuned significantly by using phase-selective chemistry of block copolymers by means of chemical, physical or electrostatic interactions, depending on their physicochemical properties. Due to selectivity for one of the two blocks,

the effective volume fraction of the two blocks will differ from the bulk state and may lead to morphological transitions.¹⁰⁰ For example, a block copolymer with spherical domains of the shorter block may transform into a cylindrical structure upon selective swelling of the shorter block. Vice versa, a cylinder-forming diblock copolymer may transform into a sphere-forming one upon selective swelling of the matrix-forming block, as shown in Figure 1.5. Thus, the selection of solvents and thus the polymer solution can change the pore diameter, the density of pores and the packing of pores.¹⁶¹

B. Controlling pore size and functionality

The absolute size of the domains is defined by the molecular weight of the copolymer and the strength of the segmental interactions between the blocks. So, the pore size and morphology of isoporous block copolymer membranes can be tuned by changing the ratio of both (or more) blocks and the molecular weight of the constituent polymer blocks¹⁶⁹ or by blending of block copolymers having different compositions.^{118, 173} While this is advantageous tailoring, it implies the need of different block copolymers to be synthesized for every modification desired in the material characteristics. In addition, there are limits in increasing the length of block copolymer chains to achieve a well-structured morphology because of the large kinetic barrier in high molecular weight copolymers for the formation of well-ordered structures. In this case, the tailoring of isoporous membranes by mixing various amounts of homopolymer, non-solvent, or ionic additives are of great interest.¹⁹²

The selection of specific pore forming blocks can be utilized as a tool to tune the functionality of pores such as pH-responsivity. *E.g.*, the isoporous membranes having P4VP as pore forming block show very small fluxes at low pH (below 4) while a very sharp increase in flux can be measured for pH above 6. The pyridine groups at the membrane surface and pore walls were protonated at low pH, and the P4VP segments stretch to minimize charge repulsion, transforming the pores into a pH-sensitive gate. Other examples for membranes having P4VP as pore forming block include PI-*b*-PS-*b*-P4VP and polystyrene-*b*-poly(4-vinylpyridine)-*b*-poly(propylene sulfide), (PS-*b*-P4VP-*b*-PPS).^{143, 190, 193} The membranes of PI-PS-PDMA block polymer do not show any pH-response but the corresponding hydrolyzed derivative PI-PS-PAA material shows opposite pH-behaviour.¹⁹⁴ Thus, block copolymers represent an extremely versatile class of materials for generating functional nanoscopic structures.

C. Influence of additives and solution composition

The segregation strength of the block copolymers in solution can be further actuated by introducing small amounts of additives such as metal salts or carbohydrates, which are selective to pore forming block.^{102, 167, 188-190} These factors include electrostatic interactions, charge dissociation, ion solvation, and physical cross-linking of chains due to the presence of ions. By this, the block copolymer concentration required for the onset of microphase separation can be varied. Sageshima *et. al.* showed that the increase in additive (iron(III) chloride, FeCl_3) concentration with respect to the PS-*b*-P4VP block copolymer concentration in a solvent of pyridine could lead to differently arranged crystal lattices such as sphere, cylinder and lamella, by selective incorporation of FeCl_3 into P4VP nanodomains, also defining different d values.¹⁹⁵ The additives lead to an increase/decrease in stretching of particular block segments, which in turn will lead to transition of morphologies from sphere to cylinders to lamella or vice versa. This phenomenon of morphological transition significantly depends on the interaction between block segment and additive which might differ in different block copolymers and solution systems. *E.g.*, the addition of cadmium(II) chloride (CdCl_2) in PS-*b*-P2VP block copolymer reduces the domain spacing while increases the domain spacing in PS-*b*-P4VP due to the selective incorporation to P2VP and P4VP domains, respectively. This different influence of CdCl_2 is due to the formation of intramolecular bond between P2VP and CdCl_2 while intermolecular bonds in case of P4VP and CdCl_2 .¹⁹⁶

D. Influence of directional fields

The orientation and lateral ordering of the nanoscopic domains during self-assembly of block copolymers can be directed by solvent annealing (uniform, gradient, and zone-annealing), by applying external directional fields such as shear stress, electric field, temperature gradients or by exploiting effects from chemically or topographically patterned substrates, or by controlled interfacial interactions.^{167, 197-199} These influences have mainly been checked for thin film fabrications. However, a similar influence can be expected for isoporous membrane fabrication.

Therefore, the ability to precisely control morphology, the length scale of microstructures, functionality and properties of domains, advantages of using polymeric material, quantitative prediction of equilibrium structures, *etc.*, makes block copolymers the pre-eminent self-assembling materials. The self-assembly of block copolymers for fabrication of isoporous membranes in flat sheet geometry has been investigated by conducting *in situ* SAXS and grazing

incidence small-angle X-ray scattering (GISAXS) experiments.^{147, 172, 200, 201} These studies support the previous explanations. In order to cover a broader range of applications, subsequently, the SNIPS process was extended on the outer surface of a HFM in order to increase the effective surface area.

1.3.7. Outside-in isoporous hollow fiber membrane fabrication by spinning

As discussed in Section 1.2.8, the HF geometry provides higher active surface area per unit volume and close packing of these self-supported membranes in filtration modules, which makes them preferable to flat sheet membranes for large-scale installations.^{3, 6, 7} The HF spinning process has been investigated vastly for the fabrication of commonly used asymmetric HFM *via* NIPS.^{43, 76, 77, 202} In the widely-used dry-jet wet spinning process for preparation of HFM, a double orifice spinneret is used for extrusion of polymer solution and bore fluid, in the outer and inner orifice, respectively. In the formation of HFM *via* NIPS, the extruded polymer solution or as-spun fiber is immersed in the precipitation bath after a short air gap distance between the spinneret and the precipitation bath. The rapid exchange of the solvent(s) with the non-solvent in the precipitation bath leads to the formation of asymmetric structure.¹⁷⁰ During the HF spinning process, additional structure-controlling factors gain importance because the shear stresses applied during extrusion develops some mechanical memories in the polymer solution. The compressible viscoelastic polymer solution shows the swelling of the extrudate after exiting the spinneret, which not only affects the membrane structure but significantly varies the performance of the formed membrane. The controlling parameters are the polymer solution (polymer characteristics, molecular weight, polymer concentration, solvent(s) and additive(s)), spinneret (design and dimensions), spinning parameters (air gap and flow rates of polymer solution and bore fluid), environmental conditions, *etc.*^{170, 203, 204} Despite having so many influencing parameters, the asymmetric polymeric membranes can still be tailored by providing possibility of wide variations in the solution and spinning conditions along with the combination of different phase inversion processes such as NIPS and TIPS in the production of HFM .

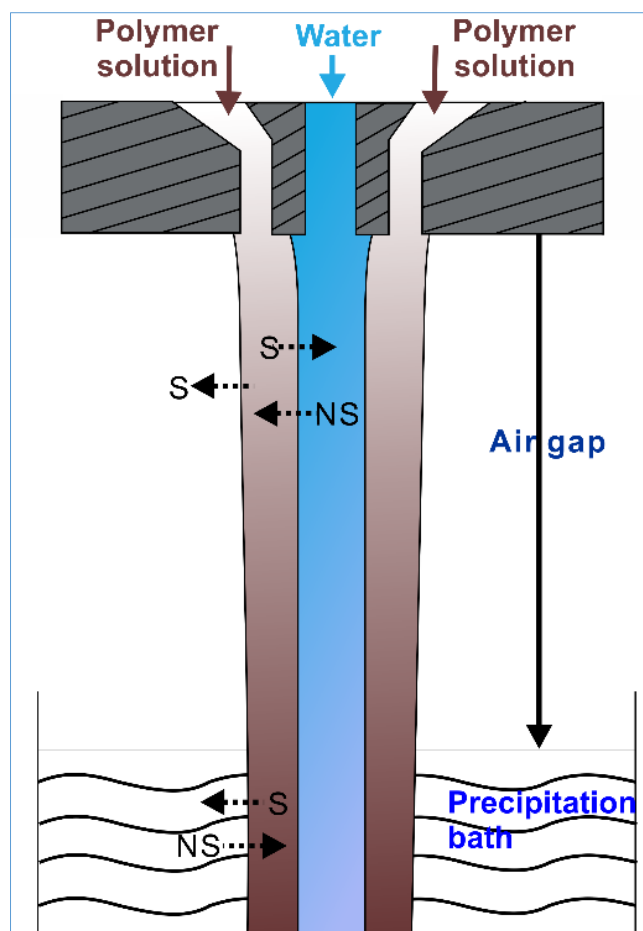


Figure 1.10. Schematic diagram of the dry-jet wet spinning process for preparation of PS-*b*-P4VP HFM. The polymer solution is extruded *via* a double orifice spinneret having non-solvent in the lumen side. After extrusion, the solvent(s) partially evaporates from the outer surface of the nascent HF causing a concentration gradient through the wall thickness of the fiber. The formation of HF is based on the non-solvent induced phase separation of polymer solution by rapidly exchanging the solvent with the non-solvent. Adapted with permission; © 2014 Elsevier Ltd.; license number: 4553090334996.¹⁷⁰

However, the fabrication of isoporous HFM by spinning the block copolymer solutions complicates the structure formation due to the narrow window of possible variations. The shear-induced free energy changes in the block copolymer microdomains during extrusion, controls the morphology and performance of the formed membranes.^{83, 170} For isoporous structure formation, the influencing parameters become more significant as the polymer solution should have a block copolymer of appropriate chemical composition and molecular weight to provide morphology of hexagonally-packed pores. Moreover, in HF spinning, the structure formation needs to take place in the air gap between the spinneret and the precipitation bath within 2 s; therefore, the composition of block copolymer solution (concentration, solvent(s) and additive(s)) is required to have enough segregation for instant evaporation-induced microphase sep-

aration. The other influencing factors are spinneret (design and dimensions), spinning parameters (air gap and flow rates of polymer solution and bore fluid), environmental conditions, *etc.*^{170, 203, 204} The schematic diagram in Figure 1.10 shows the fabrication method for the first outside-in isoporous HFM *via* dry-jet wet spinning process.

The outside-in isoporous HFM were studied to understand the influence of spinning parameters on isoporous structure formation and membrane morphology.¹⁷⁰ Subsequently, the catalytic activity was demonstrated by depositing gold nanoparticles on the outer fiber surface.²⁰⁵

Although the isoporous structure formation could be developed in flat sheet and HF membranes, the high cost of block copolymers increases the cost of integrally asymmetric isoporous membranes, which limits not only the upscaling but also the research in the field. In addition, the mechanical strength of free-standing block copolymer membranes is a challenge. Therefore, an alternative method for production of robust isoporous HFM with less consumption of block copolymer is required.

1.3.8. Fabrication of isoporous composite membranes

The alternative and desired methods for fabrication of isoporous membranes include the coating of a comparatively dilute block copolymer solution on an inexpensive, highly permeable and mechanically stable substrate membrane. The composite isoporous membranes are advantageous by providing lower consumption of block copolymer along with high mechanical strength from the robust support. The main requirement of the fabrication is a dilute block copolymer solution that is capable of providing self-assembled structures and a support membrane that is compatible to the block copolymer solution. The substrate membrane can be selected from a commercially available wide variety of polymeric or ceramic membranes in different geometries, thicknesses and characteristic properties as required. However, the selection of the dilute block copolymer solution becomes a challenge because the segregation of block segments, required for self-assembly, highly depends on the solvent selectivity.

A. Isoporous composite flat sheet membranes

a. Spray coating

The first work on isoporous composite membranes reported the use of highly diluted solutions in one solvent system for isoporous structure formation.¹⁴³ The membranes were fabricated *via* spray coating using a thin layer chromatography-fine-spray system or an airbrush system and a dip coating approach. Different dilute block copolymer solutions, 1 wt% solutions of PS-*b*-P4VP, poly(α -methylstyrene)-*b*-poly(4-vinylpyridine), or polystyrene-*b*-poly(*iso*-propylglycidyl methacrylate) in 1,4-dioxane (DOX), were spray-coated on various support materials. Yet, the major drawback of spray coating is the possibility to build up hazardous and/or explosive vapor during the coating process.

b. Dip coating

In the dip coating method, the block copolymer solutions were dip coated on a PVDF membrane using a casting machine.¹⁴³ By this, it was possible to fabricate a thin coated block copolymer layer of 11 μm . Furthermore, the membranes made by this method showed a more than 6-fold increase in water flux compared to conventional PS-*b*-P4VP membranes with similar pore sizes prepared by blade casting.

c. Roll-to-roll coating

Recently, preparation of isoporous composite flat sheet membranes has been reported by using a profile roller coating process for thin coating of dilute block copolymer solutions.²⁰⁶ The membranes were fabricated by coating a thin layer of 1 wt% PS-*b*-P4VP in DOX solution on top of a conventional PAN porous membrane. This upscalable roll to roll process offers the possibility to save >95% of block copolymer raw material as compared to the common doctor blade casting, by decreasing the block copolymer layer thickness to below 3 μm in combination with a highly open substructure.

B. Isoporous composite hollow fiber membranes

After the initial studies on outside-in block copolymer HFM, in order to enhance the mechanical strength of outside-in isoporous HFM, the idea of composite HFM fabrication came up,

which is possible in two ways either by spinning the dual-layer HFM or by coating the block copolymer solution on a robust HF substrate.

a. Dual-layer hollow fiber membranes by spinning

For fabrication of a dual-layer HFM, a triple layer spinneret is used for extrusion of two different polymer solutions. In this process, one solution is aimed to provide the selective layer (the outer most) and the other layer works as a strong support. *E.g.*, the coextrusion of the solutions of poly(ether sulfone) (PES) blended with partially sulfonated PES as the inner tube and PS-*b*-P4VP as the outer tube lead to a core-shell HFM. The fibers did not have any signs of delamination due to formation of H-bonds between the two layers. This procedure results in bendable dual layer isoporous HFM with a sufficient mechanical strength.²⁰⁷

The mechanical strength of fibers could be improved by coextrusion of the block copolymer solution providing isoporous outer surface and the second polymer solution forming the inner layer providing mechanical strength.²⁰⁷ However, the spinning process restricts the use of low polymer concentrations and big variations of spinning parameters.^{170, 208} Therefore, to reduce the high cost of block copolymers without compromising the mechanical strength of isoporous membranes, the composite membranes were prepared *via* coating.

b. Composite isoporous hollow fiber membranes by coating

The strategies to obtain isoporous HFM include spray coating and dip coating of commercially available fibers using low viscous block copolymer solutions. The spray coating method was discussed in a previous section.^{143, 209}

In the dip coating process for coating of the outer surface of HFM, first, the HFM are coated with the block copolymer solutions, and immersed in the water bath after providing a certain evaporation time. The first work on coating reported the use of a 18 wt% PS-*b*-P4VP polymer solution in DMF/THF 60/40 wt/wt on the outer surface of a PVDF HFM. However, the solution composition similar to the one commonly used for flat sheet casting provided a thick coating layer of ca. 40 μm . Recently, more works on outside-in isoporous composite HFM were reported. The use of solvent selectivity of DOX could provide isoporous structures for ca. 4 wt% of PI-*b*-PS-*b*-PDMA, PI-*b*-PS-*b*-PAA block copolymers. The functionality of the pore forming blocks could be used further to tailor the pore size.^{194, 210}

1.3.9. Characterization techniques to investigate self-assembly and membrane fabrication

In order to understand and control the structure formation in isoporous membranes, fundamental studies have mainly been focused on the effects of solvents and block copolymer concentration in the solutions using dynamic light scattering (DLS) and synchrotron SAXS. The flat sheet membrane fabrication can be studied by cryo-SAXS and -TEM to provide the visual impression of morphology at a certain time.^{118, 182, 186, 211-215} Furthermore, *in situ* SAXS and GISAXS experiments have been conducted to investigate the kinetics of structure formation of the as-cast films during isoporous flat sheet membrane fabrication for the commonly used viscous block copolymer solutions.^{147, 172, 200, 201}

The morphological investigations of membranes can be done by using optical and electron microscopy such as scanning electron microscopy (SEM), transmission electron microscopy (TEM) or atomic force microscopy. Especially SEM is also useful to study the cross sectional morphology of the membranes. These methods provide visual impressions of the final product. Further, the porosity, the pore size and the pore size distribution are commonly determined by analysis of the micrographs *via* integrating commercially available digital image processing softwares.²¹⁶ The image analysis was developed using various mathematical morphology algorithms to provide a complete pore size distribution curve for each sample. The programs determine the pore size by partitioning the images into black (dark grey/pores) and white (light grey/polymer) pixels. The software provides pore size distribution and the number of pores on the surface. With this information of number of pores in a measured area, the surface porosity can be calculated.

1.3.10. Performance characterization of isoporous membranes

The isoporous membranes are generally characterized by either checking the membrane morphology or by performance characterizations of the membranes. The isoporous membranes prepared *via* a SNIPS process provide the pore size largely in the range of ultrafiltration, ca. 15-70 nm. The pore size can be reduced by post-modifications on the membrane surface, which

can swell the chains of pore forming block. The isoporous membranes are commonly characterized by checking the water flux and performing retention tests. Since the pore forming block can have some pH sensitive functionality, the flux behavior of these membranes based on feed pH can also be a good tool to check the defect-free or uniform membrane fabrication, as the membrane would show zero flux for either low or high pH.

A. Water flux

As discussed in Section 1.2.5, the volumetric water flux (J_v) in pressure driven membrane processes is calculated as follows:

$$J_v = \frac{\Delta V}{A \cdot \Delta t \cdot \Delta p} \quad (3)$$

Where, ΔV is the volume of collected water between two mass measurements, A is the active surface area of the membrane, Δt is the time between two measurements, and Δp is the transmembrane pressure.

B. pH-responsive flux behavior

Most of the isoporous block copolymer membranes show strong stimuli (pH) response due to the pH responsive functionality of their pore forming block. *E.g.*, the isoporous membranes of PS-*b*-P4VP block copolymer show a sharp change of flux between pH 4 and 6. The fluxes at low pH (below 4) are very small. The pyridine groups at the membrane surface and pore walls were protonated at low pH, and the P4VP segments stretched to minimize charge repulsion, transforming the pores into pH-sensitive gates. Similar, influence is seen in other block copolymer membranes having P4VP as a pore forming block such as PI-*b*-PS-*b*-P4VP and PS-*b*-P4VP-*b*-PPS.^{143, 190, 193} The water flux values are a consequence of the exceptional porosity and the small thickness of the top separation layer. The PI-*b*-PS-*b*-PDMA block polymer membranes do not show any pH-response. However, the corresponding hydrolyzed derivative PI-*b*-PS-*b*-PAA material shows opposite pH-behaviour compared to PI-*b*-PS-*b*-P4VP.¹⁹⁴

C. Retention ($R\%$)

Molecular weight cut-off (MWCO) is a method of characterization used in filtration to describe pore size distribution and retention capabilities of a membrane. It is defined as the lowest molecular weight (in Daltons) of the solute with 90% rejection by the membrane. Polydextran, PEG and proteins of various molecular weights are commonly used to rate the MWCO of membranes having a pore size in the range of ultrafiltration.

The retention values are calculated as follows:

$$R\% = \left(1 - \frac{C_p}{C_f}\right) \times 100\% \quad (6)$$

Where, C_p and C_f are concentrations of solute in permeate and feed, respectively. These concentrations are measured by gel permeation chromatography (GPC).

When choosing the appropriate molecular weight cut-off for specific applications, several factors must be considered. These include sample concentration, composition, molecular shape, and operating conditions such as temperature, pressure, and feed hydrodynamics. Other variables regarding the flow of molecule passage must also be considered, *e.g.*, linear molecules, high transmembrane pressure and low sample concentration can increase molecule passage, while low temperature and membrane fouling can hinder the molecules to pass through.

2. Aim of the work

2.1. Strategy of the research

A typical ultrafiltration membrane has a pore size range of 0.005-0.1 μm , and a molecular weight cut-off range of 1-500 kDa. The membranes are easily manufactured on large scale through different methods such as phase inversion by temperature or immersion, bi-axial stretching or chemical etching. However, a well-defined regular pore structure of uniform nanometer-sized pores is difficult to achieve in these membranes. Since the main criteria of evaluation of membrane-based separation is subject to permeability-selectivity trade-offs that decide its overall worth, high number of uniform pores is the main requirement. In order to achieve high selectivity, pores on the membrane need to be relatively smaller than the particles in the mixture, and screening of these particles from surface is also preferred to reduce fouling of membranes and to maintain hygiene. While it is hard to achieve a perfection on the surface on the nanoscale with high surface porosity *via* commonly used polymers and membrane fabrication techniques, block copolymers make it possible.

This thesis reports the fabrication of isoporous membranes using block copolymers, a type of synthetic polymer membranes for liquid separation applications. The integral asymmetric isoporous membranes providing high surface porosity along with a narrow pore size distribution as a thin selective top layer, which is supported by a more open porous asymmetric structure, promise to become the prime of ultrafiltration membranes.^{87, 110, 168, 217, 218} Such block copolymer based membranes offer attractive features like tailorable pore size on the size-scale of tens of nanometer^{118, 173}, high surface porosity¹⁶⁹, sharp molecular weight cut-off¹⁷¹, thermo-responsivity^{219, 220}, pH-responsivity^{183, 190, 219}, catalytic activity²⁰⁵, and thermal stability²²¹.

Moreover, for large installations, HFM hold a prospective to be applicable in a wide area of applications due to their self-supporting geometry and higher active surface area per unit volume.^{6, 77, 222} Furthermore, the inside-out HFM offers protection of the selective inner skin along with energy-efficient purifications with well-controlled flow hydrodynamics during cross-flow

in the lumen side, where the small sweeping friction of the inlet fluid flowing across the membrane surface limits the build-up of cake layers. Easier back-flushing and cleaning thereby minimize membrane fouling, and maximize process flux and product yield.^{7, 223} Therefore, the objective of this work is to understand the self-assembly of block copolymers from solutions to flat sheet and HF membranes. Further, this knowledge is applied to develop the isoporous structure on the lumen of HFM for fabrication of technologically-relevant inside-out HFM configuration that could be potentially characterized for preliminary small-scale separations. The isoporous structure on the inner skin of the HFM is envisioned to attain specific retention conditions together with the advantages of inside-out HFM. This will give rise to various opportunities for the use of these membranes from a common need of purification of water to the solitary need of hemodialysis.^{13, 15, 168, 224, 225}

In addition, an aim is to understand the molecular self-assembly and to explore the potential applications, which motivates the studies including those on macromolecular self-assembly principles, theories, structures and properties of the assemblies, fabrication methods, *etc.*

“Research is formalized curiosity. It is poking and prying with a purpose.”

-Zora Neale Hurston

2.2. Outline of thesis

This thesis summarizes different studies to understand the structure formation in isoporous HFM, which includes the study of self-assembly from block copolymer solutions to flat sheet membranes and to HFM, in chapters 3-7. Chapters 3-6 have been completed and major parts of these sections have been published in three international peer-reviewed scientific journals. For the sake of correlation of the works and easy understandability, these sections are made distinct. The major projects are schematically pictured in Figure 2.1, highlighting their topical areas as well as the links between them.

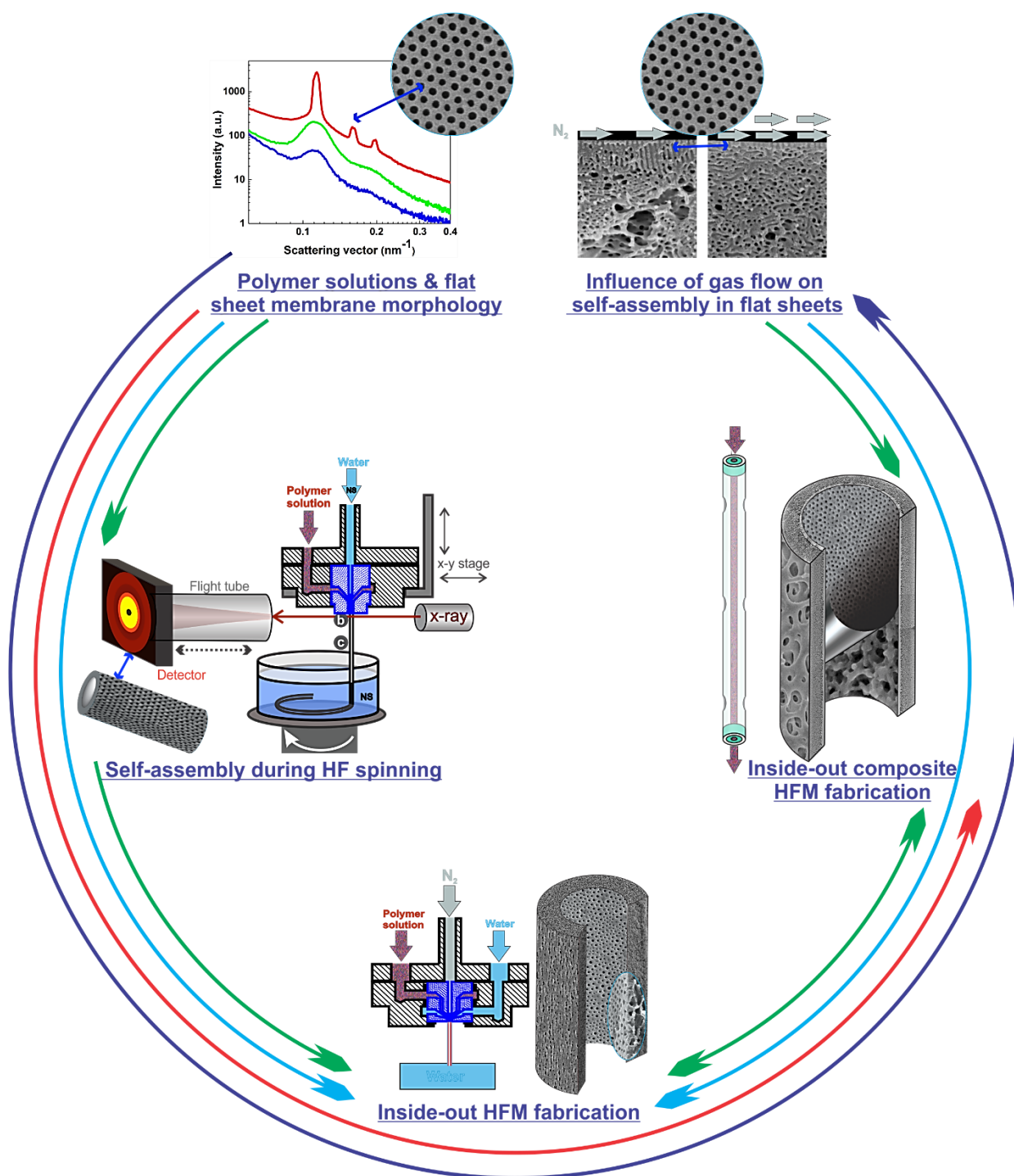


Figure 2.1. The schematically pictured outline of the thesis, highlighting the topical areas as well as the links between them.

The first project, outlined in Chapter 3, aims at the influences and benefits of additive MgAc_2 in the casting solution. In this, the pristine and MgAc_2 containing block copolymer solutions are characterized by SAXS. This work represents the influence of MgAc_2 on block copolymer self-assembly in solution. The influence of solution characteristics was studied in isoporous flat sheet membranes. The study forms the basis for the Chapter 4 of this thesis; the solutions are used for HF spinning experiments. This study also unveils the influence of only 0.04 wt% MgAc_2 on the domain spacing in dilute block copolymer solutions having 4 wt% block copolymer, which forms the basis for the Chapter 5; the solution is used for coating experiments. The work using MgAc_2 is an advancement from a previous study, where MgAc_2 was added in block copolymer solutions for isoporous flat sheet membrane fabrication.

The second project provides the first demonstration of *in situ* SAXS studies on the structure formation in outside-in isoporous HFM and both the ordered and disordered block copolymer solutions were probed *in situ*. In this work, which is summarized in Chapter 4, a comparative study is reported about the influence of shear during and after extrusion on the block copolymer microdomains for different spinning parameters and block copolymer solutions. SAXS studies were correlated with the HFM morphology as investigated by SEM.

The third project, presented in Chapter 5, introduces the idea of controlled evaporation using gas-flow and provides the first demonstration about the possibility to achieve self-assembled structures in compact geometries such as a HF membrane. This work reveals the integrally asymmetric inside-out isoporous HFM prepared using the dry-jet wet spinning technique. The inside-out configuration of membranes is technologically favored by providing good control on flow hydrodynamics and has been a long-standing goal in membrane technology.

The fourth project introduces the second finding of this dissertation that is fabrication of evaporation-induced self-assembled structures in already available compact geometries, such as a HF membrane. In this work, dilute block copolymer solutions were used to develop isoporous structures in highly permeable robust PES HFM with an inner diameter of approximately 1 mm. The requirement of a comparatively less concentrated block copolymer solution to pass through the compact geometries significantly reduces the stimulations required for self-assembly. The high polymer relaxation rates and decreased thermodynamic driving forces, as well as high capillary suction of dilute solutions in the porous substrates complicates the block copolymer self-assembly and fabrication of uniform coated layer, respectively. The isoporous structures are developed on top of $\leq 10 \mu\text{m}$ thin coated layer.

A major part of the work has been focused on the understanding of gas-flow induced controlled isoporous structure formation for the development of evaporation-induced self-assembled structures on the inner side of compact geometries. However, the effect of the gas flow rate on self-assembly is hard to understand explicitly due to many influencing parameters during the extrusion and coating processes. So, the fifth project is designed to check the influence of controlled evaporation using a gas flow in flat sheet membranes. For this, a set-up was designed to conduct the experiments that is detailed in Section 7.1. The discussion reported in this part helps in understanding the control over the kinetics of microphase separation or evaporation-induced self-assembly.

Finally, Chapter 8 concludes the highlights of all the works and gives the perspectives for the future. The additional information regarding experiments and experimental set-ups are provided in Chapter 9.

3. Influence of additive in block copolymer solution and on structure formation in flat sheet membranes

This chapter reports the characterization of block copolymers in bulk by SAXS and TEM, block copolymer solutions by SAXS, and the flat sheet membranes cast using the block copolymer solutions by SEM investigations. The aim of this work is to study the key characteristics of the block copolymer solutions prior to applying them in complicated systems of HFM fabrications. First, the highly concentrated and viscous block copolymer solutions were selected with and without additive MgAc₂ for HF spinning. The influence of solution characteristics obtained by SAXS is checked in flat sheet membranes by doing morphological characterizations. The SEM micrographs were analyzed to measure the obtained structural features. Second, the influence of additive MgAc₂ in the dilute solutions is discussed, which is aimed to understand the influence of the structure of the solution for fabrication of inside-out isoporous composite HFM via coating.

Adapted from the following research article with permission from The Royal Society of Chemistry:
“Self-Assembly of Block Copolymers during Hollow Fiber Spinning: An *In Situ* Small-Angle X-Ray Scattering Study” Kirti Sankhala, D. C. Florian Wieland, Joachim Koll, Maryam Radjabian, Clarissa Abetz, Volker Abetz, *Nanoscale*, 2019, DOI: 10.1039/C8NR06892E
(<https://pubs.rsc.org/en/Content/ArticleLanding/2019/NR/C8NR06892E#!divAbstract>)

In membrane fabrication, the self-assembly of macromolecules into well-arranged uniform pores is subject to the segregation strength of the block segments in the block copolymer solution. Therefore, in order to identify appropriate solution conditions required for steady HF spinning and the periodic nanostructure formation, the composition and molecular weight of the block copolymer and the solution compositions were kept similar to previously reported works on flat sheets and HFM.^{170,203} As discussed in Section 1.3, the segmental incompatibility of blocks is significantly tunable by varying the polymer solution due to the different solvent selectivity of the blocks of the block copolymer.^{110, 186} The kinetics of macromolecules for microphase separation and macrophase separation can be varied by incorporating the additives selective for the pore forming block. *E.g.*, the addition of carbohydrates or metal salts can influence the self-organization of PS-*b*-P4VP block copolymer due to their known interaction with the pyridine blocks. A similar influence can be achieved by adding other metal salts like copper(II), nickel(II), cobalt(II), iron(II), cadmium(II) *etc.*^{102, 167, 188-190} However, the transition metal salts are not appropriate additives for the aimed applications of these membranes due to their often toxic nature. The additives allow to reduce the block copolymer concentration required for the onset of microphase separation, which is of great economical interest for cost reduction and resources preserving applications. In addition, the membranes prepared by using highly concentrated polymer solutions tend to form compact structures and result in lesser permeability.¹⁷¹

The influence of MgAc₂ on the pore formation has been discussed previously in PS-*b*-P4VP flat sheet membranes. The addition of MgAc₂ is known to provide isoporous surface with comparatively lesser block copolymer concentration in the casting solution. This becomes even more beneficial in HFM fabrication because of the requirement of high amount of expensive block copolymer. However, such solutions had not been studied for HFM fabrication because both the micellation and the SNIPS process are highly sensitive to even marginal changes of system parameters. Therefore, in this study, MgAc₂ was added to the block copolymer solutions to actuate the self-assembly already at lower polymer concentrations due to the known complexation of Mg cations with the pyridine moieties. Since the aim has been facilitation of the isoporous structure formation for membrane fabrication, MgAc₂ concentrations were chosen in the range that were known to provide the desired integral asymmetric isoporous membranes.¹⁸⁹ In order to reduce the number of influencing factors, the concentration of additive MgAc₂ and block copolymer were varied while the solvent compositions were kept constant in

the polymer solution, as the aimed study of HF spinning is influenced by many more parameters as compared to flat sheet membrane casting.

3.1. Preparation of bulk films and their characterization

The PS-*b*-P4VP diblock copolymers used in this work were synthesized *via* sequential anionic polymerization following a protocol reported before (see Section 9.1 for more details).¹⁶⁹ For the investigation of the bulk morphology of the PS-*b*-P4VP diblock copolymers, films were prepared from block copolymer solution in chloroform. The sections from the same films were used for characterization by SAXS and TEM. The details of selected block copolymers and their bulk characterization are given in Table 3.1. SAXS experiments on the equilibrated films were performed on a Bruker Nanostar, Karlsruhe, Germany. From the SAXS curves shown in Figure 3.1 a, the domain spacing (d_{bulk}) determined from the scattering vector q^* corresponding to the primary peak is 36.5 ± 0.6 nm in PS-*b*-P4VP₁₈¹⁵⁰ and 41.2 ± 0.6 nm in PS-*b*-P4VP₁₉¹⁷⁰ (Table 3.1).

Table 3.1. Details of PS-*b*-P4VP block copolymers and their bulk characterization. For PS-*b*-P4VP_{*a*^{*b*}}, *a* denotes the amount of P4VP block in wt% and *b* denotes M_n , where M_n is number averaged molecular weight in kg mol⁻¹. \mathcal{D} is dispersity of the respective block copolymer. q_{bulk}^* is the scattering vector corresponding to the primary peak and $d_{bulk} = 2\pi/q_{bulk}^*$ is the characteristic length or domain spacing of the bulk block copolymer film. All q^* and d have an error bar of ± 0.002 nm⁻¹ and ± 0.6 nm, respectively.

Block copolymer	M_n (kg mol ⁻¹)	PS (wt%)	P4VP (wt%)	\mathcal{D}	q_{bulk}^* (nm ⁻¹)	d_{bulk} (nm)
PS- <i>b</i> -P4VP ₁₈ ¹⁵⁰	150	82	18	1.04	0.172	36.5
PS- <i>b</i> -P4VP ₁₉ ¹⁷⁰	170	81	19	1.07	0.152	41.2

In addition, TEM was employed to obtain a direct visualization of the bulk morphology and thereby provide insights regarding the spheres. The values of average center-to-center distance between spherical domains were checked manually using DigitalMicrograph (Gatan Microscopy Suite Software, Gatan GmbH, München, Germany), which is 39 ± 6 nm in PS-*b*-P4VP₁₈¹⁵⁰ and 44 ± 8 nm in PS-*b*-P4VP₁₉¹⁷⁰, measured from Figures 3.1 b and c, respectively. These values are in agreement with the d_{bulk} measured from SAXS. It is worth noting here that the preparation artifacts during sample preparation for TEM might lead to stretching or compression in different directions. In case of SAXS characterization, the average of scattering

from the full film is in one direction. In addition, the X-ray beam has a diameter of 350 μm that makes the probed sample quite large for SAXS as compared to the sample investigated by TEM.

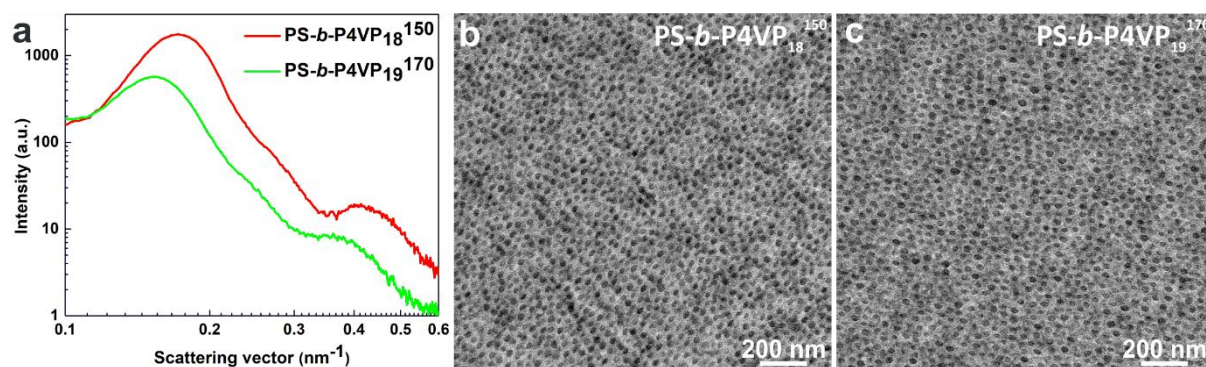


Figure 3.1. Bulk characterizations of PS-*b*-P4VP diblock copolymers. (a) SAXS curves, the curves are plotted in log-log scale and Y-offset is adjusted for better visibility. (b,c) TEM micrographs of the bulk films as described in the text.

3.2. Weakly segregated block copolymer solutions and flat sheet membrane fabrication

The solutions were prepared by stirring a specific concentration of block copolymer in a mixture of DMF/THF in equal weight ratio (wt/wt); all measurements were done in wt%. Prior to the SAXS experiments, the solutions were optimized by checking the structure formation in flat sheet membranes. The optimized concentration for selected block copolymers PS-*b*-P4VP₁₈¹⁵⁰ and PS-*b*-P4VP₁₉¹⁷⁰ were found to be 26 wt% and 25 wt% in the solvents DMF/THF 50/50 (wt/wt), respectively (Figure 3.2). The SAXS patterns of the bulk solutions show a single broad peak resembling a weakly segregated solution where the copolymers are associated in micellar aggregates (Figure 3.2 a).

Table 3.2. List of weakly segregated pristine PS-*b*-P4VP block copolymer solutions. All q^* and d have an error bar of $\pm 0.001 \text{ nm}^{-1}$ and $\pm 0.4 \text{ nm}$, respectively.

Block copolymer	Polymer solution (in DMF/THF 50/50 (wt/wt))	q^* (nm^{-1})	d (nm)
PS- <i>b</i> -P4VP ₁₈ ¹⁵⁰	26 wt% PS- <i>b</i> -P4VP ₁₈ ¹⁵⁰	0.147	42.7
PS- <i>b</i> -P4VP ₁₉ ¹⁷⁰	25 wt% PS- <i>b</i> -P4VP ₁₉ ¹⁷⁰	0.120	52.4

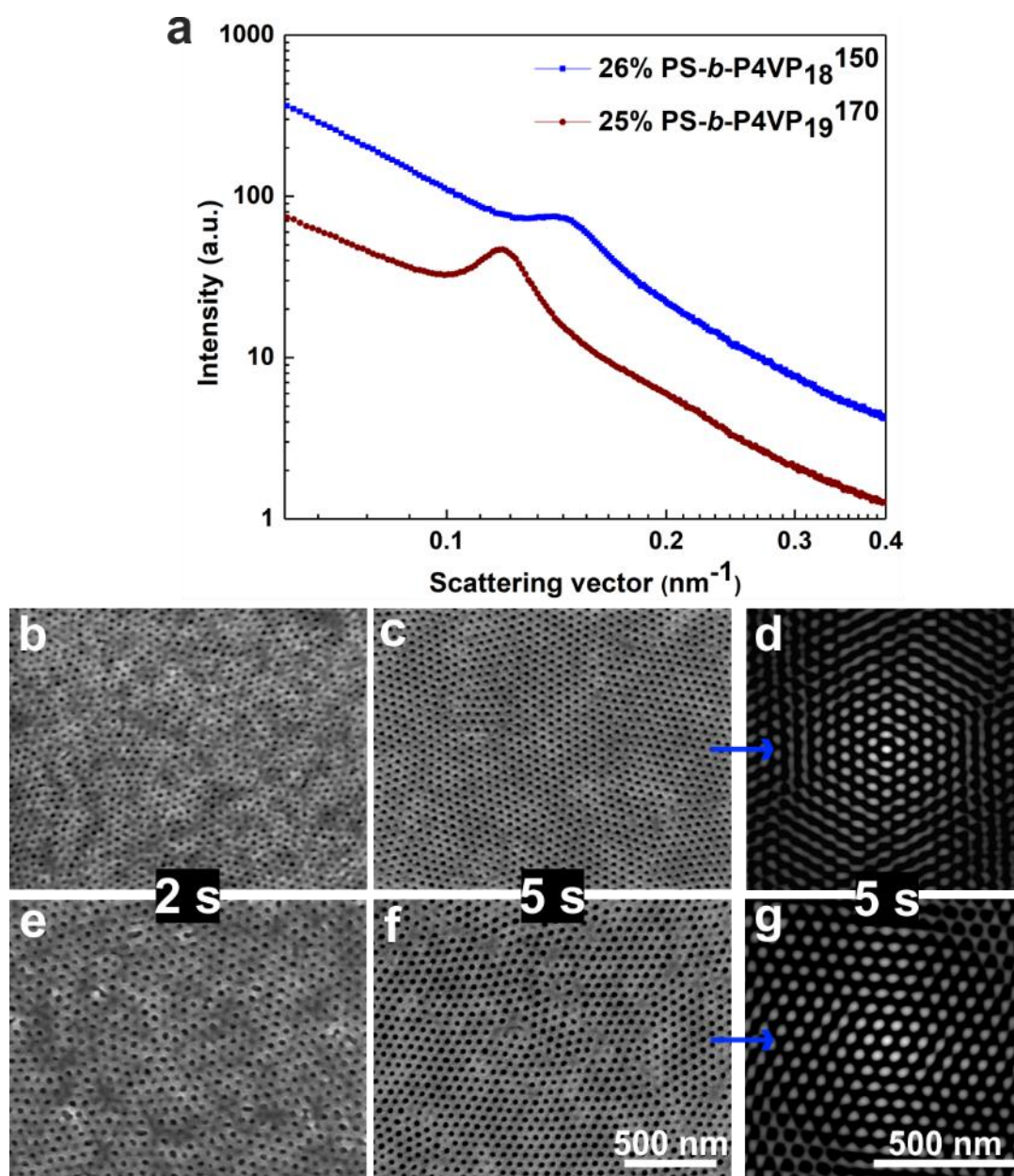


Figure 3.2. SAXS of weakly segregated casting solutions and SEM micrographs of fabricated membranes. (a) The SAXS curves of solutions, which are adjusted vertically for clarity. (b,c,e,f) SEM micrographs of the top surface of blade-cast membranes from the weakly segregated solutions 26 wt% PS-*b*-P4VP₁₈¹⁵⁰ (b, c) and 25 wt% PS-*b*-P4VP₁₉¹⁷⁰ (e, f) in DMF/THF 50/50 (wt/wt); evaporation times were 2 s (b, e) and 5 s (c, f). (d, g) The micrographs show autocorrelated patterns of SEM micrographs c and f. The micrographs b, c, e have the same scale bar as f and d has the same scale bar as g.

To obtain the average pore diameter (D_p) and the average center-to-center distance between pores (d_{c-c}), the SEM micrographs were analyzed by analySIS, named as ‘Analysis 1’. In this, d_{c-c} is an average of distances to next neighboring pore. The SEM micrographs were also analyzed by DigitalMicrograph by performing an autocorrelation analysis on the pore distribution and named as ‘Analysis 2’. This provides a visual impression of average periodic arrangements

of pores with information about D_p and d_{c-c} . In Analysis 2, D_p is calculated by the diameter of the central bright spot and d_{c-c} is calculated by taking the average of distances between the central bright spot to all nearest bright spots (located in first ring).

Table 3.3. Analysis of SEM micrographs. *Analysis 1* is done by analysisSIS and *Analysis 2* is done using DigitalMicrograph by performing autocorrelation. D_p is average pore diameter and d_{c-c} is average center-to-center distance between pores (Figures 3.2 b, c, e and f).

Polymer solution (in DMF/THF 50/50 (wt/wt))	Evaporation time and the re- spective SEM micrograph	<i>Analysis 1</i>		<i>Analysis 2</i>	
		D_p (nm)	d_{c-c} (nm)	D_p (nm)	d_{c-c} (nm)
26 wt% PS- <i>b</i> -P4VP ₁₈ ¹⁵⁰	2 s (Figure 3.2 b)	12 ± 3	47 ± 4	27	48
26 wt% PS- <i>b</i> -P4VP ₁₈ ¹⁵⁰	5 s (Figure 3.2 c)	19 ± 3	47 ± 2	21	48
25 wt% PS- <i>b</i> -P4VP ₁₉ ¹⁷⁰	2 s (Figure 3.2 e)	16 ± 5	58 ± 5	30	59
25 wt% PS- <i>b</i> -P4VP ₁₉ ¹⁷⁰	5 s (Figure 3.2 f)	25 ± 3	55 ± 2	24	53

The increase in segregation with increase in concentration due to evaporation time leads to the formation of more open pores and reduces the d_{c-c} , as detailed in Table 3.3. The morphology of the top surface of flat sheet membranes cast from these solutions for evaporation time 2 and 5 s are shown in Figure 3.2. The SEM micrographs in Figures 3.2 c and f show the hexagonal arrangements of pores by performing the autocorrelation on the SEM micrographs (Figures 3.2 d and g). For polymer solution 26 wt% PS-*b*-P4VP₁₈¹⁵⁰ in DMF/THF 50/50 (wt/wt) and the evaporation time 2 s, approx. D_p and d_{c-c} are 12 ± 3 nm and 47 ± 4 nm (Figure 3.2 b), which varies to 19 ± 3 nm and 47 ± 2 nm, respectively for longer evaporation times of 5 s (Figure 3.2 c). Similarly, for polymer solution 25 wt% PS-*b*-P4VP₁₉¹⁷⁰ in DMF/THF 50/50 (wt/wt), here D_p and d_{c-c} values change from 16 ± 5 nm and 58 ± 5 nm (Figure 3.2 e) to 25 ± 3 nm and 55 ± 2 nm (Figure 3.2 f), as the evaporation time is prolonged from 2 s to 5 s. The autocorrelation analysis on the pore distribution in SEM micrographs can be seen in Table 3.3.

3.3. Ordered block copolymer solutions and flat sheet membrane fabrication

With an increase of the PS-*b*-P4VP₁₉¹⁷⁰ block copolymer concentration from 25 wt% to 28 wt%, the macromolecules self-assemble, which leads to the formation of an ordered phase by

spontaneous packing of micelles into a periodic lattice (Figure 3.3). Due to the increased segregation, the domain spacing increases from 52.4 ± 0.4 nm to 53.7 ± 0.4 nm. As shown in Figure 3.3 and Table 3.4, the primary peak with two clear higher-order peaks correspond to the peak positions $(q/q^*)^2 = 1, 2$ and 3 , which indicate a well-developed body centered cubic (bcc) structure. We note that this data is normally not sufficient to rule out simple cubic packing, but based on experimental and theoretical results, bcc is almost undoubtedly the actual symmetry.¹⁸⁶ This structural transition in solutions from a disordered micellar liquid phase (25 wt%) to an ordered micellar or crystalline phase (28 wt%) is possible by crossing the narrow window of the block copolymer concentration, and can be considered as a reversible disorder-order transition (DOT) in solution. A similar reversible disorder-order transition in solution was observed previously for a 2D hexagonally-packed cylindrical (hcp) structure.²¹¹ This difference of structure in solutions might be a result of different block copolymer and solution compositions.

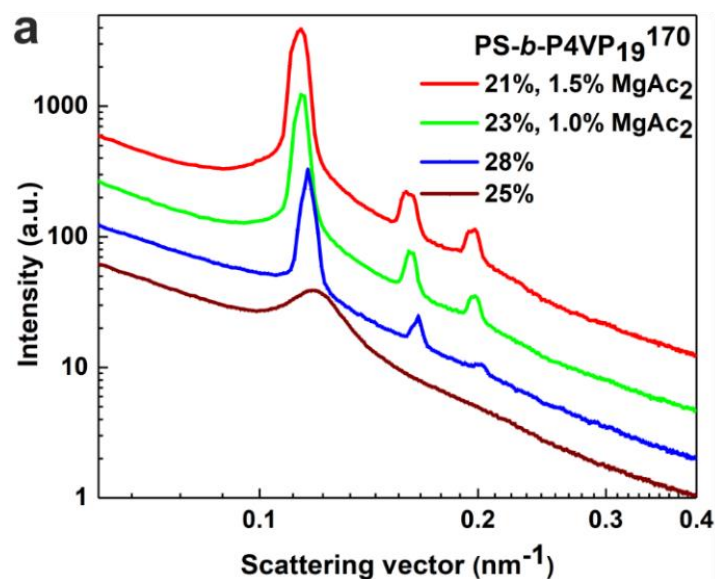


Figure 3.3. SAXS of ordered casting solutions. The SAXS curves of each solution is adjusted vertically for clarity.

Table 3.4. Details of SAXS curves of PS-*b*-P4VP₁₉¹⁷⁰ block copolymer solutions (Figure 3.3). All q^* and d have an error bar of ± 0.001 nm⁻¹ and ± 0.4 nm, respectively.

Polymer solution	Scattering vector q (nm ⁻¹)			$(q/q^*)^2$			d (nm)
	1 st (q^*)	2 nd	3 rd	1 st	2 nd	3 rd	1 st
21%, 1.5% MgAc ₂	0.114	0.161	0.198	1	1.9967	3.0042	55.1
23%, 1.0% MgAc ₂	0.114	0.162	0.198	1	2.0054	2.9997	55.1

28%	0.117	0.166	0.202	1	2.0063	2.9946	53.7
25%	0.120			1			52.4

As discussed before, in PS-*b*-P4VP block copolymers, the coordination ability of nitrogen atoms on P4VP blocks can be utilized to facilitate the structure formation using additives.^{188, 190} The addition of metal salts (here MgAc₂) tend to form cation-pyridine complexes which significantly decreases the concentration corresponding to the onset of microphase separation.¹⁸⁹ It was reported that by adding MgAc₂ in the concentration range of 0.10–0.30 wt% to the polymer solutions, no increase in viscosity was observed because it forms weaker complexes with the pyridine moieties as compared to the transition metal ions. Upon addition of 2 wt% MgAc₂, the solution viscosity appears to increase dramatically reaching values three to six times higher than the analogous solutions without MgAc₂.¹⁸⁹ For this reason, it was considered essential to increase the amount of MgAc₂ added into the viscous solution above 1 wt% and up to 2 wt%.

Interestingly, the SAXS curves in Figure 3.3 show that with addition of MgAc₂, the ordered micellar structure can be observed at comparatively low concentrations due to the selectivity of MgAc₂ to one particular block (P4VP) which increases segmental incompatibility. Such an ordered phase is observed for the first time for a diblock copolymer solution with MgAc₂ as additive. As shown in Figure 3.3 and Table 3.4, the addition of 1.0 wt% MgAc₂ in conjunction with a decreased polymer concentration of 23 wt% of PS-*b*-P4VP₁₉¹⁷⁰ leads to the formation of a lyotropic liquid crystalline phase in form of a bcc structure with a domain spacing of 55.1 ± 0.4 nm. A further increase in concentration of MgAc₂ to 1.5 wt% and a further decrease of the block copolymer amount to 21 wt% of PS-*b*-P4VP₁₉¹⁷⁰ shows a similar peak height due to more prominent micelles, with equal domain spacing 55.1 ± 0.4 nm. It also seems that under these conditions two different bcc phases are present as the scattering curves indicate a peak splitting for the higher order peaks. Moreover, the ordered solution with 1.5 wt% MgAc₂ of comparatively very low block copolymer concentration of 21 wt% shows a larger domain spacing and peak heights as compared to the solution with 28 wt% block copolymer concentration. This small increase in characteristic length points toward an increase in the volume of pore forming P4VP microdomains because the selective incorporation of MgAc₂ leads to a stronger segregation as compared to highly concentrated neat solutions.

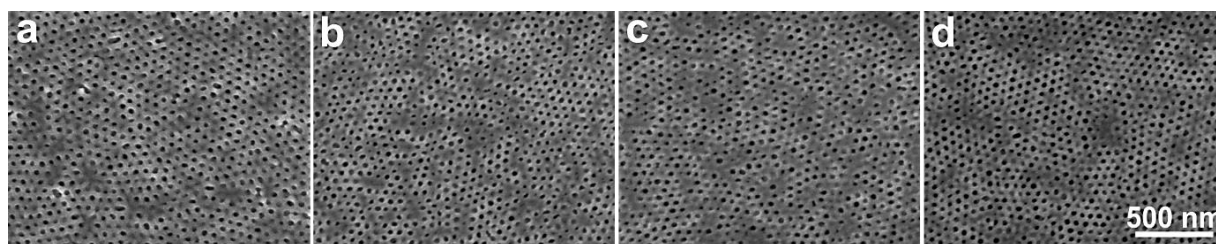


Figure 3.4. Membrane fabrication. SEM micrographs of the top surface of blade-cast membranes from the PS-*b*-P4VP₁₉¹⁷⁰ solutions having different polymer concentration (and additive) in DMF/THF 50/50 (wt/wt) and evaporation time 2 s: (a) 25 wt%; (b) 28 wt%; (c) 23 wt%, 1.0 wt% MgAc₂; (d) 21 wt%, 1.5 wt% MgAc₂.

The SEM micrographs in Figure 3.4 show the possibility to achieve hexagonally-packed pores on top of flat sheet membranes for very short evaporation times using both disordered micellar (25 wt% PS-*b*-P4VP₁₉¹⁷⁰) and ordered solutions (28 wt% PS-*b*-P4VP₁₉¹⁷⁰, 23 wt% PS-*b*-P4VP₁₉¹⁷⁰ and 1.0 wt% MgAc₂, and 21 wt% PS-*b*-P4VP₁₉¹⁷⁰ and 1.5 wt% MgAc₂). To compare the structure formation occurring at short solvent evaporation times, which would be similar to the HF spinning, the structure of the as-cast membranes were quenched by immersing them into the precipitation bath after 2 s. Since the microphase separation progresses very quickly, the morphology representing the manually hand-cast membranes for evaporation time 2 s can be significantly affected by manual inaccuracies.

Table 3.5. Analysis of SEM micrographs. *Analysis 1* is done by analySIS and *Analysis 2* is done using DigitalMicrograph by performing autocorrelation. D_p is average pore diameter and d_{c-c} is average center-to-center distance between pores for the membranes cast for 2 s evaporation time (Figure 3.4).

Polymer solution (PS- <i>b</i> -P4VP ₁₉ ¹⁷⁰ in DMF/THF 50/50 (wt/wt))	Evaporation time and the SEM micrograph	<i>Analysis 1</i>		<i>Analysis 2</i>	
		D_p (nm)	d_{c-c} (nm)	D_p (nm)	d_{c-c} (nm)
25 wt%	2 s (Figure 3.4 a)	16 ± 5	58 ± 5	30	59
28 wt%	2 s (Figure 3.4 b)	18 ± 5	54 ± 5	29	55
23 wt% and 1.0 wt% MgAc ₂	2 s (Figure 3.4 c)	25 ± 8	52 ± 5	33.5	57.8
21 wt% and 1.5 wt% MgAc ₂	2 s (Figure 3.4 d)	18 ± 6	55 ± 4	31.8	55.5

The approx. values of D_p and d_{c-c} of these membranes are given in Table 3.5, by analyzing the SEM micrographs in Figure 3.4. Since the degree of segregation is strong in the bulk state due to the high χ between PS and P4VP, the ordered structures can form quickly *via* both a disorder-order transition and an order-order transition.^{146, 186, 211, 226} The disorder-order transition is defined as the transition where long-range order appears and distinct arranged micelles can be discerned from a disordered casting solution experimentally, while the order-order transition

occurs from a bcc lattice in the casting solution to the hexagonal close packed open pores in the membrane. Radjabian *et al.* reported similar disorder-order and order-order transitions for PS-*b*-P4VP diblock copolymer solutions in DMF/THF 50/50 (wt/wt) and DOX, respectively.¹⁸⁶ A similar order-order transition was also reported by Gu *et al.* and Zhang *et al.* for PI-*b*-PS-*b*-P4VP and PS-*b*-P4VP-*b*-PPS triblock terpolymers, respectively, in the solvent(s) selective for the matrix forming or major blocks (PS), such as DOX and THF.^{201, 226}

3.4. Addition of MgAc₂ in dilute block copolymer solutions

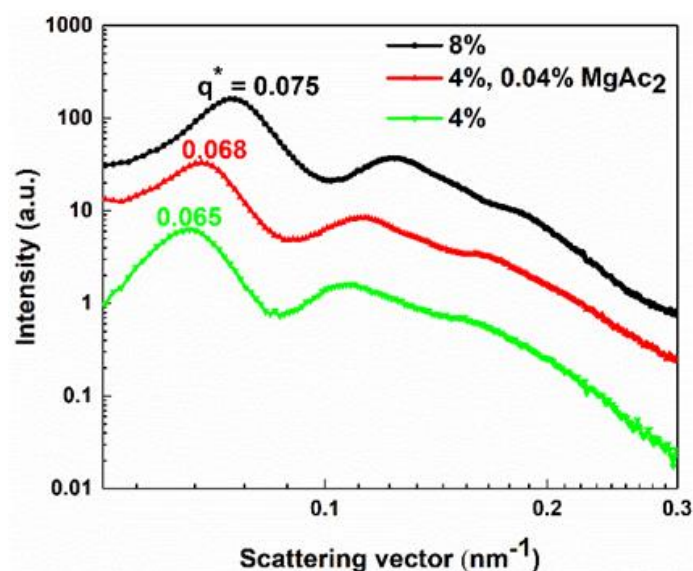


Figure 3.5. SAXS patterns of polymer solutions having 4 wt% and 8 wt% PS-*b*-P4VP₁₇¹⁶⁸ block copolymer (one with 0.04% MgAc₂) in DOX. The curves are plotted in log/log scale and the y-offset is adjusted for better visibility.

The influence of additive MgAc₂ in dilute solution is significantly different as compared to the addition in viscous solutions. As shown in Figure 3.5, in contrast to the influence of MgAc₂ observed in Section 3.3, the addition of 0.04 wt% MgAc₂ in DOX solution having 4 wt% PS-*b*-P4VP₁₇¹⁶⁸ block copolymer shows a decrease in domain spacing. In addition, an increase in polymer concentration also shows a decrease in domain spacing. A similar influence of compaction of the structures upon addition of 0.15 wt% metal salt (copper(II) chloride, CuCl₂) in solution of PS-*b*-P4VP₂₅¹⁰⁰ block copolymer in DMF/THF 30/70 (wt/wt) was also observed by Stegelmeier *et al.*¹⁷² The possible reason might be that Cu²⁺ is more electronegative than Mg²⁺. Furthermore, the cation-pyridine complexation changes the solubility of the pore forming

P4VP block in the solvent(s), mainly DMF, which decides whether a swelling or shrinkage of the micelle occurs.

In case of the solutions having 21 wt% PS-*b*-P4VP₁₉¹⁷⁰ and 1.5 wt% MgAc₂ and 23 wt% PS-*b*-P4VP₁₉¹⁷⁰ and 1.0 wt% MgAc₂, we used DMF in 50% (wt%) which is high enough for dissolving the 19 wt% P4VP segments in block copolymer. Probably, the P4VP blocks are extended due to the swelling and this facilitates the cation-complexation, which minimizes unfavorable contacts between PS and P4VP and therefore minimizes the overall enthalpic interaction. The χ parameter is effectively increased and also the size of the micelles increases, which moves the order-disorder transition farther (more discussion in the next section, in study of HFM fabrication). Therefore, in a solvent system which is more selective for the matrix forming block (*e.g.*, THF and DOX), the domain spacing might decrease with increase in viscosity of the solution due to compaction of the core, which can be expected to be even higher for more electronegative additives. A similar influence of solvent selectivity on domain spacing has been reported before.¹⁸⁶ Therefore, the characteristics of the domain spacing completely depends on the particular block copolymer solution.

3.5. Conclusion

The addition of MgAc₂ leads to an ordering in block copolymer solutions already at lower polymer concentrations as compared to the pristine block copolymer solutions. It is found that both the weakly segregated and the ordered solutions can provide isoporous structures. Two disordered block copolymer solutions (25 wt% PS-*b*-P4VP₁₉¹⁷⁰ and 26 wt% PS-*b*-P4VP₁₈¹⁵⁰ in DMF/THF 50/50 (wt/wt)) are selected to study the influence of shear-induced extrusion on the block copolymer solution characteristics and on the structure formation after leaving the spinneret during HF spinning. Also, the ordered solutions with additive MgAc₂ at comparatively lower polymer concentration (23 and 21 wt% of PS-*b*-P4VP₁₉¹⁷⁰ with 1.0 and 1.5 wt% of MgAc₂, respectively, in DMF/THF 50/50 (wt/wt)) are selected for HF study as it is of great economical interest if the amount of required block copolymer can be reduced in HF spinning. In addition, the dilute block copolymer solutions in DOX are checked for coating purpose to fabricate composite isoporous HFM. The SAXS curve shows that the addition of only 0.04 wt% MgAc₂ (with respect to the total polymer solution) can also vary the solution characteristics in dilute solution.

4. Study of structure formation in outside-in isoporous hollow fiber membranes by *in situ* small angle X-ray scattering

*The aim of this work is to understand the key factors driving the self-organization of PS-*b*-P4VP diblock copolymer, with and without the additive MgAc₂, at different distances after extrusion during HF spinning. The structure formation in HF is more sensitive towards changes in the solution compositions such as the presence of additives with reduced polymer concentration as compared to flat sheet membranes. So, the weakly segregated as well as the ordered solutions are investigated to check the influence of extrusion on the micellar lattices of microphase separated solutions and on the structure formation afterwards. Instead of the ordered solution with high polymer concentration, the ordered solution with additive MgAc₂ at comparatively lower polymer concentration is chosen while the solvent compositions are kept constant. For these experiments, we installed a lab scale HF spinning set-up into the beamline P03 at DESY, which allowed us to change the spinning parameters while simultaneously measuring the structural features by SAXS. The selected polymer solutions and the chosen spinning parameters offer a systematic and comparative study. The influence of the solution characteristics and processing parameters on the distinct microscopic mechanisms is identified and correlated to the morphology of HFM as investigated by *ex situ* SEM.*

Reproduced from the following research article with permission from the Royal Society of Chemistry: “Self-Assembly of Block Copolymers during Hollow Fiber Spinning: An *In Situ* Small-Angle X-Ray Scattering Study” Kirti Sankhala, D. C. Florian Wieland, Joachim Koll, Maryam Radjabian, Clarissa Abetz, Volker Abetz, *Nanoscale*, 2019, DOI: 10.1039/C8NR06892E (<https://pubs.rsc.org/en/Content/ArticleLanding/2019/NR/C8NR06892E#!divAbstract>)

As discussed in Section 1.3.6, two factors are of high importance in the SNIPS process: 1) Evaporation of volatile solvent(s) from the block copolymer solution where the incompatible blocks lead to the self-assembled structure by microphase separation. 2) Immersion in the coagulation bath where the precipitation traps the developed structure on the surface and generates the sponge-like substructure by the exchange of solvent by non-solvent.^{110, 169, 170} During the HF spinning process, additional structure-controlling factors gain importance because the extrusion of a compressible viscoelastic polymer solution and the swelling after extrusion impact the micellar arrangement, which in turn impact the structure formation and thus performance of the formed membrane. The controlling parameters are composition of the polymer solution (block copolymer chemical composition, molecular weight, polymer concentration, solvent(s) and additive(s)), spinneret (design and dimensions), spinning parameters (air gap and flow rates of polymer solution and bore fluid), environmental conditions, *etc.*^{170, 203} Therefore, prior to HF spinning, the block copolymer solutions were optimized as discussed in the previous chapter. Since the structure formation in HF is more sensitive towards slight changes in the solution compositions, the solvent compositions were kept constant to reduce the number of influencing parameters.

The HF spinning process has been investigated vastly for the fabrication of commonly used asymmetric HFM *via* NIPS.^{43, 76, 77, 202} However, in fabrication of isoporous HFM by spinning of the block copolymer solutions, the shear-induced changes of the free energy of the block copolymer microdomains control the morphology and performance of the formed membranes.^{83, 170} In HF spinning, the structure formation takes place in the air gap between the spinneret and the precipitation bath within 2 s, where the strain in fiber due to the gravitational force limits the range of extrusion rate and the air gap defining the evaporation time, and thus requires a good control and understanding of the process. Here, open questions remain about the parameters which direct the self-assembly of block copolymers in this very short time. After extrusion, a subtle balance exists between the block copolymers trying to reach their equilibrium state, which is disturbed due to the shear forces and the ongoing evaporation, which induces self-assembly and precipitation.

To this end, fundamental studies have been focused on the effects of the structure in block copolymer solutions and on the flat sheet membrane fabrication, but the structure formation in block copolymer HFM has not been probed by *in situ* characterization techniques so far. Therefore, it is of great interest to explore the topic categorically with insight into the behavior of

different polymer solutions at different spinning parameters after extrusion, enabling us to develop new pathways to tailor the structure formation in HFM. In order to understand the key factors driving the self-organization of PS-*b*-P4VP diblock copolymer, with and without the additive magnesium acetate (MgAc₂), at different distances from the spinneret during HF spinning, a lab scale HF spinning set-up was installed into the beamline P03 at DESY.²²⁷ The experimental set-up allowed us to change the spinning parameters while simultaneously measuring the structural features by SAXS.

In HF spinning, the isoporous structure formation occurs in the air gap between the spinneret and the precipitation bath. The parameters driving the self-assembly of block copolymers in this very short time remain doubtful due to the many influencing spinning parameters. The complexity in fabrication process increases with variation in spinning parameters due to their influence on the shear during extrusion and self-assembly afterwards. Therefore, in the next sections, the main influencing factors are discussed one by one by providing insight into the spinning process *via in situ* SAXS experiments and *ex situ* SEM investigations of fabricated HFM.

4.1. Outside-in hollow fiber membrane fabrication and experimental set-up for *in situ* SAXS

In order to achieve uniform pores on a nanometer scale on the top surface of the HFM, it is highly required to optimize the solution properties as well as to understand the correlation and influences of the spinning parameters. Therefore, for this *in situ* SAXS study, we selected the solution system that has been studied extensively for fabrication of isoporous flat sheet and HF membranes, *i.e.*, PS-*b*-P4VP diblock copolymer in the solvent mixture of DMF and THF.^{171, 203, 228}

The desired morphologies are formed by providing a distinct balance between the relaxation of the polymer chains due to the shear forces driving them out of equilibrium and the macromolecular rearrangement due to the evaporation of the more volatile solvent (THF), which fixes the PS matrix while the P4VP microdomains are highly swollen in DMF (Figures 4.1 b and c). This process of self-organization stops as soon as the HFM is immersed in the precipitation bath. Therefore, the study on the self-assembly of macromolecules in HF is focused on the

changes happening in the gap between the precipitation bath and the spinneret. The influence of the solution characteristics and processing parameters on the distinct microscopic mechanisms is identified and correlated to the membrane morphology.

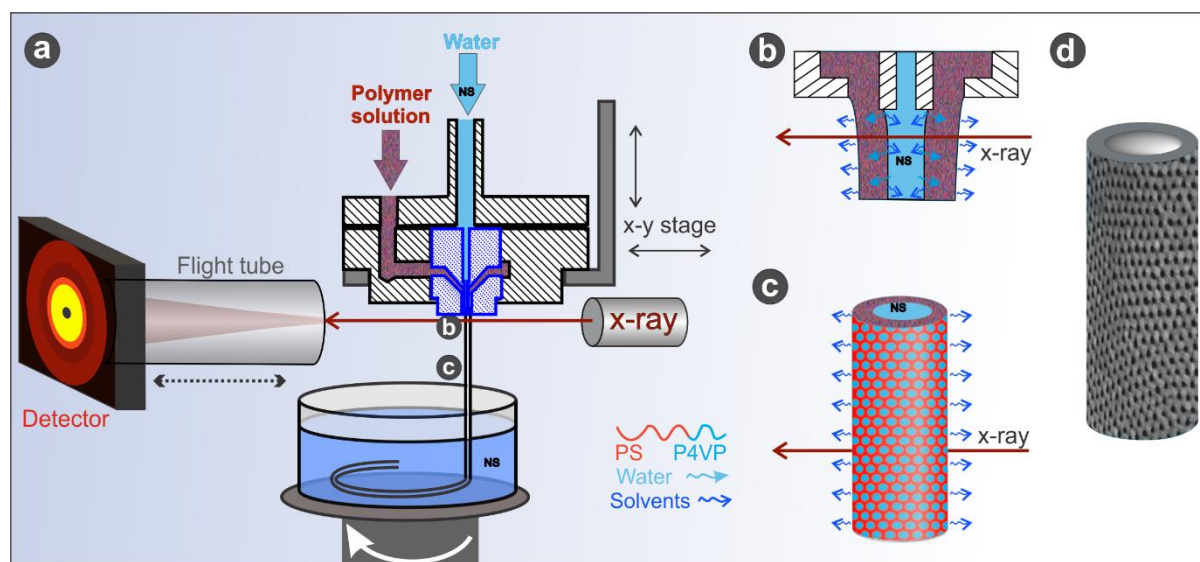


Figure 4.1. Experimental overview. (a) Set-up of spinning apparatus installed at the beamline P03 of PETRA III at DESY for *in situ* SAXS investigations. (b) As the polymer solution is extruded through the spinneret having non-solvent (NS) in the lumen, the polymer chains relax and the volatile solvents start to evaporate from the outer surface. The as-spun fiber could be investigated closest at 1 mm from the nozzle of the spinneret. (c) L_a was varied up to 80 mm, the microphase separated structures develop on the outer surface of the HF. The spun HF are collected in the precipitation bath. (d) The miniature shows an outside-in isoporous HF.

4.2. Influence of spinning parameters on structure formation in hollow fiber membranes

For the interpretation of the experimental data collected from the HF, it is important to remember the main properties controlling the structure formation. As schematized in Figure 4.1, during fabrication of isoporous HFM, the main implication is the occurrence of evaporation-induced self-assembly of block copolymers, which initiates just after extrusion. For a certain L_a , the selection of Q_p varies the evaporation time. A relatively similar evaporation time can be provided at a higher Q_p along with a higher L_a . However, the shear thinning of the polymer solution in the spinneret at the higher Q_p as well as the increase in the gravitational force acting

on the nascent fiber in the air gap have a significant effect on the kinetics of the self-assembly.¹⁷⁰

A. Influence of polymer flow rate

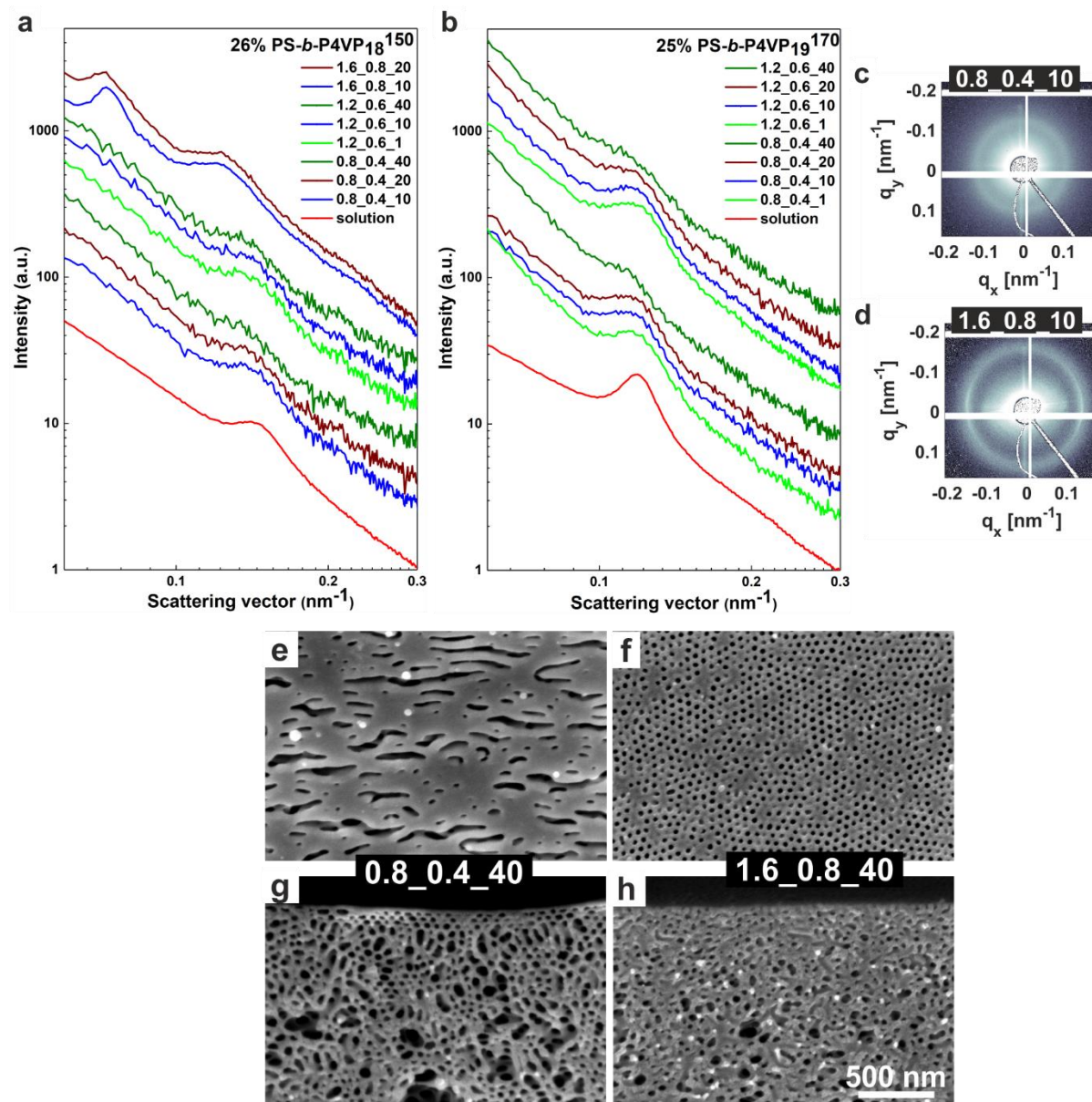


Figure 4.2. Influence of Q_p . (a, b) SAXS curves, (c, d) SAXS patterns, and (e-h) SEM micrographs of as-spun HF using block copolymer solutions of 26 wt% PS-*b*-P4VP₁₈¹⁵⁰ (a, c, d) and 25 wt% PS-*b*-P4VP₁₉¹⁷⁰ (b, e-h) in DMF/THF 50/50 (wt/wt) at different spinning parameters. The spinning parameters are mentioned as $Q_p-Q_w-L_a$. The SAXS data are plotted in log-log scale and Y-offset is adjusted for better visibility. (c, d) The images show the ring origination from the domain correlation. The fiber runs

in the vertical direction and is slightly tilted due to the movement of the precipitation bath. The SEM micrographs (e-h) have same scale bar.

Table 4.1. Details of SAXS curves of as-spun fibers using block copolymer solutions having 26 wt% PS-*b*-P4VP₁₈¹⁵⁰ and 25 wt% PS-*b*-P4VP₁₉¹⁷⁰ in DMF/THF 50/50 (wt/wt) for different spinning parameters (shown as Q_p - Q_w - L_a). All q^* (nm⁻¹) and d (nm) have an error bar of ± 0.005 nm⁻¹ and ± 1.1 nm, respectively.

L_a (mm)	26 wt% (0.8_0.4_ L_a)		26 wt% (1.2_0.6_ L_a)		26 wt% (1.6_0.8_ L_a)		25 wt% (0.8_0.4_ L_a)		25 wt% (1.2_0.6_ L_a)	
	q^*	d	q^*	d	q^*	d	q^*	d	q^*	d
Solution	0.147	42.7	-	-	-	-	0.120	52.4	-	-
1	-	-	0.144	43.6	-	-	0.120	52.4	0.120	52.4
10	0.141	44.6	0.139	45.2	0.131	47.9	0.117	53.7	0.119	52.8
20	0.138	45.5	-	-	0.133	47.2	0.116	54.2	0.116	54.2
40	0.135	46.5	0.136	46.2	-	-	0.113	55.6	0.113	55.6

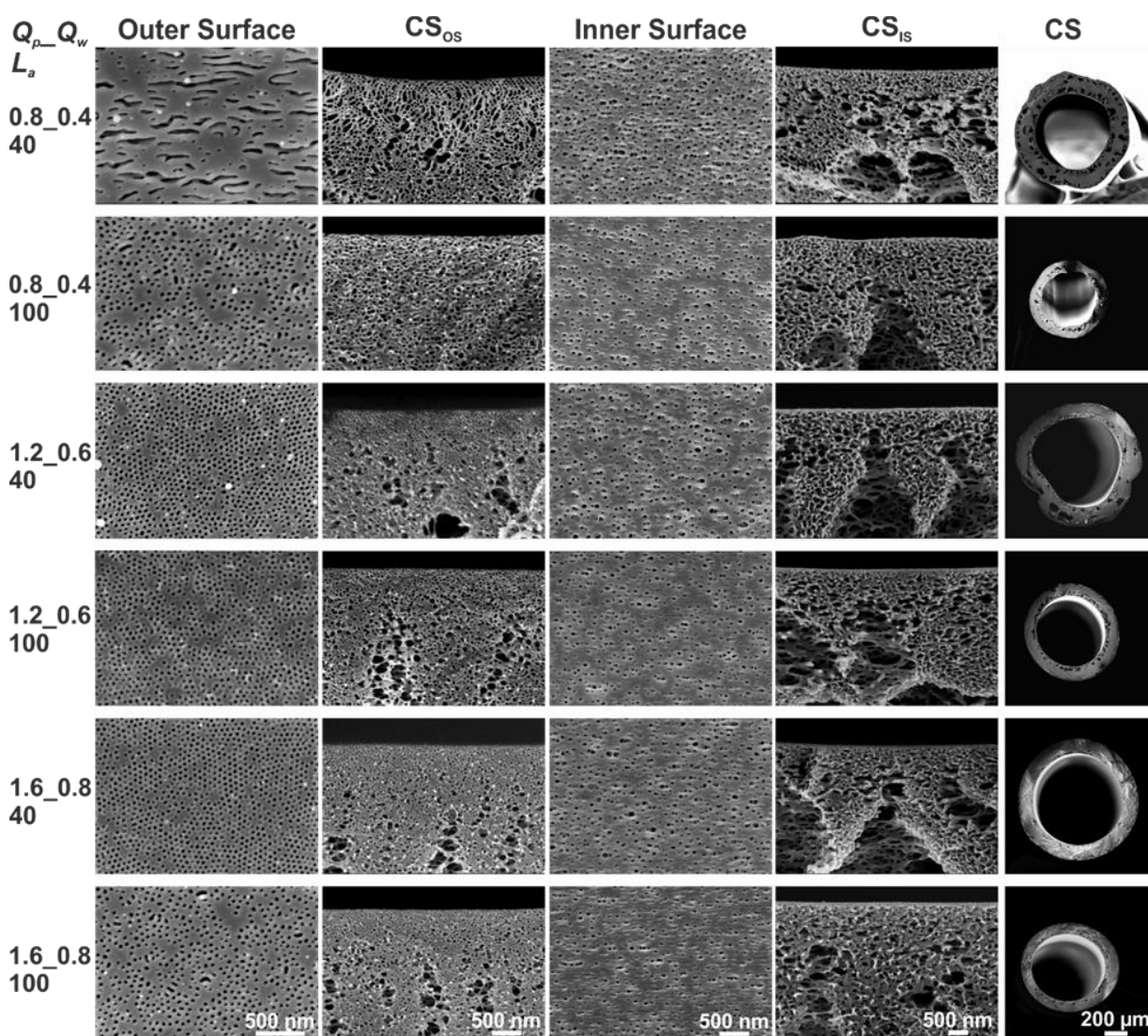


Figure 4.3. The SEM micrographs show the influence of spinning parameters (Q_p - Q_w - L_a) on the morphology of the outer surface, cross-sections near the outer surface (CS_{os}), the inner surface, cross-sections near the inner surface (CS_{is}) and the full cross-section (CS) of HFM. The HFMs were spun using block copolymer solution of 25 wt% PS-*b*-P4VP₁₉¹⁷⁰ in DMF/THF 50/50 (wt/wt) for Q_p 0.8, 1.2 and 1.6 mL/min, at $L = L_a$, 40 and 100 mm. The SEM micrographs in a column have the same scale bar.

Initially, the spinning solution is in a thermodynamical equilibrium as a weakly segregated spherical block copolymer solution. The extrusion of this viscoelastic solution through a spinneret disturbs this equilibrium by inducing uniaxial deformation as a result of the shear force. This deformation depends on various factors such as polymer solution, extrusion rate, spinneret design, die gap for extrusion, roughness of spinneret walls, *etc.* In these *in situ* experiments, all the used spinnerets were made of the same material and the dimensions of channels and orifices were kept equal, thus, providing a similar shear stress distribution throughout the experiments. As a consequence, the variables having significant impact on the shear distribution are the extrusion rate Q_p and the composition of the polymer solution which includes changes in the concentration of block copolymer and additive MgAc₂. The influence of shear deformation due to Q_p on the integral structural dimensions of weakly segregated block copolymer solution and on the self-assembly of block copolymers is shown in Figure 4.2 and Table 4.1. The comparison of scattering curves for a particular set of spinning parameters are shown in Figures 4.4, 4.6 and 4.7.

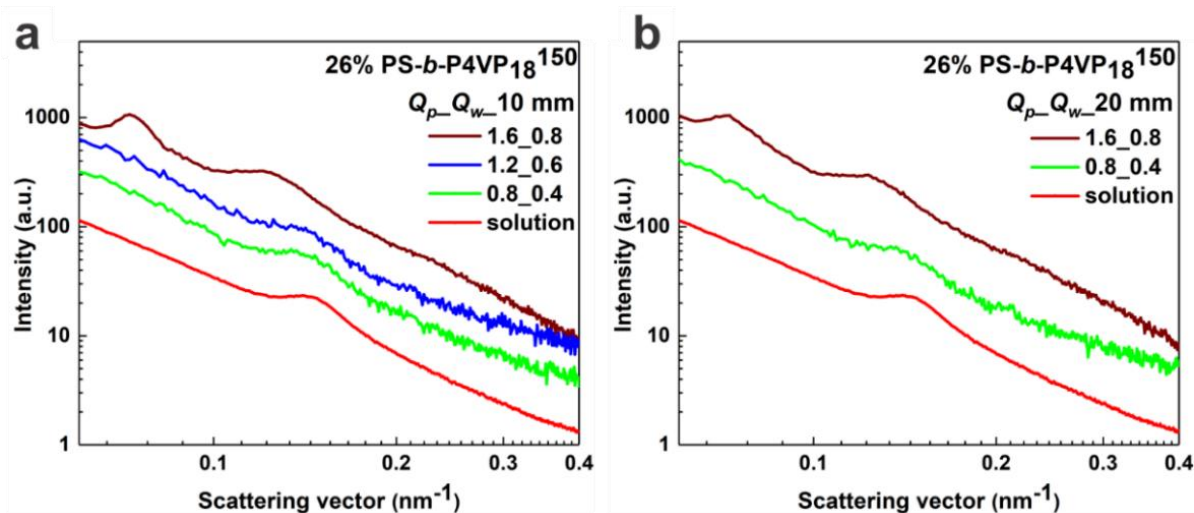


Figure 4.4. Influence of Q_p . (a,b) SAXS curves and (c,d) SAXS patterns of as-spun HF using block copolymer solution 26 wt% PS-*b*-P4VP₁₈¹⁵⁰ in DMF/THF 50/50 (wt/wt) at a particular set of spinning parameters, polymer flow rate Q_p (mL/min), bore fluid flow rate Q_w (mL/min) and air gap distance L_a (mm), mentioned as Q_p - Q_w - L_a . The SAXS data are plotted in log-log scale and Y-offset is adjusted for clarity.

The *in situ* SAXS data show that the ordering of micelles in all the polymer solutions is reduced as a course of the extrusion as compared to the conditions under rest (see the scattering curves in Figures 4.2 a, b and 4.8). It should be noted that the SAXS scans provide the structural information for all fiber materials along the beam and for an area of ca. $28 \times 14 \mu\text{m}^2$ in a single scan (more details are in Section 1.2). Therefore, the SAXS curves mainly show the influence of extrusion on structural characteristics of the as-spun fiber, which is still a viscous polymer solution within the fiber wall up to L_a of ca. 80 mm depending on the polymer solution and the thickness of the as-spun fiber.

In the scattered intensity of the weakly segregated polymer solutions of 26 wt% PS-*b*-P4VP₁₈¹⁵⁰ (Figure 4.2 a) and 25 wt% PS-*b*-P4VP₁₉¹⁷⁰ (Figure 4.2 b), no significant difference could be identified at a particular L_a for variation of Q_p from 0.8 mL/min to 1.2 mL/min. The main difference is a decrease of the overall intensity and a slight shift in the peak position with increasing L_a , which is attributed to the precipitation from the inner side of the fiber resulting in a change of the scattering contrast, and the evaporation of the more volatile solvent and relaxation from shear-induced effects, respectively. However, with further increase in Q_p , an orientation of the structures in the polymer solution becomes evident. Depending on the shear stresses, the meso-phase structures may transform from an isotropic (Figure 4.2 c) to an oriented state (Figure 4.2 d). A significant influence of the increase in Q_p to 1.6 mL/min can be seen on the orientation of the structures by development of a structure factor in the 2D SAXS images, at L_a 10 mm (Figs. 4.2 d and 4.5). The scattering image shows an orientation effect perpendicular to the fiber axis as the ring shows the maximum intensity corresponding to the perpendicular axis of the fiber; this also applies to the structure factor. This orientation of structures is accompanied by an increase in the correlation length indicating larger domains with an increase of shear (Figures 4.2 a and Table 4.1), which shows more chain orientation of the polymers and the formation of anisotropic structures. This might influence the thermodynamic driving forces which govern the self-assembly and progression of the microphase separation which affects the membrane morphology.

It is worth noting here that the influence of shear on the membrane morphology as observed by SEM and on the structure in as-spun fibers as observed by SAXS helps to understand the process. However, the spatial resolution of both methods is quite different. While the influence of spinning parameters in SAXS is measured for $28 \times 14 \mu\text{m}^2$, the SEM micrographs of cross-sections near the outer surface show the morphology only for a few microns below the surface.

In addition, SEM investigations are done in dried membranes while *in situ* SAXS experiments are conducted on as-spun fibers that almost resemble the polymer solution characteristics under shear. The influence of shear during extrusion significantly varies at different L_a due to the influence of solvent evaporation, relaxation of polymer chains and strain due to gravity.

The SEM micrographs in Figures 4.2 e-h show the influence of Q_p 0.8 and 1.6 mL/min, at L_a of 40 mm on the morphology of the outer surface and the cross-section near the outer surface of the HFM. The lower extrusion rate of 0.8 mL/min induces a lower shear rate along with a longer evaporation time. The deformation of spherical domains into ellipsoids or cylinders in the flow direction of the polymer solution can be seen in the SEM micrographs of Figures 4.2 e and g instead of the desired hexagonally-packed pores on the outer surface. However, for Q_p 1.6 mL/min, the fabrication of isoporous structure on the outer surface of HFM can be seen in Figure 4.2 f, although the evaporation time is shorter due to the higher Q_p at L_a 40 mm. The reason for a hexagonal packing of the microdomains in this comparatively short time provided in L_a 40 mm at Q_p 1.6 mL/min might be a result of an already occurred ordering of microdomains in the block copolymer solution after experiencing higher shear rates. However, at lower shear rate these microdomains tend to align and progress in the direction of shear. Thus, at a higher shear rate (Q_p 1.6 mL/min), the ordering in the weakly segregated domains tend to increase in the direction perpendicular to the fiber. Moreover, the shear-induced orientation of microdomains is higher near the outer surface which is due to the higher shear rates at the walls of the spinneret and can be seen in the SEM micrograph of the cross-section near the outer surface, see Figure 4.2 g.

The detailed influence of Q_p (0.8, 1.2 and 1.6 mL/min) and L_a (40 and 100 mm) on the morphologies of the outer surface, the inner surface and cross-sections near the outer and the inner surfaces of the HFM are shown in Figure 4.3. The values of D_p and d_{c-c} from the analysis of SEM micrographs of the outer surfaces are given in Table 4.1, which shows a decrease in D_p values with increase in Q_p . The deformation and ordering of microdomains for Q_p of 0.8 mL/min and 1.6 mL/min, respectively, is still in a metastable state which disappears with increase in L_a to 100 mm and results in less-ordered pores on the outer surface (Figure 4.3). The structures aligned on the outer surface of the HFM at Q_p 0.8 mL/min and L_a 40 mm transform into randomly located pores oriented perpendicular to the surface at L_a 100 mm. This growth of microdomains perpendicular to the surface is driven by an increase in evaporation time that

develops a concentration gradient from the top surface.^{110, 112} The isoporous structure developed at conditions of Q_p 1.6 mL/min and L_a 40 mm also vanishes with an increase in evaporation time at L_a 100 mm, respectively to a longer evaporation time. This disordering might have occurred due to the faster relaxation of microdomains after extrusion at high shear rate and due to the elongational forces as well. In average of Q_p 0.8 and 1.6 mL/min, the shear stress applied with Q_p 1.2 mL/min leads to isoporous structures for L_a 40 and 100 mm, by offering a balance between ordering in the polymer solution due to shear stresses and disordering due to the relaxation in combination with the required evaporation time. While on the other side of the HFM, on the inner surface, with increase in Q_p or shear stress at a particular L_a , the inner surface morphology gets slightly tightened, also the SEM micrographs of HFM cross-sections show lesser macrovoids due to the increase in the molecular orientation and chain packing. Therefore, a variation in Q_p strongly varies the solution characteristics during extrusion. The Q_p together with the available evaporation time drives the block copolymer microdomains to reorganize into hexagonally-packed pores on the surface. This process of self-assembly is significantly faster for more segregated or ordered block copolymer solutions because after extrusion, the block copolymer micelles try to achieve the initial equilibrium of a well-defined self-assembled nanostructure, *i.e.*, for ordered solutions containing MgAc₂. Therefore, different block copolymer solutions cause different effects of alignment as well, as seen in our experiments. So, in contrast to the flat sheet membrane, evaporation time is not the only important variable of self-assembly and structure formation in HFM fabrication, Q_p plays a key role as well under similar conditions.

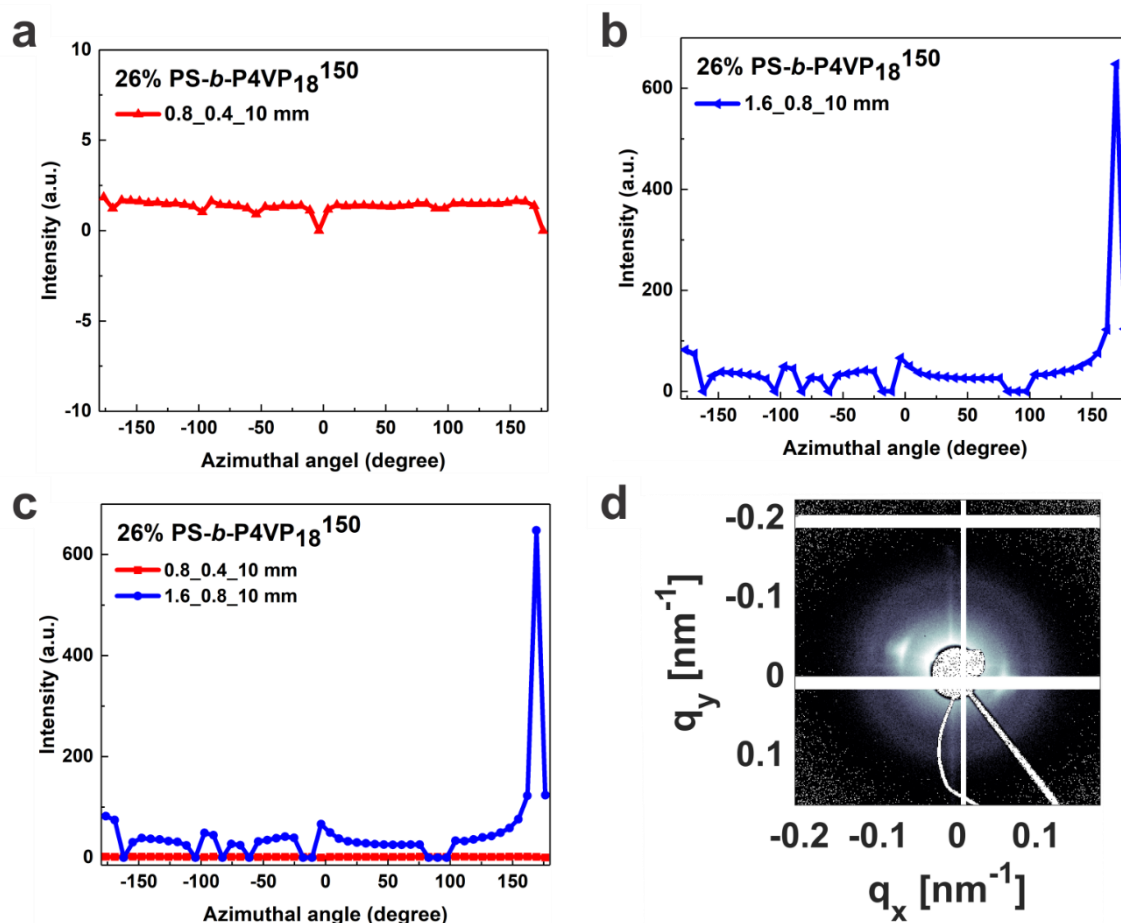


Figure 4.5. Influence of Q_p . 1D azimuthal intensity curves of as-spun HF using block copolymer solution 26 wt% PS-*b*-P4VP₁₈¹⁵⁰ in DMF/THF 50/50 (wt/wt) at a particular L_a of 10 mm for different Q_p - Q_w : 0.8_0.4 (a) and 1.6_0.8 (mL/min) (b). (c) Stacked curves. We note that in the azimuthally integrated data only one peak can be observed. This is due to the fact that the other peak lies on a dead area of the pilatus detector making it impossible to see.

B. Influence of evaporation time given by the air gap distance

While discussing evaporation-induced self-assembly, the distance between the spinneret and the precipitation bath (L_a) remains a key factor, as it defines the evaporation time at a certain Q_p . Table 4.1 and Figure 4.2 (particular sets are plotted in Figures 4.4 and 4.5) show that the structural changes occur in the nm-range on the time-scale of milliseconds before the fiber is immersed in the precipitation bath. At the solution/air interface, an increase of the evaporation time increases the interfacial chain segregation, which would result in an increase in peak-height of the scattering intensity. This behavior was observed during *in situ* SAXS study of flat sheet membranes.¹⁷² However, for the fabrication of a HF geometry, a precipitant is required on one side of the as-spun HF. The structural evaluation in this three-phase system consisting

of air on one side and precipitant on the other side of a polymer solution is significantly different, and increases the complexity in understanding the macromolecular organization in HF fabrication. For sake of simplicity, the ratio Q_p/Q_w was kept constant at two in order to provide similar conditions of coagulation from the lumen side at different volumetric flow rates (Q_p). In addition, this gives a uniform cross section and relatively similar membrane thickness as well.

In fabrication of HFM, with increasing L_a , the precipitation front moves inwards and increases the coagulation of polymer solution from the lumen side due to the solvent and non-solvent exchange between the flowing polymer solution and the bore fluid. The increase in coagulation increases the gelation/spinodal decomposition of the polymer solution from the lumen side. This behavior can be observed in the *in situ* SAXS data, which show a decrease in the peak height with increasing L_a (Figures 4.2 a, b and 4.8). This proves an increase in the coagulation from the lumen side as the number of micelles decreases. Further support to this assumption is given by the observation that the peak width gets smaller indicating a narrowing of the size-distribution for micelles due to the precipitation.

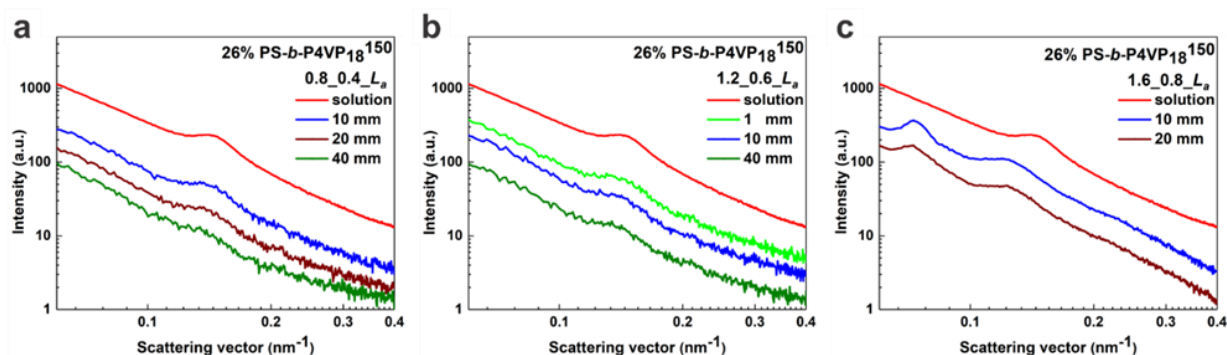


Figure 4.6. Influence of L_a . SAXS curves of as-spun HF using block copolymer solution 26 wt% PS- b -P4VP $_{18}^{150}$ in DMF/THF 50/50 (wt/wt) at different L_a (mm) for a particular set of Q_p/Q_w (in mL/min): 0.8_0.4 (a); 1.2_0.6 (b) 1.6_0.8 (c). The SAXS data are plotted in log-log scale and Y-offset is adjusted for clarity.

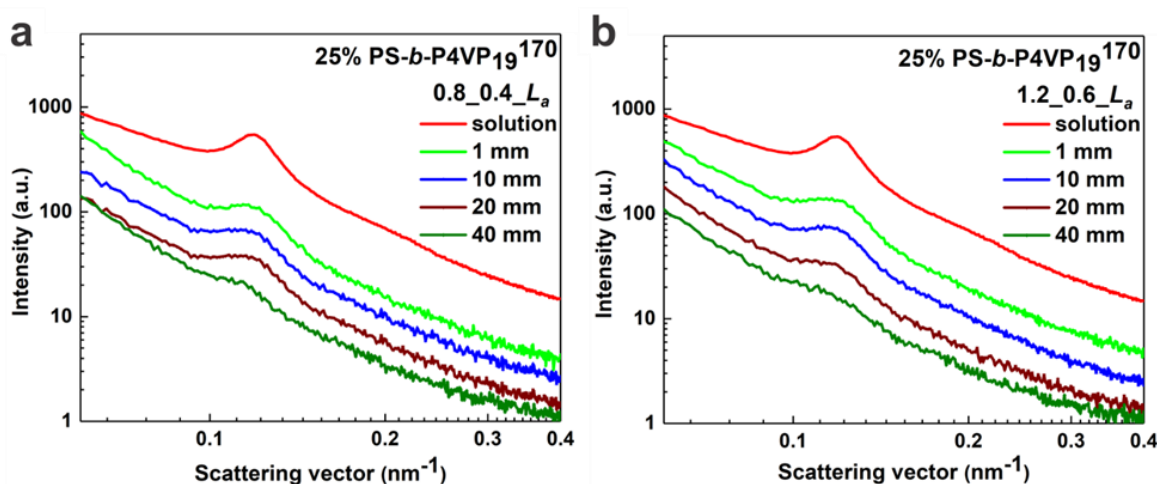


Figure 4.7. Influence of L_a . (a,b) SAXS curves of as-spun HF using block copolymer solution 25 wt% PS-*b*-P4VP₁₉¹⁷⁰ in DMF/THF 50/50 (wt/wt) at different L_a (mm) for a particular set of Q_p - Q_w (mL/min): 0.8_0.4 (a); 1.2_0.6 (b). The SAXS data are plotted in log-log scale and Y-offset is adjusted for clarity.

For a less viscous or weakly segregated polymer solution, a lower size distribution is observed, which hints at a higher mobility and, thus, kinetics in this situation (see Table 4.1). Figures 4.2 a and b show that the primary scattering peak vanishes completely for the commonly used weakly segregated solutions and significantly reduces for the ordered solutions (Figures 4.8 b and c) as well. This shows that the structure formation in as-spun fibers quenches within a short L_a . Moreover, an increase in L_a increases the strain in the nascent fiber due to gravitational force, which changes the fiber diameters and influences the structure formation and assembly of uniform pores on the top surface of membranes (Figures 4.3, 4.10, 4.11 and Table 4.3). Thus, for a uniform pore formation L_a is preferred to be ≤ 100 mm, which further significantly differs for different polymer solutions and spinning conditions.

4.3. Influence of additive MgAc₂ in the block copolymer solution in isoporous hollow fiber membrane fabrication

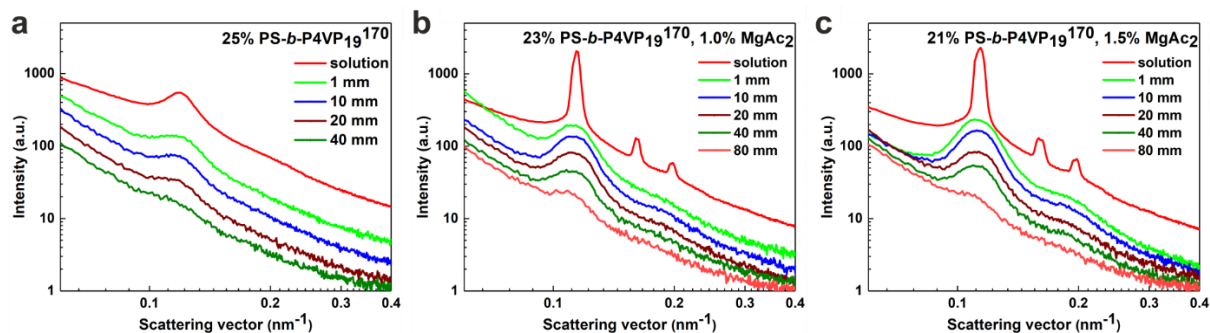


Figure 4.8. SAXS of as-spun HF using block copolymer solutions having different concentrations of PS-*b*-P4VP₁₉¹⁷⁰ and MgAc₂ in DMF/THF 50/50 (wt/wt) at Q_p 1.2 mL/min, Q_w 0.6 mL/min and different L_a (mm). Y-offset is adjusted for better presentation.

Table 4.2. Details of SAXS curves of as-spun fibers using different PS-*b*-P4VP₁₉¹⁷⁰ block copolymer solutions at different L_a , for Q_p 1.2 mL/min and Q_w 0.6 mL/min. All q^* and d have an error bar of $\pm 0.005 \text{ nm}^{-1}$ and $\pm 1.1 \text{ nm}$, respectively.

L_a (mm)	25 wt%		23 wt% and 1.0 wt% MgAc ₂		21 wt% and 1.5 wt% MgAc ₂		
	q^* (nm ⁻¹)	d (nm)	q^* (nm ⁻¹)	d (nm)	q^* (nm ⁻¹)	q^{2nd} (nm ⁻¹)	d (nm) ¹
Solution	0.120	52.4	0.114	55.1	0.114	0.161	55.1
1	0.120	52.4	0.109	57.6	0.109	0.205	57.6
10	0.119	52.8	0.111	56.6	0.111	0.193	56.6
20	0.116	54.2	0.111	56.6	0.110	0.194	57.1
40	0.113	55.6	0.108	58.2	0.107	0.200	58.7
80	-	-	0.105	59.8	-	-	-

The SAXS curves in Figure 4.8 show the influence of the extrusion parameters on the ordering of different block copolymer solutions having different amount of MgAc₂, at a certain L_a . The comparison of solutions for a particular set of spinning parameters is shown in Figure 4.9. During extrusion, the shear stresses distort the structural features of the polymer solution, *i.e.*, bcc in polymer solutions having 21 wt% PS-*b*-P4VP₁₉¹⁷⁰ and 1.5 wt% MgAc₂, and 23 wt% PS-*b*-P4VP₁₉¹⁷⁰ and 1.0 wt% MgAc₂ in DMF/THF 50/50 (wt/wt). After extrusion, the sharpness and intensity of the primary peak decreases and the peak position shifts to a slightly lower q as compared to the respective solution. The scattering pattern of the as-spun fiber, at L_a 1 mm, from spinning of 25 wt% PS-*b*-P4VP₁₉¹⁷⁰ solution does not show a significant change in the peak position as compared to the steady solution while the peak gets wider and loses the intensity, as discussed in Section 2.1 (Figures 4.2 b or 4.8 a). However, in case of the ordered solutions, the higher order peaks disappear and with increasing L_a even the shoulder becomes gradually harder to discern (Figures 4.8 b and c). This confirms that the extrusion of an ordered solution results in a lesser or only partially ordered solution afterwards.

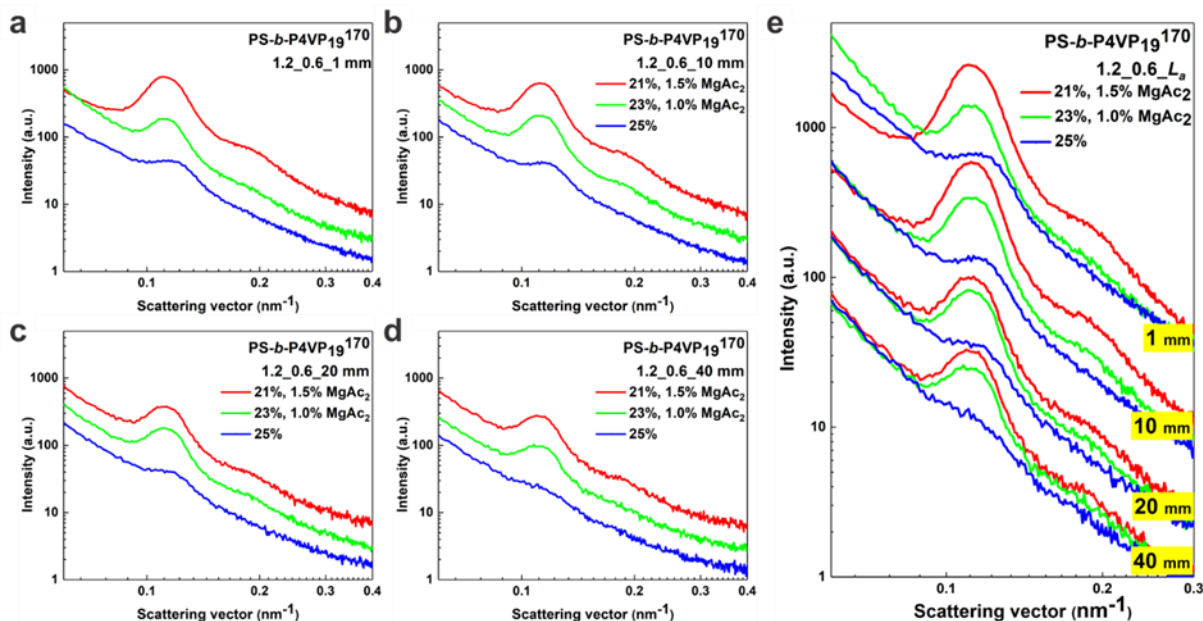


Figure 4.9. Influence of polymer solution. (a-d) SAXS curves of as-spun HF using different block copolymer solutions 25 wt% PS-*b*-P4VP₁₉¹⁷⁰, 23 wt% PS-*b*-P4VP₁₉¹⁷⁰ and 1.0 wt% MgAc₂ and 21 wt% PS-*b*-P4VP₁₉¹⁷⁰ and 1.5 wt% MgAc₂ in DMF/THF 50/50 (wt/wt). The curves are plotted for Q_p 1.2 mL/min and Q_w 0.6 mL/min, at different L_a : 1 mm (a); 10 mm (b); 20 mm (c); 40 mm (d). (e) The sets of SAXS curves a-d are stacked together. The SAXS data are plotted in log-log scale and Y-offset is adjusted for clarity.

Interestingly, just after extrusion at L_a of 1 mm, the scattering curve from the polymer solution 23 wt% PS-*b*-P4VP₁₉¹⁷⁰ with 1.0 wt% MgAc₂ in DMF/THF 50/50 (wt/wt) shows only one broad peak with an increase in domain spacing as compared to the respective solution, see Figure 4.8 b and Table 4.2. However, the second shoulder in the scattering curves appears at L_a of 10 and 20 mm with a decrease in domain spacing, which again disappears for L_a ca. 40 mm and shows an increase in domain spacing. This trend in SAXS curves and domain spacing values hint at ongoing structural transitions in the block copolymer solution. We suggest that the competing interactions of shear stresses during extrusion, relaxation after extrusion, and the evaporation-induced increase in segregation of block copolymers are responsible for this behaviour. During extrusion, the structural ordering of the block copolymers is disturbed and due to the shear stresses the ordered micelles might enlarge showing an increase in domain spacing. After extrusion, these structures in an as-spun polymer solution try to achieve the initial equilibrium of block copolymer solution by releasing the shear effects and show a decrease in domain spacing. On the other hand, with increasing L_a the influence of evaporation on the self-assembly and the precipitation from the lumen side on coagulation increases significantly. Thus, the observation of the second shoulder for block copolymer solutions of 23 wt%

with 1.0 wt% MgAc₂ shows that up to 20 mm the bulk relaxation dominates which is overwhelmed by the segregation and self-assembly afterwards.

A similar trend in the height of the second shoulder and in the domain spacing can also be seen during the spinning of the solution containing 21 wt% PS-*b*-P4VP₁₉¹⁷⁰ and 1.5 wt% MgAc₂ in DMF/THF 50/50 (wt/wt) (see Figure 4.8 c and Table 4.2). However, here the second shoulder is stronger and can be seen up to L_a ca. 40 mm. This indicates that with increase in the concentration of MgAc₂ from 1.0 wt% to 1.5 wt% and, respectively, with decrease in the total P4VP segments with decrease in block copolymer concentration, the cation-pyridine complexation gets stronger and the structural ordering gets kinetically trapped. So, due to the higher MgAc₂ concentration, the initial structural properties of block copolymer solutions are more dominating, induced by the increased effective χ parameter, as compared to the solution with 23 wt% block copolymer and 1.0 wt% MgAc₂. The solution scattering curves in Figure 3.3 show that the increased addition of MgAc₂ leads to more prominent microphase separation in the solution of polymeric amphiphiles, which might be due to lower mobility of polymer chains or reduced micelle mobility, and all together lowers the structural transitions.

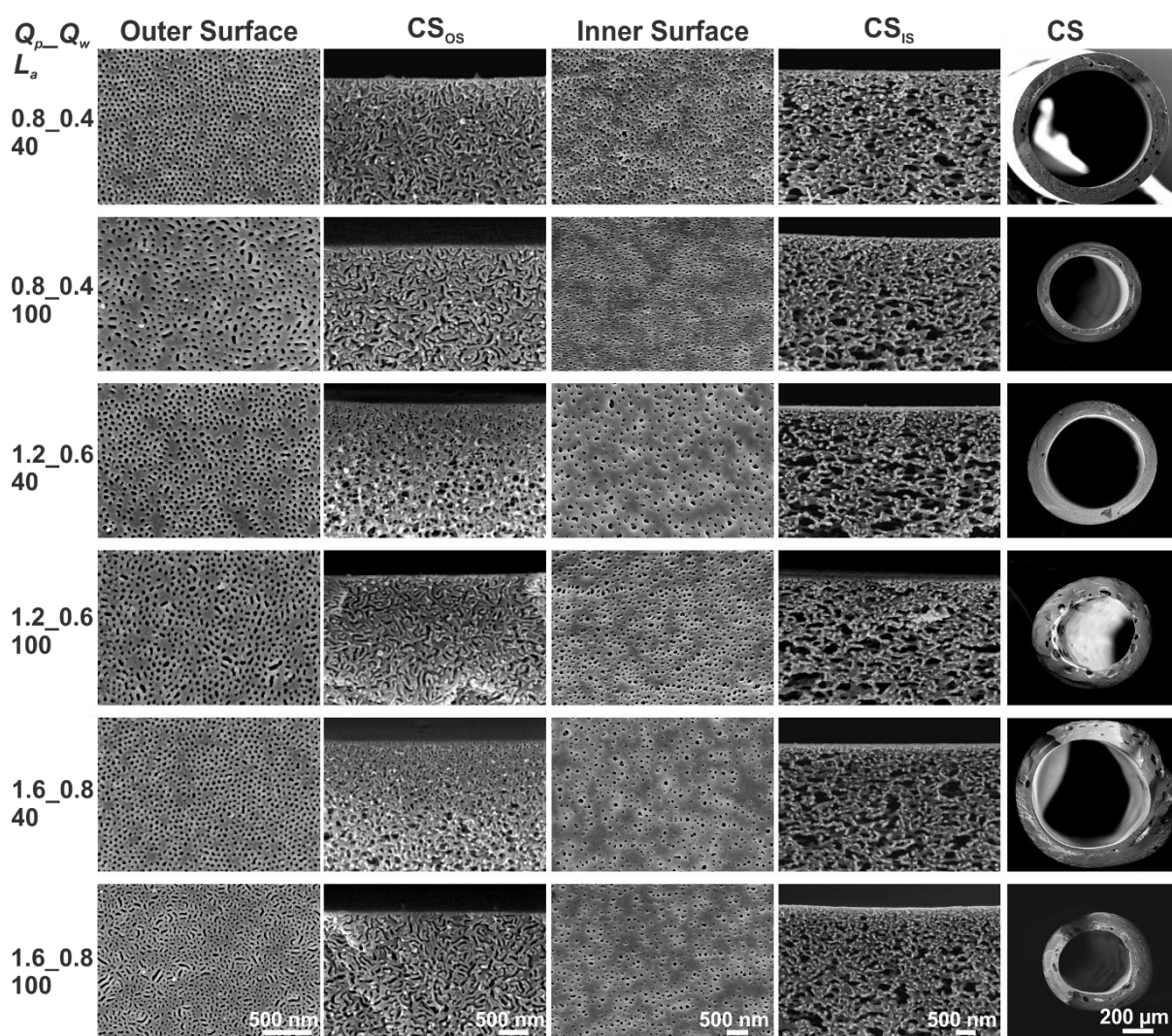


Figure 4.10. The SEM micrographs show the influence of spinning parameters (Q_p - Q_w - L_a) on the morphology of the outer surface, cross-sections near the outer surface (CS_{os}), the inner surface, cross-sections near the inner surfaces (CS_{is}) and the full cross-section (CS) of HFM. The HFM were spun using block copolymer solution of 21 wt% PS-*b*-P4VP₁₉¹⁷⁰ and 1.5 wt% MgAc₂ in DMF/THF 50/50 (wt/wt) for Q_p 0.8, 1.2 and 1.6 mL/min, at $L = L_a$, 40 and 100 mm. The SEM micrographs in a column have the same scale bar.

The SEM micrographs in Figure 4.10 show the influence of spinning parameters; Q_p of 0.8, 1.2 and 1.6 mL/min, and L_a of 40 and 100 mm, on the morphology of HFM spun using an ordered block copolymer solution with 21 wt% PS-*b*-P4VP₁₉¹⁷⁰ and 1.5 wt% MgAc₂ in DMF/THF 50/50 (wt/wt). The influence of solution characteristics on the formation of isoporous structures can be seen in the SEM micrographs of the outer surface of the HFM spun using two different solutions, in Figures 4.3 and 4.10. The HFM with isoporous outer surface could be achieved for a wider range of Q_p (0.8, 1.2 and 1.6 mL/min) at L_a 40 mm using an ordered solution containing MgAc₂ (Figure 4.9) as compared to the pristine weakly segregated solution having

higher polymer concentration of 25 wt% PS-*b*-P4VP₁₉¹⁷⁰ in DMF/THF 50/50 (wt/wt) (Figures 4.3 and 4.11). For Q_p 0.8 mL/min, at L_a 40 mm, formation of isoporous structures can be observed for the ordered solution containing MgAc₂, while the pristine weakly segregated solution shows a random alignment of cylinders on the outer surface. This shows that the shear-induced ordering for isoporous structure formation is more probable even at lower shear rates for already ordered solutions, after losing the crystallinity during extrusion, whereas for the weakly segregated solutions the requirement of higher shear rate can be expected for ordering of the microdomains. This metastable hexagonal ordering of microdomains on the outer surface disappears for all three Q_p values (0.8, 1.2 and 1.6 mL/min) within L_a of 100 mm, and the SEM micrographs of cross-sections near the outer surface show the random cylindrical growth of micelles in this short evaporation time (see Figure 7). However, for the weakly segregated solution, in Figure 5, such random cylindrical ordering at the cross-section near the outer surface is missing and a rather asymmetric structure can be recognized, and the self-assembled isoporous structures can be seen for Q_p of 1.2 mL/min, up to L_a of 100 mm (Figure 4.10). An influence of solution characteristics can also be observed on the morphology of the inner surface of HFM, where the pores look more elongated in Figure 4.3 as compared to Figure 4.10. In addition, the morphology of cross-sections near the inner surface is significantly different. Therefore, the HFM morphology completely depends on the solution characteristics and the spinning parameters. The isoporous structure formation and growth of microdomains is faster and facilitated in ordered solutions containing MgAc₂ as compared to the pristine solutions.

SEM micrographs of the outer surface of the HFM and their analysis

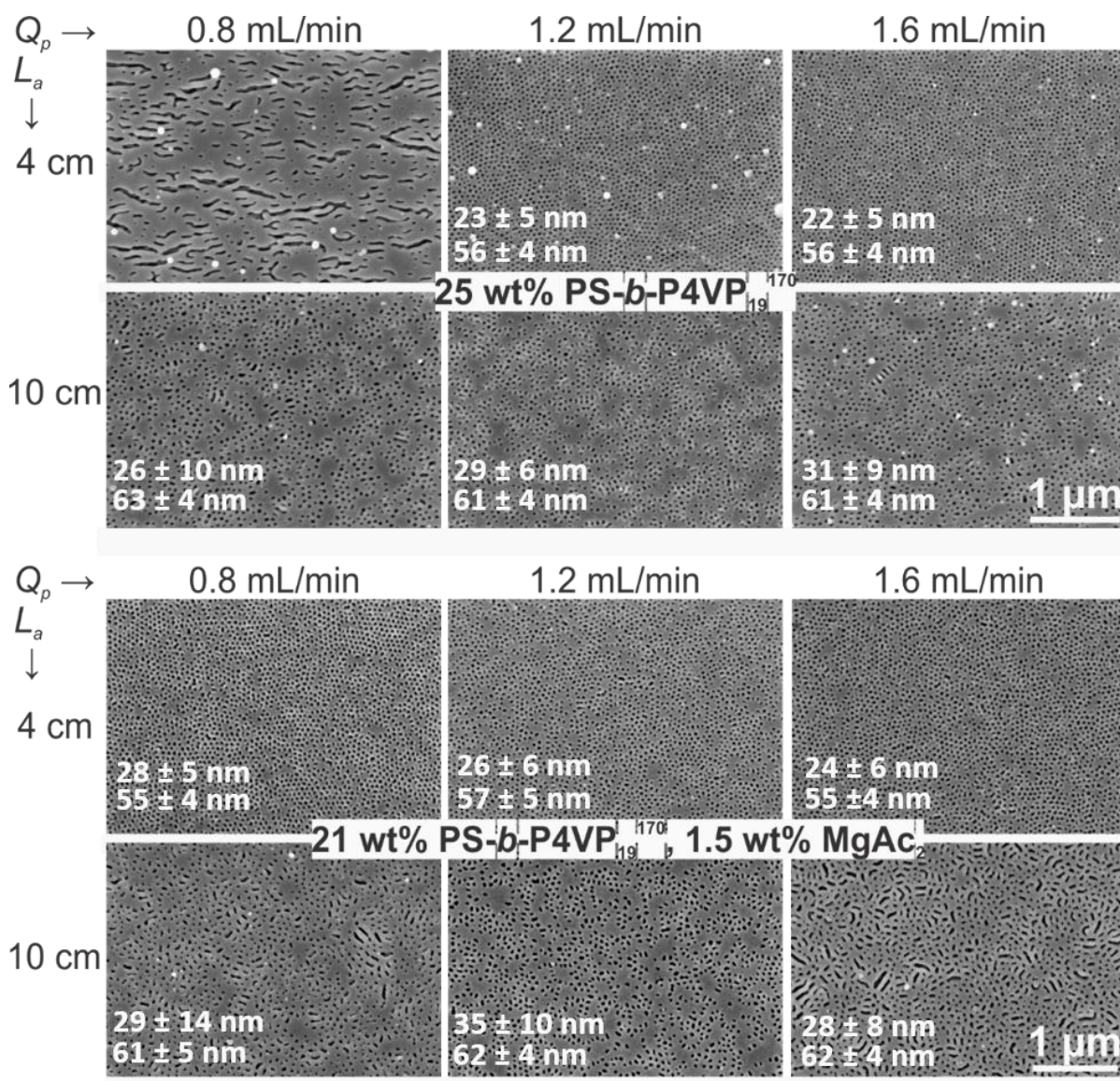


Figure 4.11. The SEM micrographs show the influence of spinning parameters (Q_p , Q_w , L_a) on the morphology of the outer surface of HFM. The HFM were spun using block copolymer solutions of 25 wt% PS-*b*-P4VP₁₉¹⁷⁰ and 21 wt% PS-*b*-P4VP₁₉¹⁷⁰ and 1.5 wt% MgAc₂ in DMF/THF 50/50 (wt/wt) for Q_p 0.8, 1.2 and 1.6 mL/min, at L_a 40 and 100 mm. The numbers on each micrograph show D_p (average pore diameter) in top and d_{c-c} (average center-to-center distance between pores) in second row, the analysis of micrographs is done by analySIS.

Table 4.3. Analysis of SEM micrographs of cross-sections of HFM, as shown in Figures 4.3 and 4.10. D_{out} is outer diameter and D_{in} is inner diameter of HFM.

25 wt% PS- <i>b</i> -P4VP ₁₉ ¹⁷⁰						
$Q_p \rightarrow$ $L_a \downarrow$	0.8 mL/min	1.2 mL/min	1.6 mL/min	0.8 mL/min	1.2 mL/min	1.6 mL/min
	D_{out} (μm)			D_{in} (μm)		
40 mm	1006 \pm 20	1069 \pm 66	1037 \pm 12	678 \pm 32	735 \pm 74	773 \pm 10
100 mm	686 \pm 3	785 \pm 51	809 \pm 33	439 \pm 47	545 \pm 54	584 \pm 33
21 wt% PS- <i>b</i> -P4VP ₁₉ ¹⁷⁰ and 1.5 wt% MgAc ₂						
$Q_p \rightarrow$ $L_a \downarrow$	0.8 mL/min	1.2 mL/min	1.6 mL/min	0.8 mL/min	1.2 mL/min	1.6 mL/min
	D_{out} (μm)			D_{in} (μm)		
40 mm	961 \pm 66	873 \pm 68	935 \pm 76	733 \pm 73	645 \pm 32	700 \pm 76
100 mm	687 \pm 43	712 \pm 19	673 \pm 54	515 \pm 42	468 \pm 19	435 \pm 40

4.4. Conclusion

The synchrotron SAXS measurements provide insight into the microscopic processes relevant for ordering of microdomains and their self-assembly after extrusion of concentrated block copolymer solutions. For this, the ordered solution having MgAc₂ with comparatively lower polymer concentrations and the weakly segregated pristine PS-*b*-P4VP block copolymer solutions were extruded. These structural features are correlated to the final morphology of the HF membranes, investigated by *ex situ* SEM. The SAXS data shows that the shear stresses during the spinning of a block copolymer solution results in disordering of an already ordered solution and reduces the micellization in a weakly segregated solution as well.

5. Fabrication of integral inside-out isoporous block copolymer hollow fiber membranes

Fabrication of evaporation-induced self-assembled structures on easily accessible surfaces and under normal evaporation conditions (e.g., flat sheet membranes and outer surface of HFM) is a conventional strategy while achieving such evaporation-induced microphase separated structures in compact geometries has been a long-standing goal. The fabrication of self-assembled structures on the lumen of HFM remains a challenge due to the requirement of additional structure-controlling evaporation conditions. As discussed in the previous chapter, while the preparation of outside-in isoporous membranes is already challenging, the preparation of inside-out isoporous HFM with an inner diameter of less than 1 mm is even more demanding. This study reports for the first time the preparation of an inside-out isoporous integral asymmetric HF membrane, in which the idea of gas flow was coined for the controlled evaporation required for self-assembly of block copolymers.

Adapted with permission from the following research article:

“A Pathway to Fabricate Hollow Fiber Membranes with Isoporous Inner Surface”, Kirti Sankhala, Joachim Koll, Maryam Radjabian, Ulrich A. Handge, Volker Abetz, *Advanced Materials Interfaces* 4 (7), 1600991, 2017; (<https://onlinelibrary.wiley.com/doi/full/10.1002/admi.201600991>)

Publisher: John Wiley and Sons; Copyright © WILEY-VCH Verlag GmbH & Co. KGaA, Weinheim; License number: 4553120468198.

As discussed in Section 1.2.8, the inside-out HFM provide the following advantages compared to outside-in HFM: (1) The conservation of the selective surface from abrasions during processing and module fabrication. (2) The fluid flowing in the lumen side is delivered into the lumens equally and enhances the flux since separation is a pressure driven process. (3) The inside-out cross-flow filtration mode limits the build-up of cake layers. However, if cake layers are formed, then they can be easily removed by back-wash and aeration, and hence maintain the permeate along with more hygienic system.⁶

5.1. Membrane fabrication *via* dry-jet wet spinning technique

In this study, the traditional dry-jet wet spinning technique is modified to fulfill the conditions required to complete the SNIPS process, which is required to achieve an isoporous structure on the lumen side of a HFM. A schematic depiction of the spinning process is provided in Figure 5.1. A triple orifice spinneret (Figure 5.1 a) was used to extrude the bore fluid, polymer solution, and water at controlled volumetric flow rates. The triple orifice spinneret had die gaps of 0.34 and 0.15 mm for polymer solution and water, respectively (for more details see Section 9.7). Afterwards the as-spun fiber is passed through a certain air gap before being immersed into the coagulation bath of water. As solvent evaporation is the preliminary requirement of SNIPS process for microphase separation and solidification of the isoporous surface later on, a gas (N₂) flow was introduced in the lumen of polymer solution flow. This gas stream suppressed the swelling of the extruded polymer solution, which otherwise would result in blocked fibers. Moreover, to initiate the formation of a fiber and subsequently strengthen the fiber, the polymer solution was extruded with a circlet flow of strong precipitant (water) on the outer side (Figure 5.1 b). The elementary experiments were performed on laboratory scale, using a spinning set-up having high-precision pumps, while the fibers were collected manually.

A solution of 27 wt% PS-*b*-P4VP₁₇¹³⁹ block copolymer in a binary mixture of DMF/THF 50/50 (wt/wt) was used. The concentration was optimized by checking the structure formation in flat sheet membranes.^{169, 170}

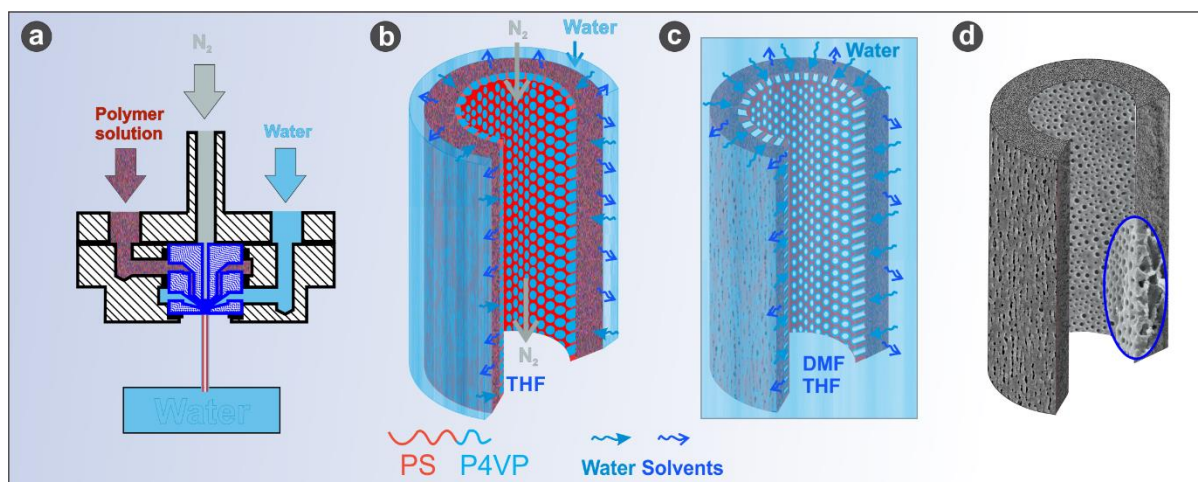


Figure 5.1. Preparation of inside isoporous HFM. (a) A triple orifice spinneret is used for HF spinning. Schemes b and c describe the SNIPS process, required for the formation of an isoporous structure on the inner surface of HF membrane. (b) After extrusion through the spinneret, N_2 is the central fluid in the lumen of nascent fiber and water is in the circlet. (c) The as-spun fiber is immersed into the precipitation bath of water where the non-solvent replaces the solvents. (d) The miniature inside-out isoporous HF.

5.2. Structure formation on the inner surface

In the dry-jet wet spinning for fabrication of inside-out isoporous HFM, after leaving the spinneret, the polymer chains relax in the presence of the compressible bore fluid of N_2 . The gas flow initiates the evaporation of the volatile solvents (mainly THF) on the inner surface. The evaporation of more volatile solvent THF solidifies the PS matrix while P4VP domains remain swollen in DMF. This evaporation-induced microphase separation of block copolymers depends on the evaporation conditions along with the quality of ordering already available in the block copolymer solutions. The evaporation time is controlled by the air gap distance (L_a) and the polymer flow rate (Q_p), while the rate of evaporation is mainly controlled by bore fluid (N_2) flow rate (Q_{N_2}). The SNIPS process on the inner surface of HFM completes by quenching the self-assembled structures by non-solvent induced phase separation. The phase separation on the inner surface takes place by the intrusion of water from outside to the lumen side through the polymeric fiber wall (Figure 5.1 c). In the precipitation bath, the solvents are replaced by non-solvent and due to the selective swelling of the P4VP domains by DMF the exchange with water leads to open pores. Therefore, one extra factor is emphasized in this work, *i.e.*, the rate of intrusion of water, which is fast across the partially precipitated polymeric wall.¹⁷² This was also observed in the previous chapter reporting *in situ* SAXS experiments during HF spinning

that with increase in L_a the peak height decreases due to the decrease in number of micelles, while, in that case the precipitation front is moving from inner side to outer side.

The coagulation of polymer solution is highly influenced by the factors controlling the wall thickness of the fiber, *e.g.*, the polymer concentration, Q_p , die gap for the polymer solution, miscibility of the solvents with water, air gap distance, *etc.* A higher solution concentration and Q_p would yield a higher shear stress in the flow chamber of the spinneret and result in an increase in the alignment of polymer chains, which in turn decreases the rate of intrusion of water.²²⁹

5.3. Influence of spinning parameters on hollow fiber membrane morphology

The spinning factors influencing the shear-induced structural changes are analogous to the ones discussed for outside-in isoporous HFM in Section 4.3. The only difference from the latter is the change in evaporation conditions. In the inside-out isoporous HFM fabrication the evaporation-induced self-assembly is controlled *via* gas flow.

The experiments for inside-out HF spinning were conducted in the optimized range of parameters such as Q_p was varied between 1.5 to 3 mL/min and L_a was varied as 5, 10 and 15 cm, where Q_p and L_a are adjusted respectively to regulate the evaporation time and time required for intrusion of water to the inner side. For example, a low Q_p (< 1.5 mL/min) and a high L_a (> 10 cm) provide a longer evaporation time prior to immersion into the precipitation bath, leading to the disappearance of a well-organized self-assembled structure, while $Q_p > 3$ mL/min is found to provide lesser evaporation time required for structure formation. After some preliminary hit-and-trial experiments, Q_{N_2} and Q_w were fixed to 1 mL/min, to form a lumen in the as-spun polymer solution and to provide enough precipitation from the outer side. The influence of Q_p and L_a on a particular section of HFM, *e.g.* inner surface, cross-section near the inner surface, outer surface, cross-section near the outer surface is shown in Figures 5.2-5.5.

A. Influence on the morphology of inner surface

Figure 5.2 shows that with increase in Q_p at a particular L_a of 10 cm, the appearance and disappearance of an isoporous structure can be observed. As discussed in the previous chapter, the increase in Q_p orients the block copolymer microdomains perpendicular to the surface helping in the structure formation, while it decreases the evaporation time at a particular L_a . The evaporation time is provided to achieve the desired state of evaporation-induced self-assembly leading to swelling of P4VP domains in DMF and for fixing of the PS matrix by evaporation of THF in case of already oriented microdomains. The self-assembly of block copolymers as hexagonally arranged microdomains is a metastable state of ordering, this duration is further shortened during HF spinning due to the ongoing relaxation of polymer chains after shear-inducing extrusion, which makes the structural evaluation quite complex in isoporous HFM fabrication.

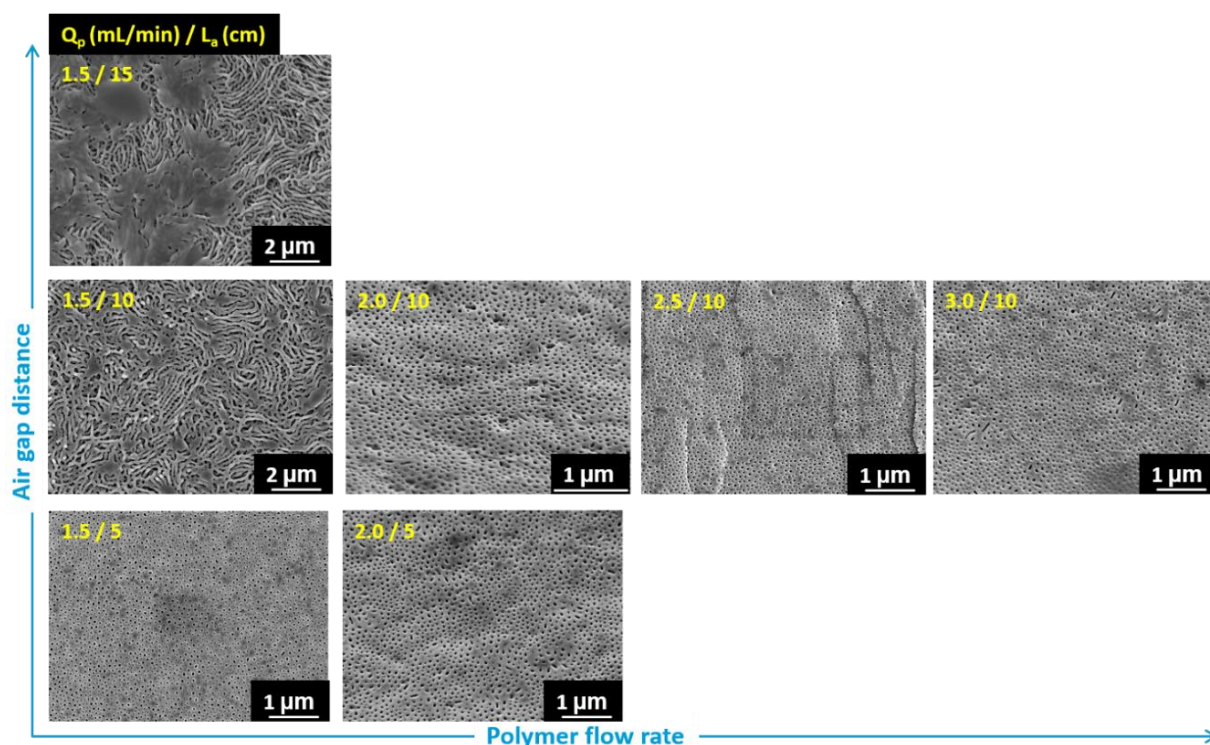


Figure 5.2. The SEM micrographs represent the isoporous structure formation on the inner surface of the HFM. The varying parameters are Q_p and L_a , which are mentioned on the SEM micrographs as Q_p/L_a , while Q_{N2} and Q_w were kept 1 mL/min.

The cross-section near the isoporous inner surface of the HF shown in Figure 5.6 b resembles a thin selective layer of a few nm on top of its membrane body that provides mechanical support

to the selective layer. Fast evaporation due to gas flow leads to a stronger concentration gradient perpendicular to the inner surface of the spun solution and is therefore enhancing the initiation of microphase separation or ordering of micelles assisting the P4VP domains to orient perpendicularly.¹⁰⁵ In consequence, also the usually required evaporation time prior to quenching is shortened. Short evaporation is also favorable to get a thin selective layer on top of a porous support layer which will decrease its hydraulic resistance and increase the permeability.²²³

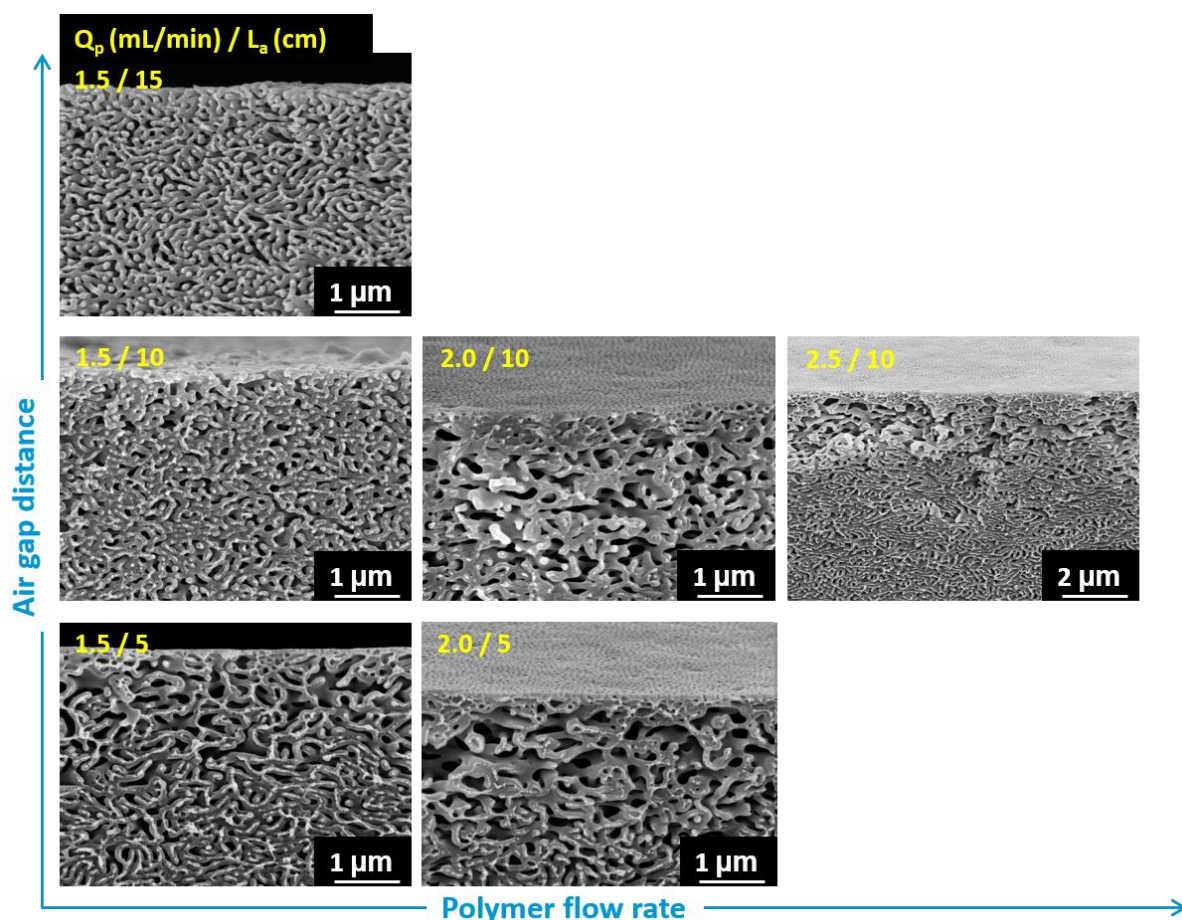


Figure 5.3. The SEM micrographs represent the morphology of cross-section near the inner surface of the HFM. The varying parameters are Q_p and L_a , which are mentioned on the SEM micrographs as Q_p/L_a , while Q_{N_2} and Q_w were kept 1 mL/min.

With increase in L_a , more evaporation of the volatile solvent increases the polymer concentration, which densifies the substructure near the inner surface of the HFM. The influence on the cross-section near the inner surface can be seen in Figure 5.3. At Q_p 1.5 mL/min, with increase in L_a from 5 to 15 cm the structure in the cross-section near the inner surface gets denser due

to the increase in total evaporation of solvent(s). A similar effect on the cross-sectional morphology can be observed with increase in polymer concentration and Q_p . A higher solution concentration and Q_p would yield a higher shear stress in the flow chamber of the spinneret and result in an increase in the alignment/packing of polymer chains, which also delays the intrusion of water. *E.g.*, at L_a 10 cm, with increase in Q_p from 1.5 to 2.5 mL/min the structure in the cross-section near the inner (Figure 5.3) and the outer surface (Figure 5.5) gets denser, which is also true for the overall cross-sectional morphology.

B. Influence on the morphology of outer surface

The effect of L_a (5-15 cm) on the outer surface and outer surface cross-section is not highly pronounced due to the coextrusion of water around the polymer solution while, as discussed in the previous section, the increase in Q_p shows a strong influence on membrane porosity.

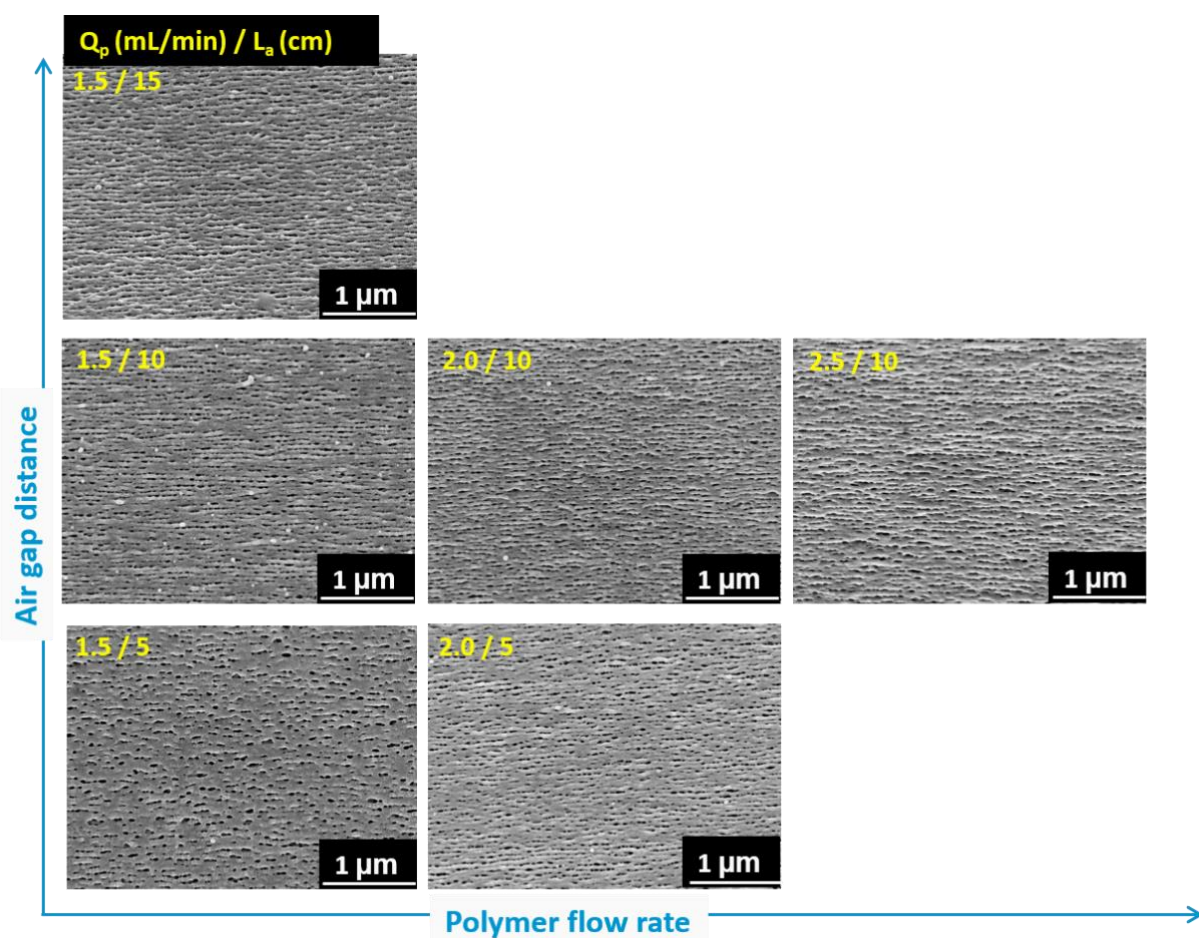


Figure 5.4. The SEM micrographs represent morphology of the outer surface of the HFM. The varying parameters are Q_p and L_a , which are mentioned on the SEM micrographs as Q_p/L_a , while Q_{N_2} and Q_w were kept 1 mL/min.

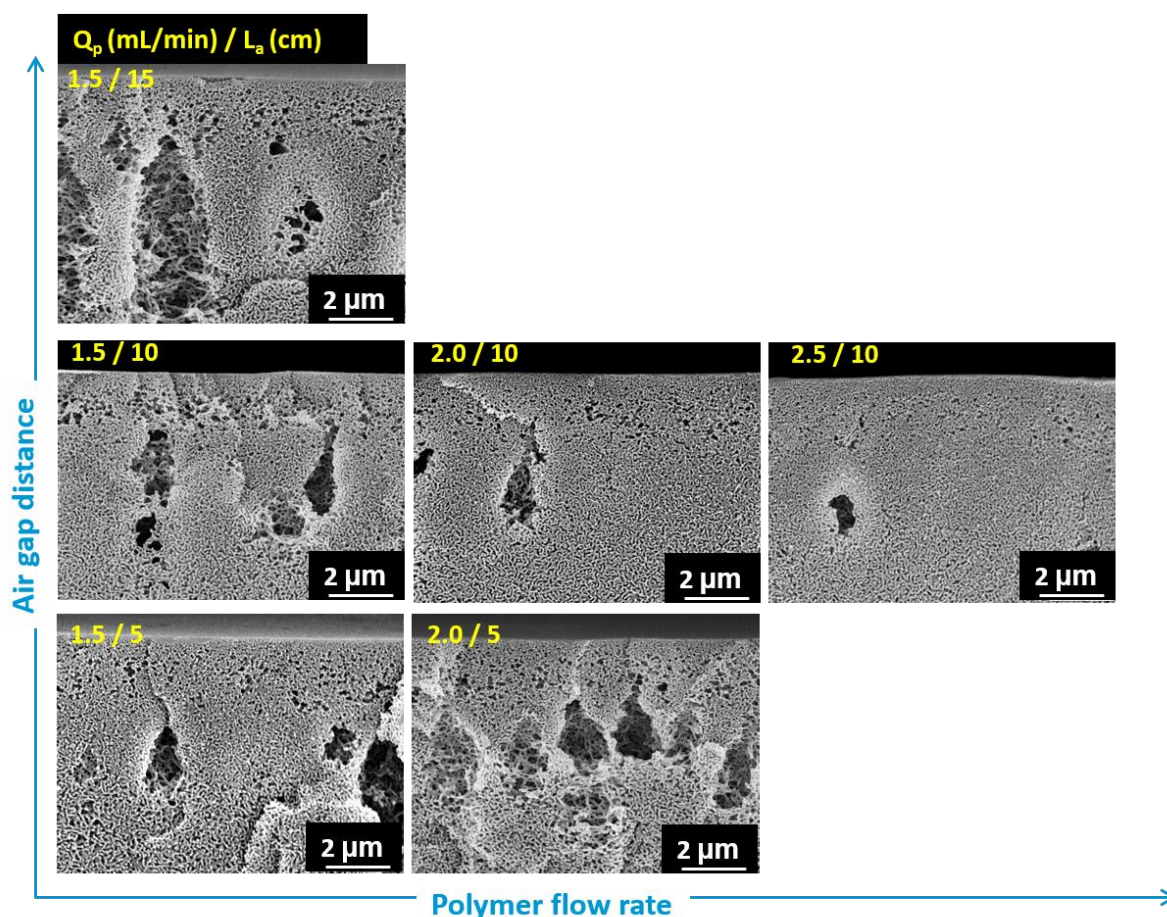


Figure 5.5. The SEM micrographs represent the morphology of cross-section near the outer surface of the HFM. The varying parameters are Q_p and L_a , which are mentioned on the SEM micrographs as Q_p/L_a , while Q_{N_2} and Q_w were kept 1 mL/min.

C. Optimized parameters

Figure 5.6 provides a complete overview of the structure of the inside-out isoporous HFM for the optimized spinning parameters of this particular block copolymer solution, which are Q_p 2 mL/min, Q_{N_2} 1 mL/min and circlet fluid (water) flow rate Q_w 1 mL/min, at L_a of 5 cm. The SEM micrograph of the inner surface displays the self-assembled pores. The cross-section near the isoporous inner surface of the HF shown in Figure 5.6 resembles a thin selective layer of a few nm on top of its membrane body. The elongated pores on the outer surface and an open spongy network of highly interconnected pores can be seen in the cross-section near the outer surface of the HF, respectively. The complete cross-section of the HF is of a uniform circular shape. As seen in the cross-section at higher magnification, the small voids near the outer surface are formed due to intrusion of water from the outer side of the HF. The position, size and

quantity of these voids differ with variation in L_a , Q_p , polymer concentration, solvent composition *etc.*^{202, 230}

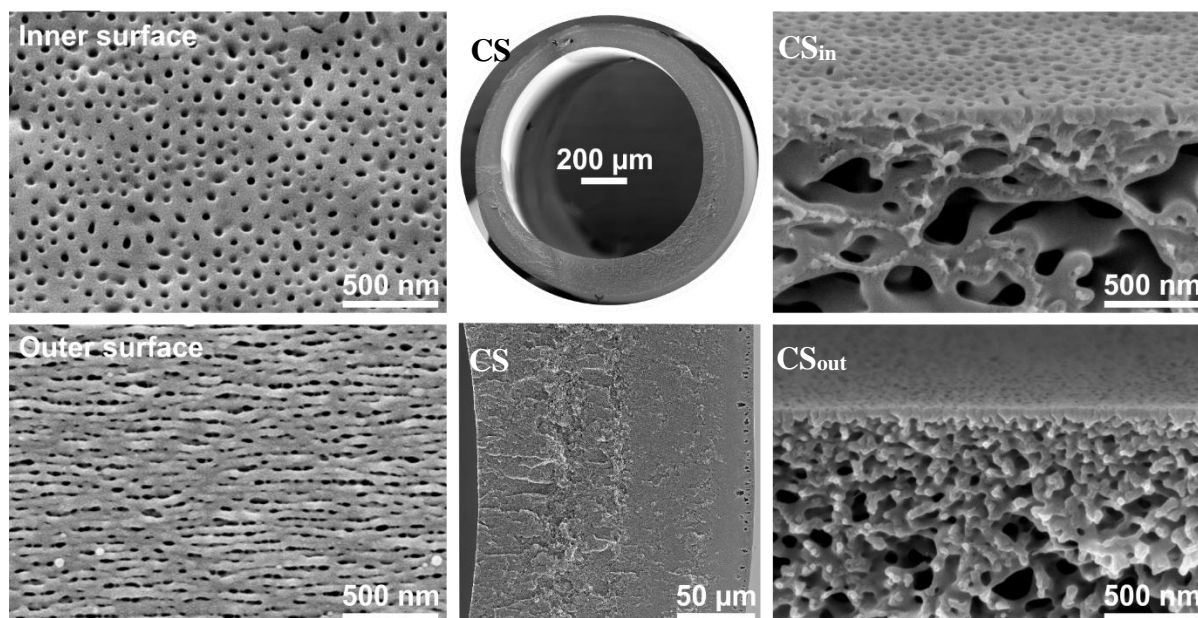


Figure 5.6. SEM characterization of the HF membrane spun from the polymer solution of a 27 wt% PS-*b*-P4VP₁₇¹³⁹ block copolymer in DMF/THF 50/50 (wt/wt). Spinning parameters were Q_p 2 mL/min; Q_{N_2} 1 mL/min; Q_w 1 mL/min; L_a 5 cm. CS represents cross-section, CS_{in} shows cross-section near the inner surface, and CS_{out} shows cross-section near the outer surface.

D. Other polymer solutions for isoporous hollow fiber membrane fabrication

The fabrication of inside-out isoporous membranes was also tried with different block copolymer solutions. A different block copolymer was dissolved in the solvent systems of DMF/THF 50/50 (wt/wt) and DMF/THF/DOX 33/33/34 (wt/wt/wt). The SEM micrographs in Figure 5.7 and 5.8 show the membrane morphology in different sections. For these membranes, the substructure morphology near the inner surface looks different from the one shown in Figure 5.3. The possible reason is the low wt% of P4VP in that block copolymer.

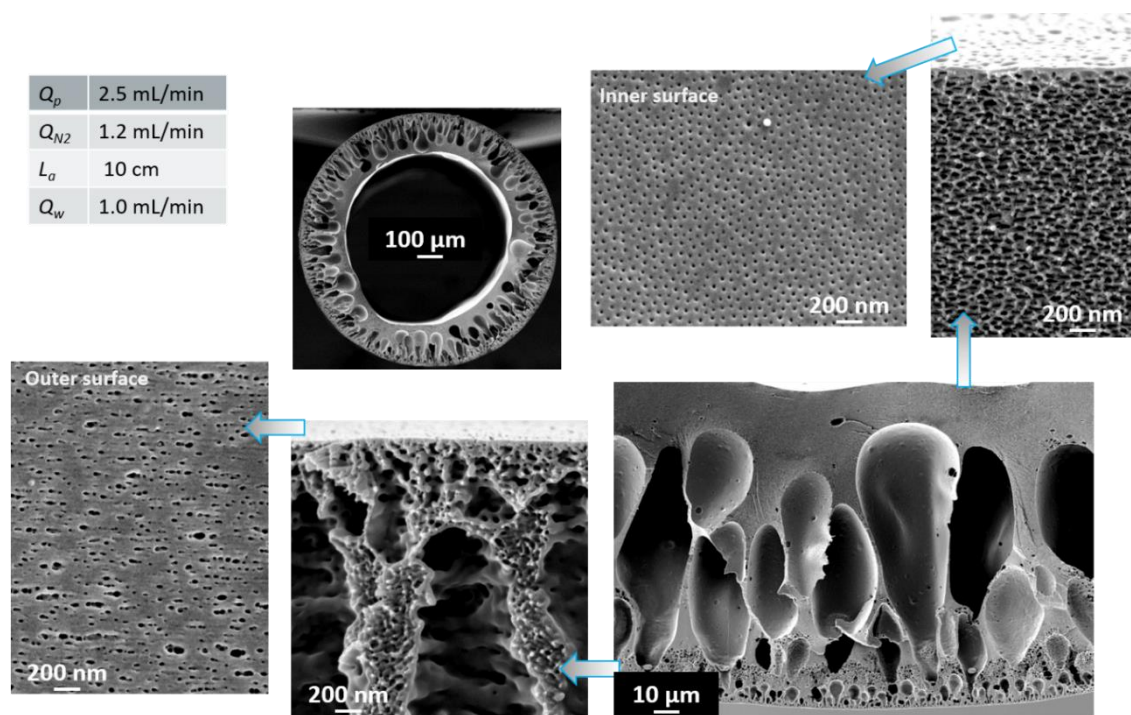


Figure 5.7. SEM micrographs represent the morphology of the cross-section near inner surface, the inner surface, the outer surface and cross-sectional view of the HF membrane. The HFM were spun from the polymer solution of a 30 wt% PS-*b*-P4VP₁₄⁸⁹ block copolymer in DMF/THF 50/50 (wt/wt). Spinning parameters were Q_p 2.5 mL/min, Q_{N2} 1.48 mL/min, Q_w 1 mL/min and L_a 5 cm.

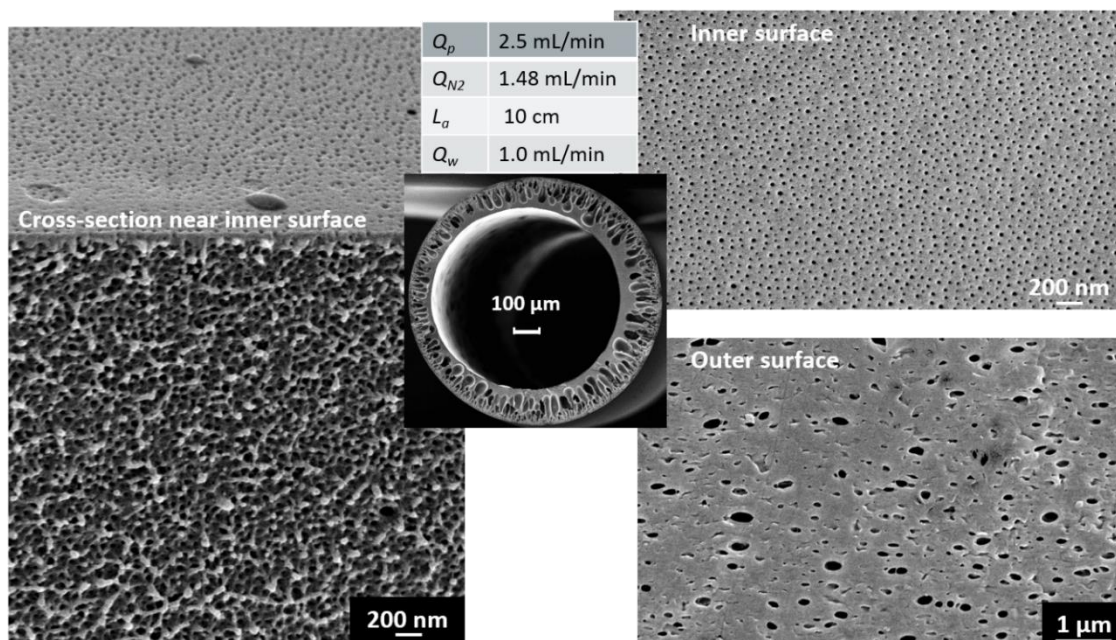


Figure 5.8. SEM micrographs represent the morphology of the cross-section near inner surface, the inner surface, the outer surface and cross-sectional view of the HF membrane. The HFM were spun from the polymer solution of a 30 wt% PS-*b*-P4VP₁₄⁸⁹ block copolymer in DMF/THF/DOX 33/33/34 (wt/wt/wt). Spinning parameters were Q_p 2.5 mL/min, Q_{N2} 1.48 mL/min, Q_w 1 mL/min and L_a 5 cm.

5.4. Membrane characterization

The membrane performance was checked for the optimized inside-out isoporous HFM, as shown in Figure 5.6. The spinning parameters were Q_p 2 mL/min, Q_{N_2} 1 mL/min, Q_w 1 mL/min, and L_a 5 cm. The volumetric water flux (J_v) for these membranes is $170 \pm 20 \text{ L m}^{-2} \text{ h}^{-1} \text{ bar}^{-1}$, which was measured in dead end-mode, at 2 bar transmembrane pressure. The inside-out isoporous HFM showed $92 \pm 2 \%$ retention for PEG molecules of M_w 400 kDa. The retention experiments were conducted in cross-flow mode.

5.5. Conclusion

This chapter showed the possibility to fabricate inside-out isoporous HFM. The gas flow in the lumen side is required to trigger the microphase separation that was quenched by controlled macrophase separation in the precipitation bath. The key to this development is the ability to control the formation of an isoporous structure *via* the SNIPS method in the dynamic process of dry-jet wet HF spinning by introducing a precise gas flow in the lumen of the nascent fibers. The interplay between evaporation of volatile solvent from the inner surface and intrusion of water from outside to the inside of the HF is controlled. The membrane exhibits similar structural properties analogous to those seen for outside-in isoporous HFM.

6. Fabrication of inside-out isoporous composite hollow fiber membranes

In this chapter, a successful method to develop isoporous structures in compact geometries is highlighted by introducing an inside-out configuration of isoporous composite HFM. For this work, a highly permeable and robust PES HFM with an inner diameter of approx. 1 mm is selected as a compact geometry. The isoporous structures are developed on top of a thin coated layer ($\leq 10 \mu\text{m}$) by depositing a thin selective layer of dilute block copolymer solutions onto the lumen side of PES support HFM, followed by the SNIPS method. The solvent selectivity of blocks and the consequential segmental incompatibility enable the use of a wide range of block copolymer concentrations to achieve an isoporous surface that can further be controlled by other coating parameters. SEM and TEM helped to elucidate the coating mechanisms and adhesion of two chemically distinct polymer layers. The highly asymmetric membrane has a significant difference in pore sizes on the inner and the outer surfaces from ca. 25 nm to 2.5 μm , respectively, and shows water flux of $260 \pm 50 \text{ L m}^{-2} \text{ h}^{-1} \text{ bar}^{-1}$ and MWCO of 300 kDa for PEG.

Reprinted with permission from the research article:

“Setting the Stage for Fabrication of Self-Assembled Structures in Compact Geometries: Inside-Out Isoporous Hollow Fiber Membranes”, Kirti Sankhala, Joachim Koll, Volker Abetz, *ACS Macro Letters* 7 (7), 840-845, 2018; (<https://pubs.acs.org/doi/10.1021/acsmacrolett.8b00402>)

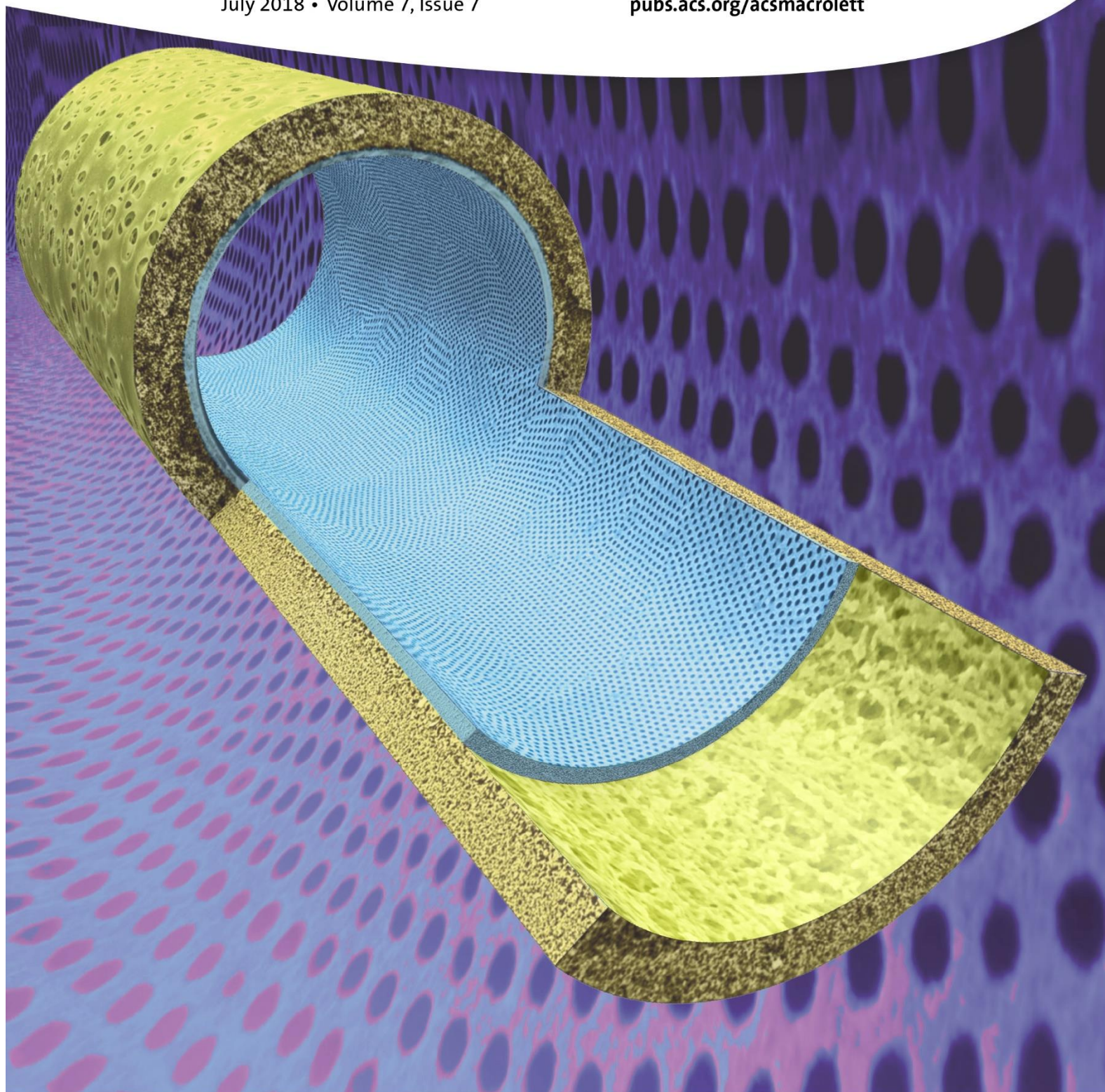
Cover Picture: *ACS Macro Letters* 7 (7), 2018

Copyright © 2018, American Chemical Society

ACS *Macro Letters*

July 2018 • Volume 7, Issue 7

pubs.acs.org/acsmacrolett



ACS Publications
Most Trusted. Most Cited. Most Read.

www.acs.org

The inside-out isoporous HFM reported in the previous section conveyed the notion to control over self-assembly by using N_2 flow for the first time, especially during the complex dynamic process of HF spinning. However, the high costs and mechanical strength of integral asymmetric block copolymer HFM is quite a challenge. In order to solve these issues, previously dual-layer composite HFM were proposed by spinning and coating methods in outside-in HFM configuration. The spinning process requires a certain concentration of the block copolymer to attain enough viscoelasticity in the polymer solution for the continuous extrusion. In addition, a big variation in spinning parameters is restricted as the process involves significant viscous stresses on the polymer chains during extrusion, thus the fabrication of dual-layer isoporous HFM remains expensive.^{170, 208} This makes the preparation of composite membranes *via* coating of dilute block copolymer solutions onto a mechanically stable and inexpensive support HF a method of choice. The additional advantages of block copolymer coating are that it can be processed easily onto the support membrane matrix owing to the solvent or solvent mixture in the solution, which helps to coat the irregular surfaces and small defects. However, the requirement of comparatively less concentrated block copolymer solution to pass through the compact geometries significantly reduces the stimulations required for self-assembly. The high polymer relaxation rates and decreased thermodynamic driving forces, as well as high capillary suction of dilute solutions in the porous substrates complicates the block copolymer self-assembly and fabrication of uniform coated layer, respectively.

In this chapter, a successful method to develop inside-out isoporous composite HFM is discussed, introducing a technologically favored inside-out configuration for isoporous composite HFM with large bore diameters. The membranes were prepared by depositing a thin selective layer of dilute block copolymer solutions onto the lumen side of a mechanically robust PES support HFM, afterwards the conditions required to complete the SNIPS process were studied.

The highly influencing and interrelated factors such as substrate properties (hydrophilicity or hydrophobicity, roughness on the inner surface, and porosity), composition of the coating solution, polymer solution flow rate Q_p , time for polymer solution flow t_p , N_2 flow rate Q_{N_2} , time for N_2 flow t_{N_2} , and water flow rate Q_w make this system of pumping coating solution in the lumen side intricate and demanding. For the sake of easy understanding, each influencing factor is discussed in the following sections.

6.1. Influence of substrate hollow fiber membrane

The key question in this study sought to get robust support membranes providing as high flux as possible along with a surface compatible with the coating solution. The inner surface, the porosity of the substructure near the inner surface, and the fiber diameter of support membranes are key parameters in fabrication of composite membranes. In contrast with the outside-in composite membranes, here, the capillary force acting on the polymer solution in the fiber-lumen makes the system different and more challenging. The capillary force in the lumen influences the thickness of the coated layer, which is controlled by the bore gas flow. Moreover, the capillary behaviour of pores affects the intrusion of polymer solution and changes the porosity of the support membrane. So, for easy flow of a polymer solution through the fiber lumen, it is preferred to have fibers of bore diameter ≥ 1 mm. The porosity and solubility of substrate HFM have an influence on the substructure of the coated block copolymer layer as well, where a slight intrusion of block copolymer solution into the support assures a strong adhesion of the two chemically distinct polymers.

Support membranes

In order to achieve the separation on the top surface of the final integral asymmetric block copolymer layer on the lumen side and to reduce the hydraulic resistance, highly porous PES HFM were selected as substrate. The coating process is applicable to a wide range of polymers, *e.g.* PES, PVDF, PEI, *etc.* PVDF HFM has been reported for coating of block copolymer solutions on the outer side of HFM.^{194, 209} The coating on the lumen side of PEI HFM is possible without any pretreatment but due to the very low water flux the PEI HFM were not considered for this study. In this work, two different commercial PES HFM were chosen to validate our process; PES1 and PES2 HFM. The morphological characterization of these membranes is done by SEM, as shown in Figure 6.1.

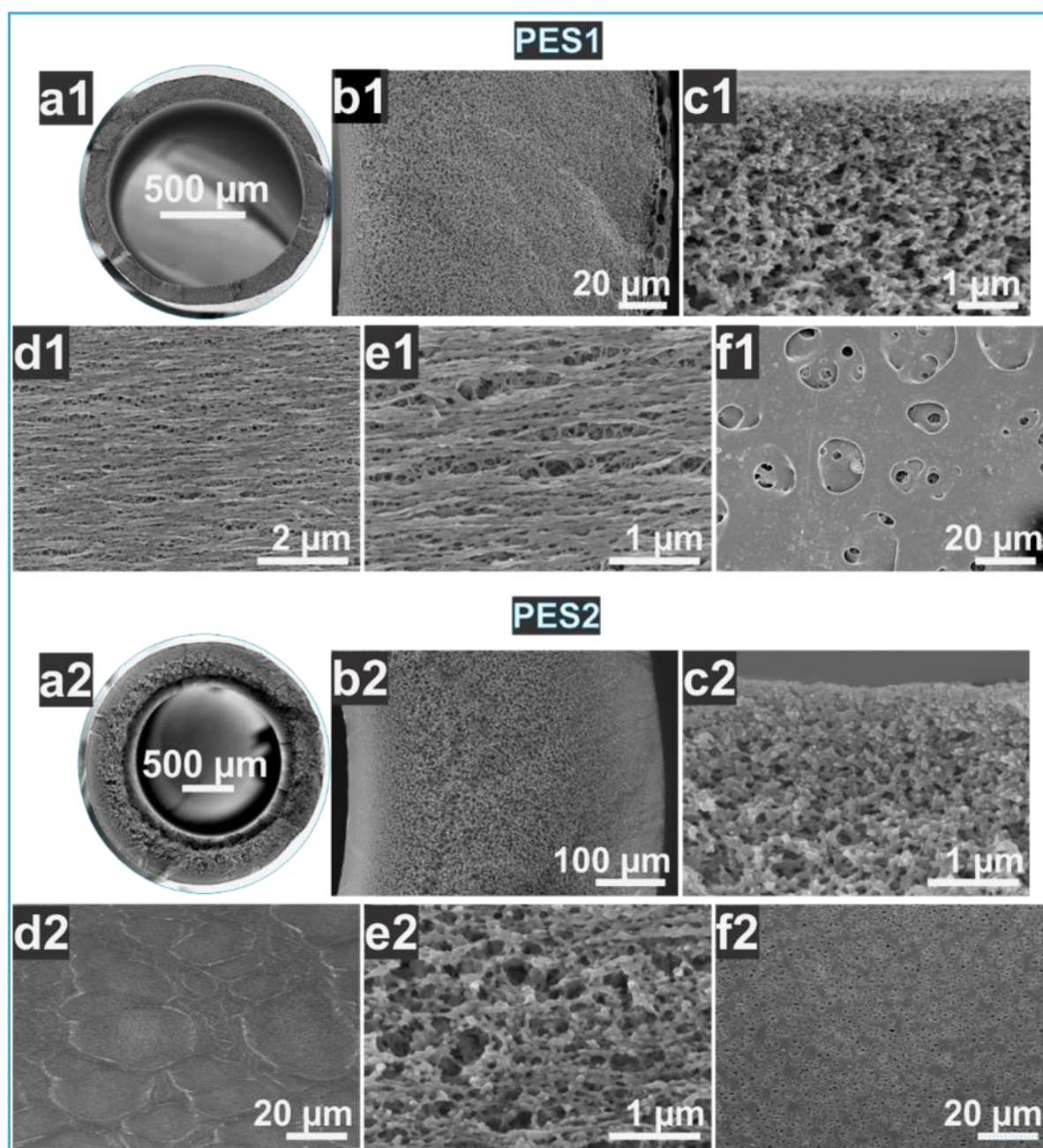


Figure 6.1. SEM micrographs of two different pristine support membranes used in this study. (a1-f1) PES1 HFM. (a2-f2) PES2 HFM. (a1,b1,a2,b2) Cross-section of the support HFM. (c1,c2) Cross-section near the inner surface. (d1,e1,d2,e2) Inner surface. (f1,f2) Outer surface.

The PES1 support membranes were purchased from Spectrum Labs, Germany, which have an inner diameter of 1 mm and MWCO 750 kDa (as mentioned by the supplier). The water flux for these membranes is ca. $2000 \text{ L m}^{-2} \text{ h}^{-1} \text{ bar}^{-1}$. The PES2 support membranes were kindly provided by Cut Membrane Technology GmbH, Germany. The PES2 support membranes have an inner diameter of 1.5 mm and the pore size on the inner selective surface is ca. $0.2 \text{ } \mu\text{m}$ (as mentioned by the supplier). The water flux for these membranes is ca. $500 \pm 100 \text{ L m}^{-2} \text{ h}^{-1} \text{ bar}^{-1}$.

¹. Both PES1 and PES2 membranes were measured at 2 bar transmembrane pressure, in dead end-mode, in inside-out direction using a home-made laboratory scale automatic water-flux measurement set-up. Prior to coating, these commercially available high flux support HFM were rinsed with 30 wt% hydrogen peroxide (H₂O₂) solution several times and then immersed for one hour in H₂O₂ solution in order to clean the inner surface and remove the influence of surface-treatments on commercial fibers, if there are any. Afterwards, the HFM were washed using water and dried at room temperature. These HFM show improved surface wettability for block copolymer solutions.

Pretreatment of substrate fibers

The substrate fibers can be pretreated prior to conveying the coating solution in order to reduce the suction of block copolymer solution in the porous support.²⁰⁹ The pretreatment agents are required to have good miscibility with the solvent used in the coating solution and are preferred to be a non-solvent for the support HF. Unfortunately, PES highly swells in organic solvents such as DOX and then shrinks during precipitation which also increases the strain between these two differently porous PES and block copolymer layers. The difference in the substructure which is more tightly packed near the inner surface and still more open afterwards tend to tear off the top surface; the PES2 support membranes were more tightly packed near the inner surface as compared to PES1. While the pretreatment using a non-solvent such as PEG or glycerine hinders the further adhesion on the inner surface. Therefore, the selection of an appropriate support membrane and the pretreatment agent is very important.

6.2. Fabrication of inside-out composite hollow fiber membrane

The selective skin layer of the composite ultrafiltration membrane was prepared on the inner surface of the PES HF substrate *via* pumping coating. A schematic depiction of the coating process on the lumen side of a support HF is provided in Figure 6.2. The first step is the preparation of a module holding support HFM (Figure 6.2 a); the details about module fabrication are given in Section 9.8. Afterwards, three fluids were subsequently introduced into the lumen side of the substrate fibers for a certain time. 1) The polymer solution, which consists of PS-*b*-

P4VP diblock copolymer in DOX or DOX/DMF as coating material (Figure 6.2 b). 2) The gas flow (mainly N_2), to remove superfluous polymer solution and to provide sufficient evaporation conditions required for block copolymer self-assembly (Figure 6.2 c). 3) Water, to allow precipitation of the coated layer and complete the exchange of solvents by non-solvents (Figure 6.2 d). To control the flow rates micro-precision pumps were used. The HFM with the thin film selective layer were then washed and kept in DI water. After solvent removal, the membranes were kept at room temperature for 24 h for drying. The performance tests were conducted with a wet membrane while for microscopical characterizations the membranes were kept in an oven for graded drying up to 60 °C.

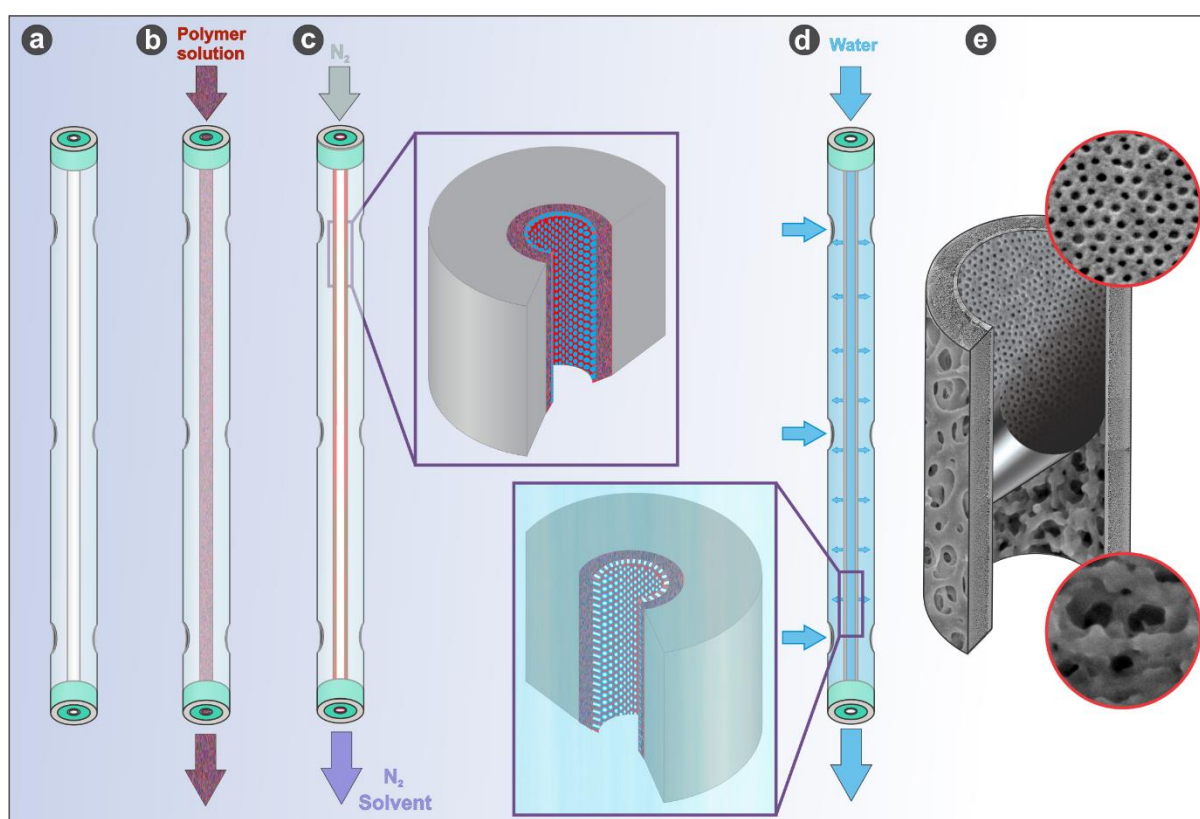


Figure 6.2. (a-d) A schematic diagram demonstrating the mechanism of inside-out isoporous composite HFM fabrication. (a) A module holding H_2O_2 treated PES support HFM. (b) The block copolymer solution is then pumped into the lumen of support fiber. (c) Afterwards, N_2 is conveyed in the lumen; the enlarged section shows the microphase separation on the lumen side. (d) Then, the coated fiber is exposed to water flow, and the enlarged section displays the pore opening on the inner surface of composite membrane. (e) The scheme of coated HFM.

6.3. Selection of polymer solution and the structure formation

The self-assembly and isoporous structure formation requires selecting a suitable block copolymer solution since this parameter governs the membrane morphology, solubility and diffusivity in the support membrane, which in fact affect the complete membrane morphology and the performance. Moreover, uniform coating without dewetting or suction of the polymer solution remains the main challenge in coating of highly porous support HF. Here, we used PS-*b*-P4VP₁₇¹⁶⁸ (subscripts denote the amount of respective block in wt% and superscript denotes the total molecular weight in kg mol⁻¹). In the common isoporous membrane fabrication, 15-35 wt% block copolymer is dissolved in the solvent mixture of DMF/THF or DMF/THF/DOX.^{169, 182, 231} However, such viscous solutions cannot be easily pumped through a HFM. Since self-assembly is a result of segmental incompatibility between the repulsive blocks, therefore, by selecting a right solvent or solvent mixture the structure formation in solution can be influenced. The micellar structures can be achieved in 1-3 wt% of PS-*b*-P4VP solution using DOX as a solvent offering rather rigid micellar cores for P4VP.¹⁸⁶ As DOX is selective for PES substrate and thus penetrates into it, the block copolymer concentration in the coating solution increases which enhances the microphase separation. It was not possible to obtain open pores using DOX solutions with 1-8 wt% of block copolymer concentration and evaporation times of 10-60 s for both PES1 and PES2 HFM (Figure 6.3). These fibers became impermeable. A possible reason could be the slow evaporation rate in the lumen side which leads to almost closed domains of P4VP on the top surface, as compared to using DOX as a single solvent in flat sheet membrane fabrication by blade casting¹⁸⁶ or by spray coating¹⁴³. Moreover, here, the absence of a commonly used more volatile cosolvent (THF) lacks a strong, highly directional field due to a fast increase in concentration gradient from the top surface, leading to a lesser segregated system and overall a comparatively relaxed system for self-assembly.^{103, 110, 112, 155} Consequently, an increased swelling of the P4VP blocks was required. In this case, a block copolymer of lower molecular weight of ca. 100 kDa and higher P4VP segments of ca. 25 wt% might lead to isoporous structures due to higher mobility or faster self-assembly of shorter chains.

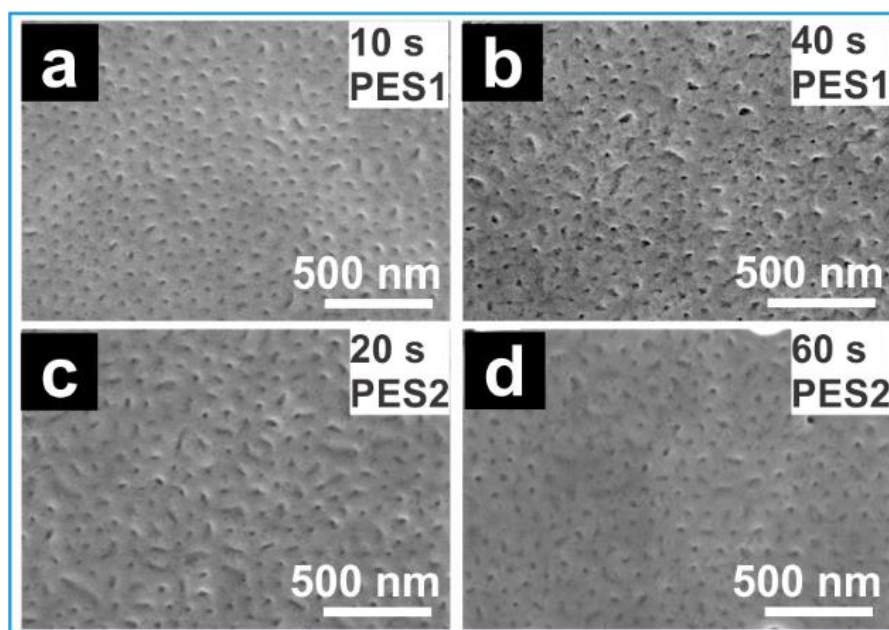


Figure 6.3. The SEM micrographs show inner surface morphology of HFM coated using a solution of 2 wt% PS-*b*-P4VP¹⁶⁸ block copolymer in DOX, where Q_p : 1.0 mL min⁻¹; t_p : 10 s; Q_{N2} : 1.0 mL min⁻¹; t_{N2} : as mentioned on the micrograph; and Q_w : 3.0 mL min⁻¹. (a,b) PES1 HFM. (c,d) PES2 HFM.

In order to increase swelling of the P4VP blocks, 5-10 wt% of DMF was added in the DOX solutions. The addition of DMF increases the solubility of P4VP blocks and the micellization decreases; due to which the ordering transition in the solution shifts towards higher polymer concentration (Figure 6.4).

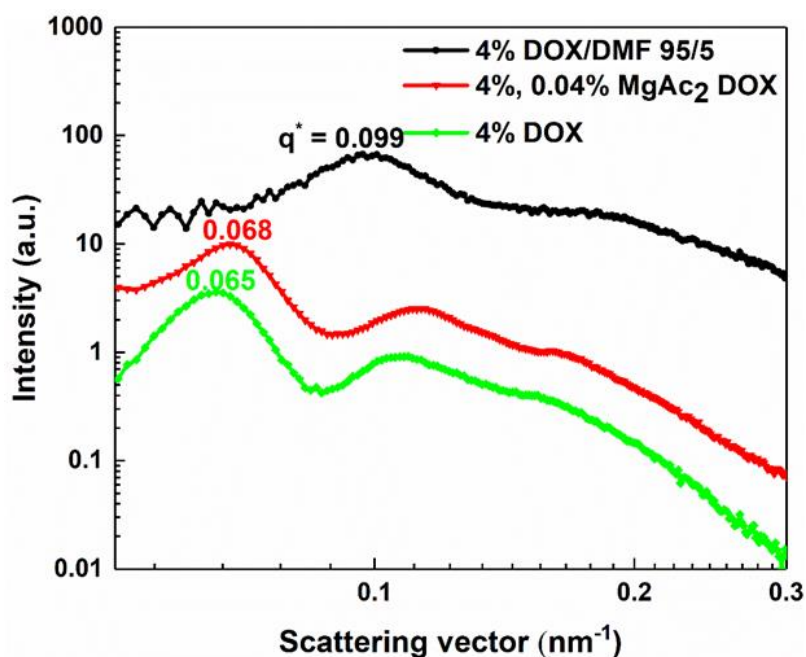


Figure 6.4. SAXS patterns of polymer solutions having 4 wt% PS-*b*-P4VP₁₇¹⁶⁸ block copolymer (one with 0.04% MgAc₂) in DOX and solvent mixture of DOX/DMF 95/5 wt%. The curves are plotted in log/log scale and the y-offset is adjusted for better visibility.

The addition of 5-10 wt% DMF in DOX solution leads to dissolution of the inner skin of the support fiber instead of only swelling it. The main work was focused on the more robust PES2 HFM because the highly porous and thinner PES1 HFM dissolves too fast in the DMF of the coating solutions. The influence of varying the time of N₂ flow (20 and 40 s) between solvent flow (DOX/DMF 90/10 (wt/wt) for 10 s) and water flow can be seen as the dissolution of the inner surface and membrane permeability (Figure 6.5).

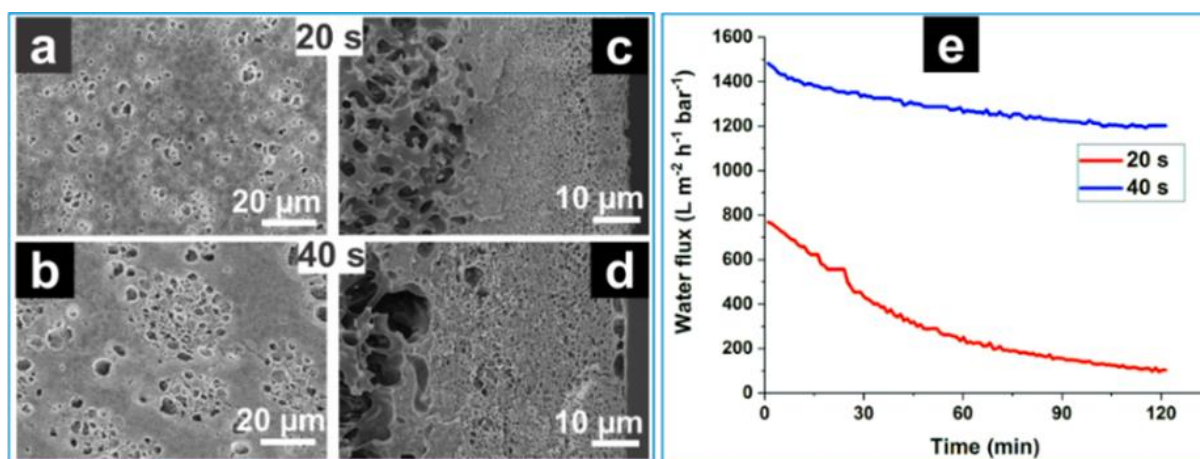


Figure 6.5. Influence of DOX/DMF 90/10 (wt/wt) on PES2 substrate HFM. (a,b) Inner surface morphology. (c,d) Cross-section near the inner surface. (e) Water flux measurements. The parameters were as following, solvents flow rate Q_s : 1.0 mL min⁻¹; flow time for solvents t_s : 10 s; Q_{N_2} : 1.0 mL min⁻¹; t_{N_2} : 20 s (a,c) and 40 s (b,d); and Q_w : 3.0 mL min⁻¹.

By selecting the right block copolymer solution of 4 wt% PS-*b*-P4VP₁₇¹⁶⁸ in DOX/DMF 90/10 and suitable coating parameters, isoporous structures could be fabricated on the inner surface (Figure 6.6).

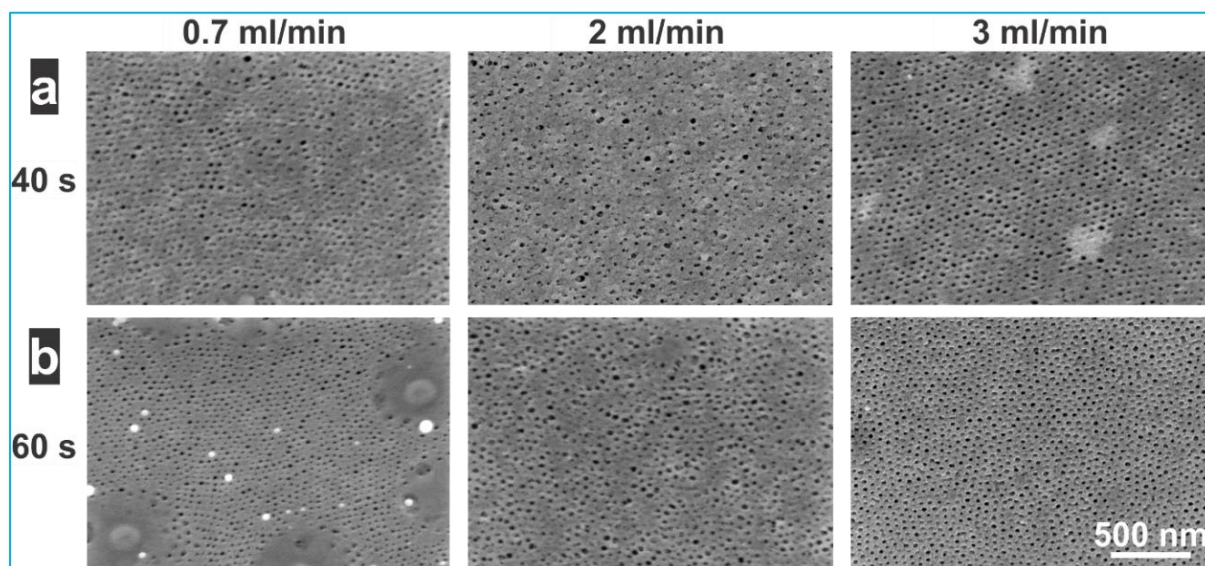


Figure 6.6. The SEM micrographs show the morphology of the inner surface of the coated membranes. The H_2O_2 treated PES2 HFM were coated with the polymer solution of 4 wt% PS-*b*-P4VP₁₇¹⁶⁸ in solvent mixture of DOX/DMF 90/10 (wt/wt). The coating parameters were Q_p : 1.0 mL min⁻¹; t_p : 10 s; Q_{N2} (0.7 mL min⁻¹, 2.0 mL min⁻¹, and 3.0 mL min⁻¹); t_{N2} (40 s and 60 s); and Q_w : 3.0 mL min⁻¹. All micrographs have the same scale bar.

As discussed in Chapter 3, the PS-*b*-P4VP supramolecular assemblies can be facilitated by addition of metal salts. The SAXS results in Figure 6.4 show that the addition of MgAc₂ (1 wt% of block copolymer concentration) increases the structure ordering with a shift of the maxima in SAXS towards higher scattering vectors and thus decreases the domain spacing. The slightly more viscous block copolymer solution showed good spreading and controlled sinking of the solution into the HF support without dewetting and resulted in a uniform coated layer. For the used block copolymer and PES2 HFM, the optimized polymer solution is 4 wt% PS-*b*-P4VP₁₇¹⁶⁸ and 0.04 wt% MgAc₂ in the solvent mixture of DOX/DMF 90/10 (wt/wt). The optimized solution is still comparatively dilute for self-assembly which leads to high relaxation rates of the macromolecules and therefore requires a good control over kinetics and thermodynamics of microphase separation, as schematized in Figure 6.2. The successful fabrication of an isoporous structure on the inner surface is shown in Figure 6.7 for the varying coating parameters.

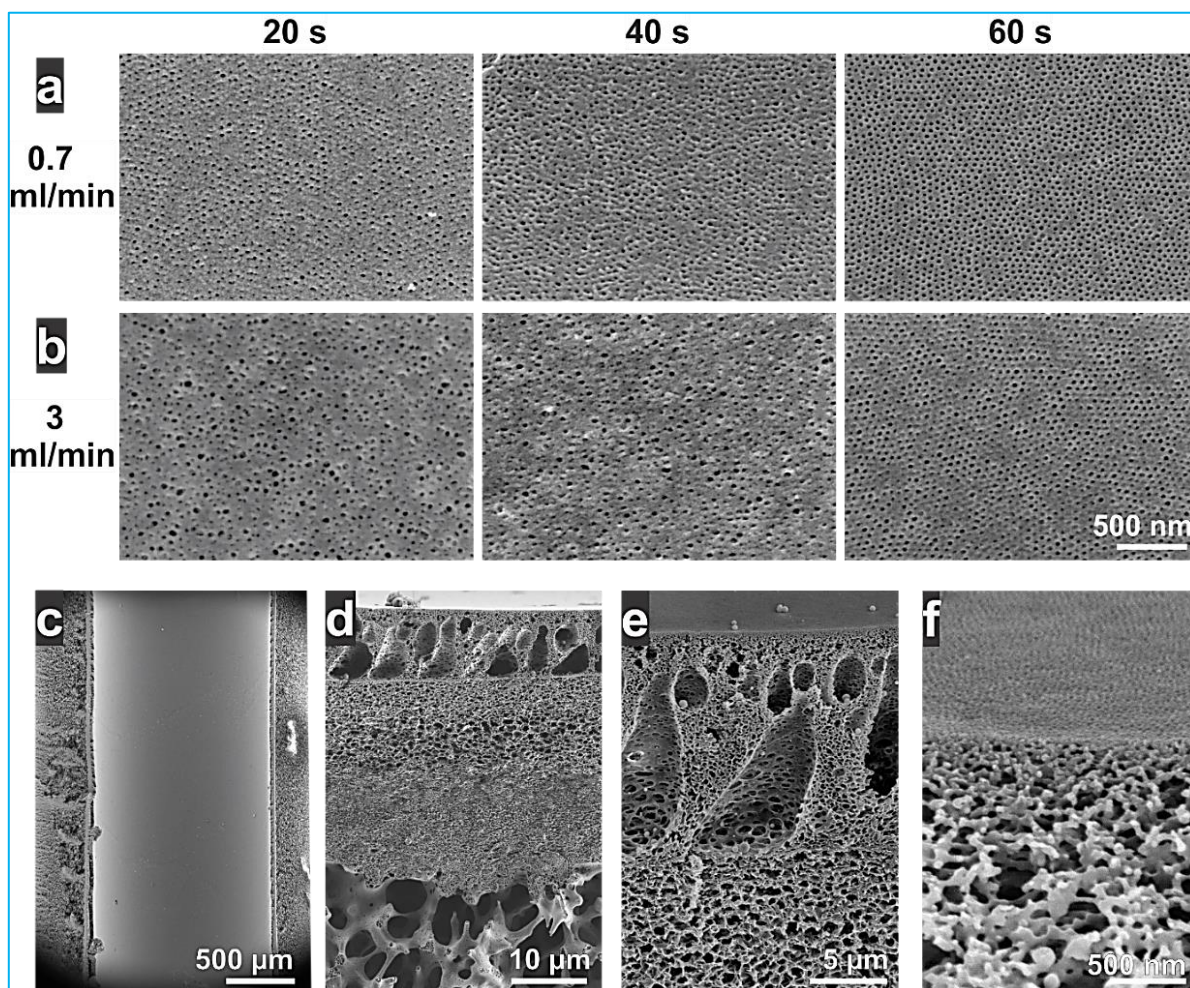


Figure 6.7. The H_2O_2 treated PES2 membranes were coated with the polymer solution of 4 wt% PS-*b*-P4VP₁₇¹⁶⁸ and 0.04 wt% MgAc_2 in solvent mixture of DOX/DMF 90/10 (wt/wt). (a,b) The SEM micrographs show the morphology of inner surface of HFM. The coating parameters were Q_p : 1.0 mL min^{-1} , t_p : 10 s, Q_{N2} (0.7 and 3.0 mL min^{-1}) and t_{N2} (20 s, 40 s and 60 s), and Q_w : 3.0 mL min^{-1} ; all micrographs have the same scale bar. (c) The inner view of the coated HFM. (d-f) The SEM micrographs show the cross-sectional morphology where thickness of the coated layer is around 10 μm . (c-f) The coating parameters were Q_p : 1.0 mL min^{-1} , t_p : 10 s, Q_{N2} : 0.7 mL min^{-1} , t_{N2} : 60s, and Q_w : 3.0 mL min^{-1} .

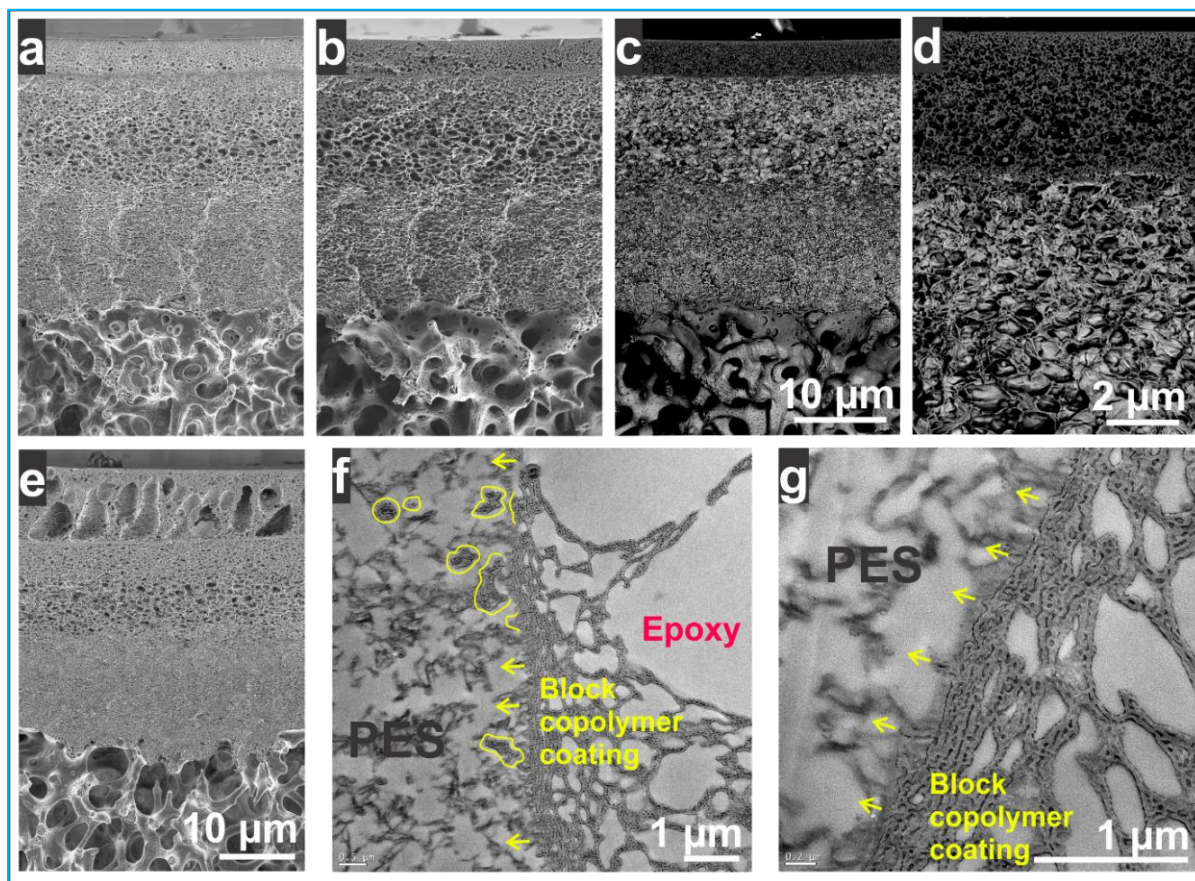


Figure 6.8. The PES2 HFM were coated with the solution of 4 wt% PS-*b*-P4VP₁₇¹⁶⁸ and 0.04 wt% MgAc₂ in solvent mixture of DOX/DMF 90/10 (wt/wt). Thickness of the coated layer is ca. 5 μm. The coating parameters were Q_p : 1.0 mL min⁻¹, t_p : 10 s, Q_{N2} : 1.0 mL min⁻¹, t_{N2} : 60s, and Q_w : 3.0 mL min⁻¹. (a,e) SEM micrographs show the surface of the cross-sectional morphology by using in-lens detector. (b) Topographical image using secondary electron detector (HE-SE2). (c,d) The compositional contrast is shown by energy specific separation of backscattered electrons using energy selective backscattered electrons (EsB) detector. Micrographs a-c have the same scale bar. (f,g) Bright-field TEM images of cross sections from I₂-stained films showing the interface of PES support and coating layer. The selectively stained P4VP domains appear black and PS is dark grey. The yellow arrows and marked areas show intrusion of block copolymer into the PES matrix by forming connected pores.

6.4. Coating parameters influencing the fabrication of composite isoporous hollow fiber membranes

The homogeneous PS-*b*-P4VP₁₇¹⁶⁸ block copolymer solution was incorporated into the lumen side of PES support HF (Figure 6.2 b) using a high precision pump. Here, polymer solution flow rate Q_p and time for flow t_p influence the intrusion of block copolymer solution into the support membrane due to the capillary forces in the lumen side. Therefore, in order to reduce

the time t_P required to fill the fiber lumen and complete wetting of the inner skin with polymer solution a certain Q_P is required. Otherwise, either pinholes generate on the inner surface due to the capillary suction of polymer solution or more intrusion of solution into the substructure will result in a rather dense interface due to more dissolution of the PES inner layer and will further deform the support. After some preliminary coating experiments with the selected PES2 support membranes, Q_P was fixed to 1 mL min^{-1} for t_P 10 s. The controlled dissolution of the inner skin of PES HF and intrusion of block copolymer solution confirm the attachment of the two chemically distinct polymer layers with interconnected pores (Figures 6.8 f and g).

Afterwards, N_2 flow is conveyed in the fiber lumen which is full of polymer solution (Figure 6.2 c) to remove the excess polymer solution while allowing a fine coating of block copolymer solution on the inner surface. The kinetics of the block copolymer chains and their self-assembly is influenced by the rate of evaporation which is controlled by Q_{N_2} , while the evaporation time is controlled by t_{N_2} . With increasing t_{N_2} , the increased dissolution of the inner skin of the PES HF deforms the inner surface morphology and changes membrane performance (Figure 6.5). The development of structure and increasing segregation of the block copolymer with increasing Q_{N_2} and t_{N_2} is shown in Figures 6.6 and 6.7. It was observed that Q_{N_2} higher than 1.0 mL min^{-1} tends to tear off the inner layer of PES2 support HFM, however, the self-assembly and isoporous structure formation is facilitated. Thus a support HFM having an asymmetric open porous structure is suitable for such coating experiments instead of the one having a tightly packed substructure near the inner surface. Further, depending on the non-uniform porosity on the inner surface of the support membrane and the coating solution, the coated layer provides spongy or macrovoid substructures (Figures 6.8 a and e). Therefore, for the optimized polymer solution and the used PES 2 support HFM, we optimized Q_{N_2} as $0.7\text{-}1.0 \text{ mL min}^{-1}$, and the evaporation time around 60 s for the fabrication of a smooth, uniform and well attached isoporous coating layer on the lumen side (Figures 6.7 and 6.8).

After providing sufficient evaporation in a controlled manner for a predetermined period, water is introduced in the lumen in order to freeze the isoporous structure and complete the exchange of solvents by non-solvent water (Figure 6.2 d). Here, the flow rate drives the exchange rate of solvents by non-solvent, so, a higher flow rate is preferred, *i.e.*, Q_w 3.0 mL min^{-1} , to provide enough non-solvent for replacing the solvents in a short time. Afterwards, the module is being immersed into the coagulation bath of water for another 48 h.

6.5. Membrane performance

The novel composite membranes show a promising initial water flux ($J_{v\ composite}$) of 260 ± 50 L m^{-2} h^{-1} bar^{-1} in wet conditions and has MWCO 300 kDa for PEG molecules. Figure 6.9 shows a similar flux tendency for pristine and coated membranes and the MWCO is similar to previously reported isoporous membranes of similar pore size. This proves the defect free fabrication of composite isoporous HFM.

A. Membrane water flux

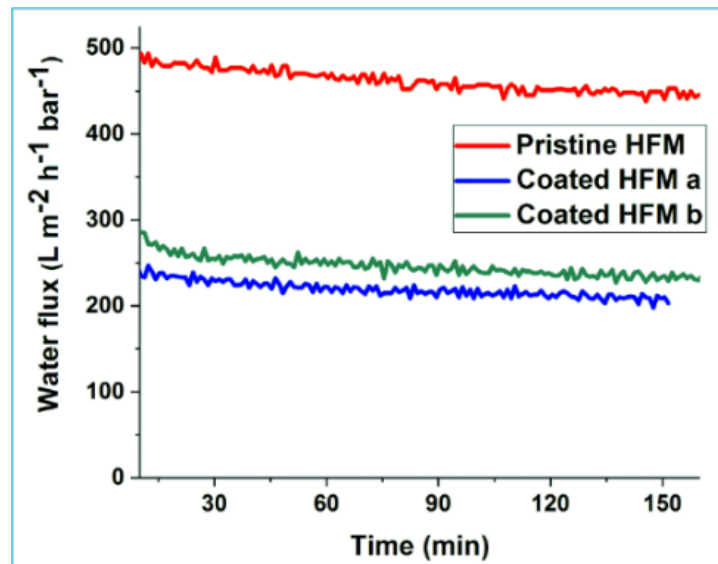


Figure 6.9. Comparison of water flux measurements for pristine and composite HFM. The H_2O_2 rinsed PES2 HFM (pristine) were coated with the polymer solution of 4 wt% PS-*b*-P4VP₁₇¹⁶⁸ and 0.04 wt% MgAc₂ in a solvent mixture of DOX/DMF 90/10 (wt/wt). The coating parameters were set to Q_p : 1.0 mL min^{-1} , t_p : 10 s, t_{N2} : 60s, and Q_w : 3.0 mL min^{-1} . Q_{N2} was varied as 0.7 mL/min (coated HFM a) and 1.0 mL min^{-1} (coated HFM b). On average, the PES2 and coated HFM show water flux ca. 500 ± 100 L m^{-2} h^{-1} bar^{-1} and 260 ± 50 L m^{-2} h^{-1} bar^{-1} , respectively.

B. Membrane water flux from the block copolymer layer

By considering the two layers of composite membranes contributing to the total resistance of flow, a two-resistor series model can be applied:

$$\frac{1}{J_{v\ composite}} = \frac{1}{J_{v\ PES}} + \frac{1}{J_{v\ BCP}} \quad (7)$$

Where, $J_{v\ composite}$: water flux of composite HFM ($260\text{ L m}^{-2}\text{ h}^{-1}\text{ bar}^{-1}$) and $J_{v\ PES}$: water flux of pristine PES2 HFM ($500\text{ L m}^{-2}\text{ h}^{-1}\text{ bar}^{-1}$). This provides the water flux from block copolymer layer ($J_{v\ BCP}$) of ca. $540\text{ L m}^{-2}\text{ h}^{-1}\text{ bar}^{-1}$. This supports the statement that with decreasing the layer thickness we could increase the water flux.

For $J_{v\ composite}$, the flow resistance contributed by the support HFM is calculated as 52% of the overall resistance.

C. Membrane water flux from the active layer predicted by Hagen-Poiseuille Equation

In order to evaluate the experimentally obtained water flux (J_v) of the composite membrane the the Hagen-Poiseuille law for a laminar flow in simple straight cylinders was applied to the structural features of optimized composite HFM, assuming that the flux is mainly hindered by the most active top layer (as discussed in Section 1.2.5).

$$J_v = -N_p \cdot \frac{\pi D^4}{128 \eta l} \cdot \Delta p \quad (4)$$

Where, N_p : the average number of pores per unit area on the membrane surface; r : the pore radius; Δp : pressure drop; η : viscosity of water ($8.94 \times 10^{-4}\text{ Pa s}$ at $24\text{ }^\circ\text{C}$)²³²; l : length of open pores.

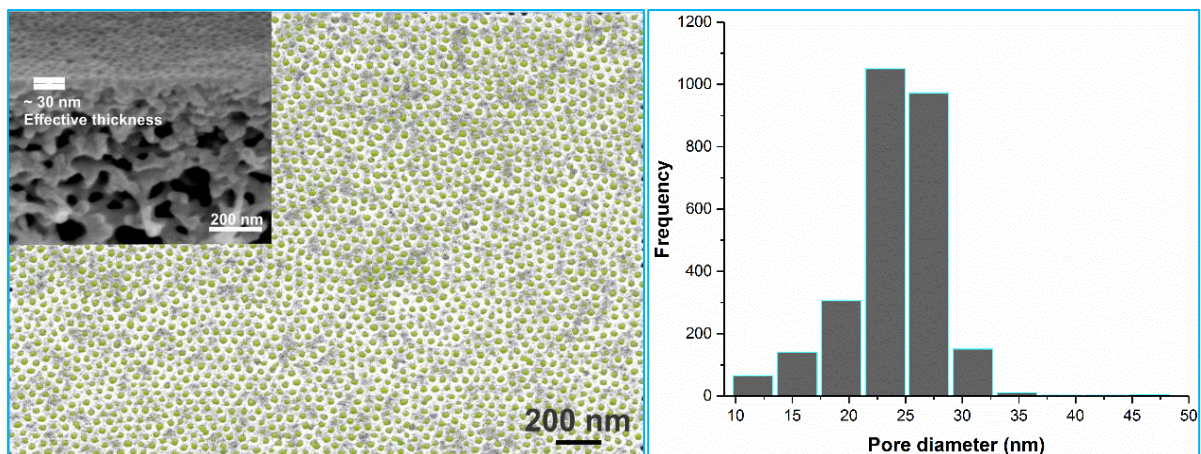


Figure 6.10. The adjusted SEM micrograph of membrane surface to find edges and maxima for structural analysis by IMS V15Q4. The SEM micrograph in inset shows the cross-section near the inner isoporous surface highlighting the active layer thickness (l). The graph in right shows the pore size distribution (N_p : 2709, in $5.7\text{ }\mu\text{m}^2$ of the measured area) of the membrane surface. The coating parameters for this membrane were Q_p : 1.0 mL min^{-1} , t_p : 10 s, Q_{N2} : 0.7 mL min^{-1} , t_{N2} : 60s, and Q_w : 3.0 mL min^{-1} .

From the SEM micrographs analysis, the average pore diameter is 24 nm, N_p is 4.8×10^{14} pores m^{-2} (N_p : 2709 in $5.7 \mu\text{m}^2$ of the measured area), l is 30 nm, and Δp corresponds to 2 bar transmembrane pressure. The calculated water flux J_v for these structural features is ca. $52,465 \text{ L m}^{-2} \text{ h}^{-1} \text{ bar}^{-1}$. The theoretically calculated water flux (J_v : by Hagen-Poiseuille equation) is much higher than the experimentally obtained value (P_{BCP} : calculated for the block copolymer layer by applying the two-resistor series model).

The main difference between theoretically calculated (J_v) and experimental water flux (J_{vBCP}) comes from the dry-state pore size (as calculated from the SEM micrograph) to the wet-state pore size in real conditions when P4VP polymer chains swell in water. Also, the contribution from membranes thickness of both block copolymer and PES layers as compared to the length of pores in active layer is not considered in the calculation. However, the flow resistance from ca. $500 \mu\text{m}$ thick substrate layer cannot be ignored. The other possible reason is the lower and inhomogeneous porosity on the inner surface of support HFM, which is more porous in the pits on the inner skin (this can be seen in the SEM micrograph of inner surface, Figure 6.1d2). The denser parts of the inner surface hinders the flow due to the lack of connectivity of pores and this resistance of flow from the support HFM is calculated as around 52% of the overall resistance for $J_{v \text{ composite}} 260 \pm 50 \text{ L m}^{-2} \text{ h}^{-1} \text{ bar}^{-1}$.

6.6. Conclusion

In this chapter, a novel method for fabrication of inside-out isoporous composite HFM fabrication was reported. The method efficiency is shown by investigation of the morphology of the modified membranes and the membrane performance. The composite membranes show a promising initial water flux of $260 \pm 50 \text{ L m}^{-2} \text{ h}^{-1} \text{ bar}^{-1}$ in wet conditions, higher than the previously reported outside-in isoporous composite HFM²⁰⁹ and comparable to single layer isoporous HFM¹⁷⁰. The optimized coating parameters and process conditions highly depend on the diameter of lumen, morphology and material of support membrane, and the block copolymer solution used for coating.

7. Influence of controlled evaporation by gas flow on the evaporation-induced self-assembly of block copolymers

Since the gas flow induced self-assembly seems to be the only possible way to achieve evaporation-induced self-assembled structures in the compact geometries, therefore it is of great interest to understand the evaporation-induced self-assembly of block copolymers by providing controlled evaporation by gas flow. The gas flow can not only trigger and control the microphase separation but also facilitates the structure formation in isoporous membranes. In this study, we describe a correlation of gas flow induced evaporation with the development of lateral order of microphase separated structures on top followed by the orientation in perpendicular direction as pores which further connects with the asymmetric structure, a result of macrophase separation of the disordered solution. The as-formed structure is trapped by non-solvent induced phase separation. The morphological structures were investigated by SEM. The preliminary results show that gas flow during casting can significantly improve the structure formation and broaden the block copolymer concentration range and casting conditions suitable for the SNIPS process. The knowledge is advantageous for all the self-assembly processes including the membrane fabrication via SNIPS.

‘Block copolymers, self-assembly and isoporous membranes’ are discussed in section 1.3. In the conventional isoporous membrane fabrication, the evaporation-induced self-assembly of block copolymers is achieved under normal environmental conditions. The transition from a disordered into an ordered phase takes place by changing thermodynamic or physical field strength. As discussed before, the mechanism can be enhanced by changing temperature, chemical potential (concentration, solvent(s), carbohydrates or salt addition), mechanical fields (pressure, shear, extension, humidity), as well as of electric field. In this study, the evaporation-induced self-assembly of block copolymers is achieved by providing controlled evaporation *via* gas flow. Thus, the factor controlling the microphase separation, *i.e.*, ‘rate of evaporation’ which controls the built-up concentration gradient perpendicular to the film surface can be considered as the directional field for self-assembly. The stability range of the hexagonal packing phase is limited for a particular solution at particular fabrication conditions. This variability has a favorable effect on the production and optimization of materials. In addition, the artificial evaporation *via* gas flow makes it possible to achieve self-assembled structures on the inner surfaces of a compact geometry. This opens new possibilities where self-assembled structures can be applied in different aspects.

The self-assembly of microdomains is a non-equilibrium/metastable state where initially the disorder-order structural transition occurs which then again start to disorder to an amorphous mesoscale structure. Thus, the requirement of artificial evaporation conditions makes the SNIPS process more intricate and exciting. The controlled and continuous evaporation of solvents develops a stronger gradient for microphase separation. Phillip et al. discussed the structure development on the top surface and perpendicular orientation of pores by stating “*fast evaporation is needed for perpendicularly oriented cylinders*”. Where, two conditions of evaporation were considered, one is normal evaporation in which the cast film was exposed to open atmosphere and to slow down the evaporation the cast film was covered using a Petri dish.¹¹²
¹⁶⁴ The evaporation prompted thermodynamic and kinetic parameters influences the lateral order formation and the perpendicular elongation of pores. This perpendicular orientation of pore-forming domains can reach the length up to approximately 500 nm. Further, the ternary phase diagram shown by Abetz explains the development of integral asymmetric membranes explicitly.¹¹⁰ Subsequent, in order to further understand the self-assembly, the question arises “*How fast or slow evaporation is suitable for the various solvent systems as compared to the normal evaporation conditions?*” and “*How the kinetics of microphase separation will be driven depending on the volatility and selectivity of solvents?*”

In the previous chapters 5 and 6, the gas flow induced structure formation has been studied in fabrication of inside-out isoporous HFM *via* spinning and coating. In both the studies, the microphase separation was initiated by providing a gas (N₂) flow in the lumen of a nascent hollow fiber of diameter less than 1 mm, subsequently in the precipitation bath the SNIPS process completes with macrophase separation on the inner surface. In these studies, the self-assembly was controlled on the inner surface of a HF where many additional influencing factors do not allow a very straight forward correlation between air flow induced microphase separation or rate of evaporation and self-assembly and structure formation. Moreover, the inside-out (composite) HFM fabrication further demands a detailed study of influence of gas flow on structure formation, *i.e.*, influence of rate of evaporation of solvents. The two methods for fabrication of HFM, by spinning the block copolymer solution or by coating on the lumen side of a highly porous support HFM are completely different and have different controlling factors for structure formation. Therefore, to understand the influence of gas flow explicitly, a comparatively less complex system is selected, *i.e.*, flat sheet membrane fabrication.

This chapter reports an empirical study showing the influence of rate of evaporation on isoporous structure formation, length of cylindrically orientated domains and progression of these microphase separated block copolymer domains. For preparation of isoporous flat sheet membranes *via* a SNIPS process with controlled evaporation, the casting experiments were conducted in a way that the gas flow rate and the time of gas flow can be precisely regulated. The main components of the procedure are illustrated in Figure 7.1. Specific details for the preparation of isoporous membranes under controlled casting conditions and their influence are discussed in the following sections.

7.1. Envelope design

As a prerequisite for performing the experiments providing controllable laminar gas flow on the top surface of flat sheet membranes, an envelope is designed according to the experimental requirements, which is shown in Figure 7.1. The envelope dimensions were decided according to the dimensions of glass plates, as typically used for casting of flat sheet membranes on small scale. The used glass plates have the dimensions of 20 x 10 x 0.5 cm³ (length × width × height) and the envelope has the dimensions of 20 x 10 x 2.3 cm³ (length × width × height) on the inner side, providing a gap of 1.8 mm above the glass plate, which decreases further when using a

substrate for casting. The envelope was manufactured by an in house 3D-printer, Project MJP 3600 printer, using polytetrafluoroethylene (PTFE). In order to provide a laminar flow on the top surface of an as-cast polymer solution, the distance from the connecting tube to the glass plate was increased by incorporating a triangular shape in the front, which ends at the glass plate with a fine grid. This perpendicular grid was developed during printing by providing the gap and the material continuously in a thickness of 0.5 mm for each one.

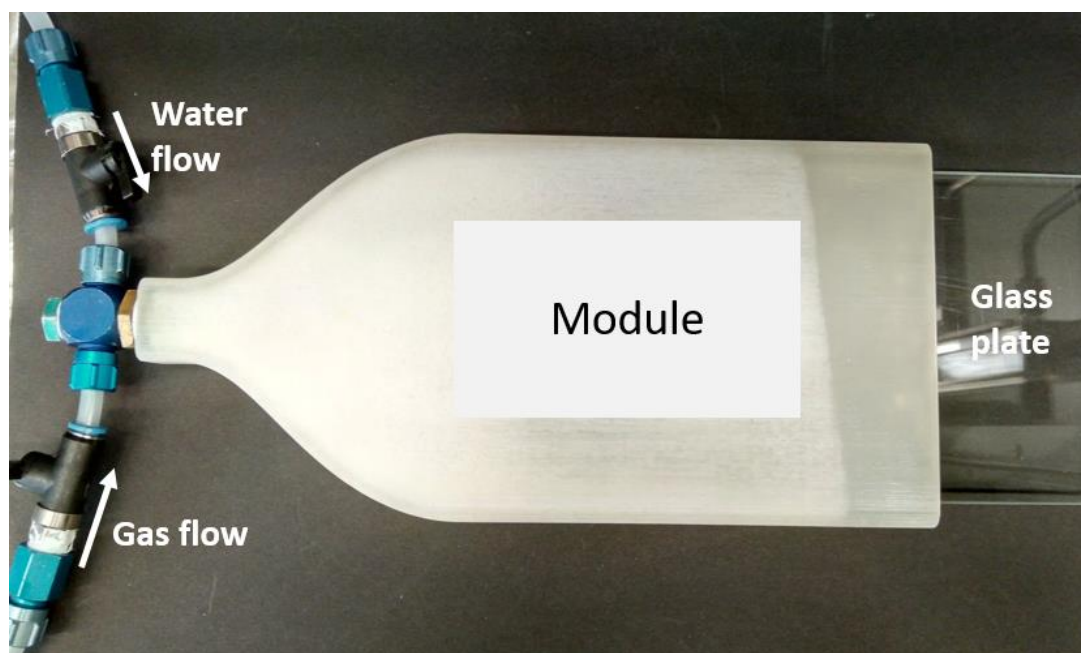


Figure 7.1. Set-up used for casting of flat sheet membranes on the glass plate. The gas and water flow rates are precisely controlled using high precision pumps.

7.2. Flat sheet membrane fabrication

Flat sheet membranes were prepared by providing controlled evaporation *via* gas flow on top. A doctor blade of gap height 200 μm was used for the casting of the polymer solution either on glass plates or on the substrates. For the casting of viscous polymer solutions a non-woven support was used. The casting was done carefully to get the selected evaporation time for a certain gas flow rate. For this, the doctor blade was placed on the glass plate, which was moved into the envelope while casting, and after a certain time the non-solvent flow was introduced from the same entrance as gas flow without lacking a sec. These two fluids were sequentially introduced into the envelope for a certain time by using valves (the switching): (1) the gas flow

(mainly N₂), to provide sufficient evaporation conditions required for self-assembly. (2) Water, to allow precipitation of the film and complete exchange of solvents by non-solvents. To control the gas flow rates, a mass flow controller (Bronkhorst 5000 mln/min N₂; Accuracy of <1% of the set point) was used and for the water flow a variable area flowmeter (Krohne DK 800; Accuracy of <4% of the set point) was used. The membranes were then washed and kept in DI water. After complete solvent removal, the membranes were kept at room temperature for 24 h for drying. The membranes were kept in an oven for drying up to 60 °C for microscopical characterizations.

7.3. Results

The flat sheet membranes were cast using a block copolymer solution of 27 wt% PS-*b*-P4VP₁₇^{139k} in DMF/THF 50/50 (wt/wt) for Q_{N_2} in the range of 1500-6000 mL/min and for t_{N_2} of 2-8 s. Figures 7.2-7.4 show the influence of casting parameters on the structure formation on the top surface and cross-sections near the top surface. Interestingly, the isoporous structure can be obtained for a wide window of casting parameters without any significant influence in the structure of the top surface, as shown in Figure 7.2. However, the cross-sectional morphology highlights the influence of rate and amount of solvent(s)-evaporation. For the low Q_{N_2} of 1500 mL/min, a growth in the length of cylindrical pores can be seen for t_{N_2} from 2 s to 8 s (Figure 7.3). For higher Q_{N_2} of 6000 mL/min, the perpendicular orientation of pores as cylinders vanishes and a rather disorderd orientation of cylinders can be seen for t_{N_2} from 2 s to 8 s (Figure 7.3). Figure 7.4 shows that with increase in rate and time of evaporation the substructure gets denser and the number of macrovoids decreases.

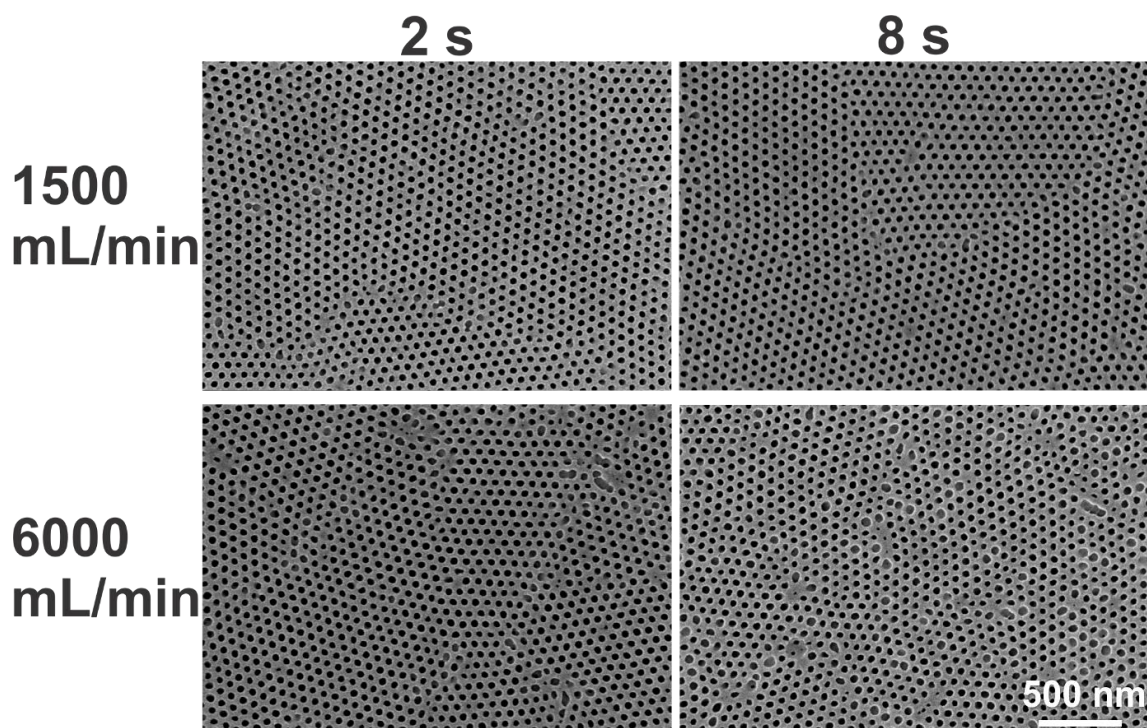


Figure 7.2. SEM micrographs of the top surfaces of the flat sheet membranes cast using block copolymer solution of 27 wt% PS-*b*-P4VP₁₇^{139k} in DMF/THF 50/50 (wt/wt). The membranes were cast for Q_{N2} of 1500 and 6000 mL/min and for t_{N2} of 2 and 8 s.

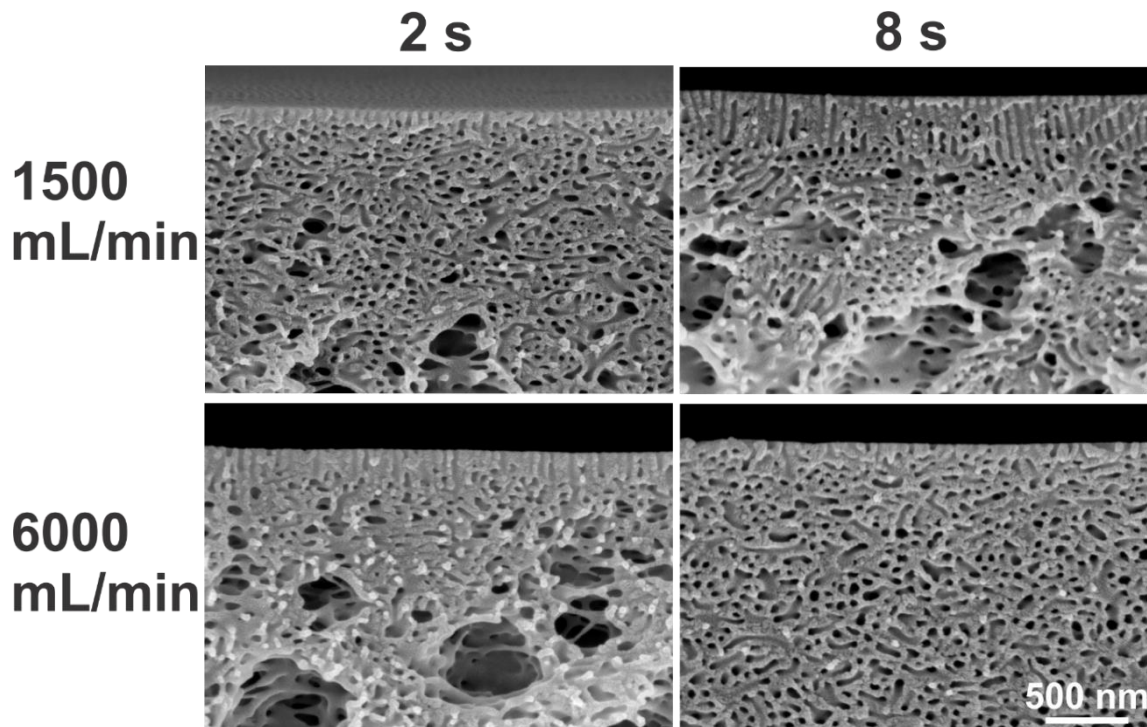


Figure 7.3. SEM micrographs of the cross-sections near to the top surfaces of the flat sheet membranes prepared using the block copolymer solution of 27 wt% PS-*b*-P4VP₁₇^{139k} in DMF/THF 50/50 (wt/wt). The casting parameters were Q_{N2} of 1500 and 6000 mL/min and t_{N2} of 2 and 8 s.

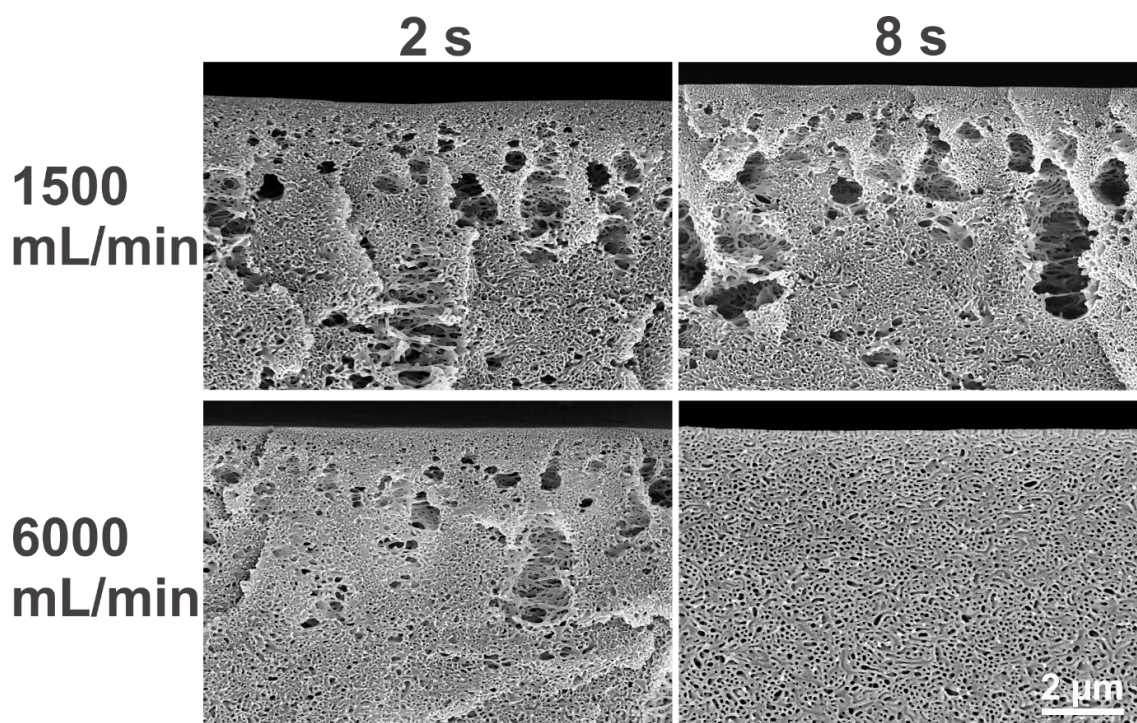


Figure 7.4. SEM micrographs of the cross-section of the flat sheet membranes near to the top surface. The membranes were cast using block copolymer solution of 27 wt% PS-*b*-P4VP₁₇^{139k} in DMF/THF 50/50 (wt/wt), for Q_{N_2} of 1500 and 6000 mL/min and for t_{N_2} of 2 and 8 s.

7.4. Evaporation-induced self-assembly of block copolymers *via* gas flow

As discussed in section 1.3.5, the prepared block copolymer solution remains homogeneous within the metastable regime, unless any possibility to reduce the Gibbs energy. As the block copolymer solution is exposed to environment or gas flow, by allowing the evaporation of solvents, the demixing happens *via* nucleation and growth and the microphase separation takes place spontaneously. The SNIPS process resulting in isoporous membranes demands a good control over self-organization of macromolecules forming highly segregated microdomains of the minority blocks (P4VP) in the matrix of majority blocks (PS). In this process of evaporation-induced self-assembly, the evaporation of volatile solvent(s) solidifies the respective block segments, and the decrease in temperature plays an important role in phase transitions between different ordered states or between the disordered and an ordered state because of the contribution TdS to the free energy (where T is temperature and dS is change in the entropy).¹⁰³ The increased rate of evaporation fixes the matrix forming blocks because of its selectivity to more volatile solvents while allowing the swelling of pore forming block in a comparatively less

volatile solvent. The increase in rate and time of evaporation leads the segregation of microdomains in a certain depth of the substructure.

A. Difference from the conventional evaporation-induced self-assembly

In case of evaporation *via* gas flow, the concentration of the solvent(s) in the air is less likely to go up with time because of continuously replacing the solvents with gas flow, thus encouraging the diffusion of volatile solvent(s) from the as-cast membrane (free venting condition). Therefore, no evaporation-equilibrium is generated in the enclosed area and the concentration of the evaporating substance in the air keep removing, enhancing the capacity for the evaporation. Further, with increase in gas flow rate, the boundary layer at the evaporation surface decreases with flow velocity due to decreasing the diffusion distance in the stagnant layer. Furthermore, in case of casting in the envelope, the evaporation of solvent(s) happens faster as there is less exertion (due to low pressure) on the surface keeping the molecules from launching themselves. This is significantly higher in flat sheet membranes as compared to the lumen of a HFM because of the surface area, as there are more surface molecules per unit of volume that are potentially able to escape.

B. Influence of the gas flow rate

In the endothermic process of evaporation, heat is absorbed during evaporation and an increase in evaporation lowers the free energy on surface. The higher the temperature of the substance the greater the kinetic energy of the molecules at its surface and therefore the faster the rate of their evaporation. By increasing the rate of evaporation, a faster temperature drop provides a faster increase in concentration on the top surface and the development of concentration gradient development from the top surface. Due to this, the sudden loss of entropy change strongly influences the degree of order and the phase transitions.

So, initially the self-assembly of block copolymers initiates on the surface but with the passes of time and increase in diffusion of solvent molecules towards the surface, the microphase separation occurs in the substructure as well. Figure 7.5 shows the stacked SEM micrographs representing a complete cross-sectional view of a flat sheet membrane, which was provided a longer evaporation time of 8 s and high gas flow rate of 4500 mL/min.

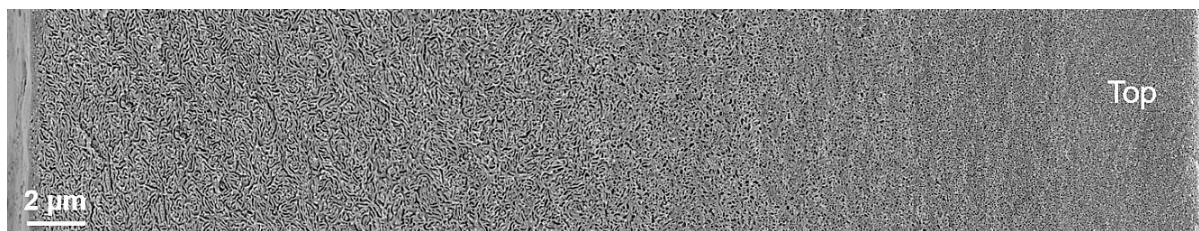


Figure 7.5. Cross-sectional view of an isoporous membrane showing the progression of microphase separation of block copolymers. A set of SEM micrographs is stacked continuously from top to bottom. The as-cast polymer solution was provided t_{N_2} of 8 s and Q_{N_2} of 4500 mL/min.

C. Benefits over conventional evaporation under environmental conditions

This novel approach towards fabrication of isoporous membranes can provide a faster development of self-assembled pores on the top surface. A faster membrane fabrication is always appreciated in order to reduce the production cost by decreasing the time required for evaporation because the higher evaporation time demands slower casting of polymer solution and comparatively longer way to the water bath.

In addition, humidity has been a big challenge in fabrication of conventional block copolymer membranes. In case of normal evaporation conditions, the thermodynamically driven system tries to minimize the overall free energy in the system. The decrease in the temperature on the surface due to evaporation can lead to condensation of water, depending on the humidity in the atmosphere. Therefore, the humidity in the atmosphere of as-cast film plays a significant role; higher humidity can hinder the self-assembly process by increasing the condensation and increasing the heat of system. Thus, the idea of using gas flow for evaporation-induced self-assembly offers the freedom of membrane fabrication at any place irrespective of the humidity levels while the temperature should be considered as well.

7.5. Conclusion

The evaporation-induced self-assembly of block copolymers *via* gas flow promises to be an efficient tool for controlled bottom-up fabrications such as isoporous membranes. In case of volatile solvent(s) in the block copolymer solution, the rate and time of gas flow controls the evaporation of solvents and thus the kinetics of microphase separation. The results show that gas flow during casting can significantly improve the structure formation and broadens range

of the block copolymer concentration in solution and the casting conditions suitable for a usual SNIPS process. The concept significantly holds the potential to be applied in fabrications of other self-assembled structures in compact geometries using various block copolymer solutions or to achieve different morphology as required in the aimed application.

8. Summary and outlook

“All knowledge is connected to all other knowledge. The fun is in making the connections.”

-Arthur Aufderheide

The fabrication process (SNIPS) to prepare isoporous flat sheet membranes and the self-assembly of block copolymers had been well studied. The isoporous flat sheet membranes were cast using polymer solutions with and without additives. It was known that by using additives, the concentration required for structure formation can be reduced. These additive-containing solutions had not been tried in the more-recently introduced outside-in isoporous HFM, instead the experimental conditions were optimized to achieve isoporous structure in commonly used viscous solutions. In this study, the solutions having MgAc_2 as additive were characterized *via* SAXS and the structure formation was checked in both flat sheet and HF membranes.

The microphase separation of block copolymers during isoporous flat sheet membrane fabrication had already been investigated by conducting SAXS and GiSAXS experiments. Such fundamental studies of exploring the macromolecular behavior by SAXS characterizations always looked fascinating to me and led me to the idea of investigating the structure formation by conducting *in situ* SAXS experiments during HFM fabrication. The first ever *in situ* SAXS experiments during spinning of block copolymer HF revealed interesting facts about shear-induced self-assembly in block copolymers. The same experiments revealed the influence of MgAc_2 in self-assembly of block copolymers in solutions and during spinning. The study of effects of polymer flow rate on self-assembly will be helpful for further development of block copolymer HF spinning and isoporous membrane fabrication. Moreover, this study will be

helpful in understanding the development and loss of hexagonally-packed microphase separated domains along with the influence of MgAc_2 .

The next exciting step of this dissertation was the development of inside-out HFM. The control over self-assembly of macromolecules and trapping the structure at the right time is exciting and playful. Although the HF spinning itself has many controlling parameters, playing the puzzle of self-assembly with gas flow made this work much more interesting. After many hit and trials, it was possible to control the structure formation in the kinetic process of HF spinning using the gas flow. This work led to the novel idea of using gas flow to achieve evaporation-induced self-assembly. However, due to the lower density of gas than water, the spun HF tend to float in the precipitation bath instead of properly submersing into the water. This Buoyancy force becomes a challenge for smooth spinning of HFM in a manual small-scale set-up. Therefore, the future work will focus on modification of the spinning process to achieve stable HF spinning and smart techniques for collecting the spun fibers.

“The mind that opens to a new idea never returns to its original size.”

-Albert Einstein

After the successful fabrication of integral asymmetric inside-out isoporous HFM, the idea of coating on the lumen side of robust HFM came up. A method to develop self-assembled structures on the lumen side of compact geometries like the lumen of a HFM was reported *via* a cost-effective and scalable coating method followed by SNIPS. The strategy was validated on the example of a 4 wt% PS-*b*-P4VP block copolymer solution to coat the inner surface of a microfiltration PES HFM with inner diameter of 1.5 mm. Again, the coating of block copolymer solution and the isoporous structure on the lumen side were achieved using gas flow. This success in the fabrication of inside-out isoporous composite HFM opens many new applications for isoporous membranes because of the possibility to fabricate robust HFM with far less consumption of expensive block copolymer. The required block copolymer concentration was further reduced by addition of MgAc_2 in the polymer solution. The membranes hold potential

to be explored and applied in the fields of bioreactors, protein separation, pharmacy, food industry, and wastewater treatment, among others. Moreover, by coating the outer surface, a bifunctional separation system can be fabricated which may offer a different avenue towards biotechnological applications such as diffusion of different molecules in opposite directions, where, the support fiber can trigger catalytic reactions as well. However, in order to achieve specific separation conditions from the top isoporous layer, the further work will also be focused on reduction of the resistance of flow through the interface and the support HFM. For this, the control over infiltration of block copolymer solution into the support by pretreatments and a different support HF (providing lower resistance and not swellable by the solvent(s) used in the coating solution) will be considered.

This novel approach of inside-out HFM fabrication may provide valuable perceptions for the fabrication of inside isoporous HFM, also with other block copolymers. Further, the surface area is decreased in inside-out HFM as compared to outside-in HFM, while the configuration provides better control on flow hydrodynamics. Therefore, to increase the active surface area while keeping the direction of filtration as inside-out, one can simply apply the technique on the lumen side of multi-bore HFM. Moreover, the multi-bore inside-out HFM will offer highly robust membranes applicable for high-pressure applications.

The idea of using gas-flow brought two novel HFM. However, the difference of evaporation-induced self-assembly under environmental conditions and *via* gas flow was still not explicitly understood. Therefore, the gas flow induced structure formation was studied in flat sheet membranes, as the flat sheet membranes offer fewer variables. The preliminary studies were conducted for the most studied block copolymer solution of PS-*b*-P4VP in DMF/THF 50/50. However, this brought many more questions as the microphase separation highly depends on the volatility of used solvents and the selectivity of solvents to the block segments of the copolymer.

Nevertheless,

“We absolutely must leave room for doubt or there is no progress and no learning ...”

-Prof. Richard P. Feynman

The additional outlook beyond the topic of the main research is about spreading the awareness and knowledge about the field to a larger audience in the society. Even though, the development in the field of membrane technology has been going on for half a century, the knowledge about membranes and their requirements is not readily available in school and college courses, and people are away from the knowledge of their very basic need of filters such as one required for water purification. Being a membranologist focused on water purification, my perspective is also to spread knowledge and awareness from the smart storage of all types of water to saving water, to recycle wastewater, and to reuse water in a safe way.

9. Experimental section

9.1. Materials

The asymmetric PS-*b*-P4VP diblock copolymers were synthesized by Brigitte Lademann *via* sequential anionic polymerization following a protocol reported before.^{118, 169} Tetrahydrofuran (THF, Th. Geyer GmbH & Co. KG, Renningen, Germany) was purified by sequential distillation from *sec*-butyl lithium (*sec*-BuLi) (1.4 M in cyclohexane, Sigma-Aldrich, Schnelldorf) under purified argon atmosphere. Styrene (S) (≥ 99 wt% with *p*-*tert*-butylcatechol as stabilizer, Sigma-Aldrich, Schnelldorf, Germany) was purified from basic aluminum oxide (Macherey-Nagel, Duren, Germany) and subsequently distilled from dibutylmagnesium (MgBu₂) (1.0 M in heptane, Sigma-Aldrich, Schnelldorf) under high vacuum. 4-vinylpyridine (4VP) (99 wt% with <1000 ppm *p*-*tert*-butylcatechol as inhibitor, Sigma-Aldrich) was once distilled under reduced pressure from calcium hydride (CaH₂) and twice from ethylaluminum dichloride (EtAlCl₂). The polymerization of styrene was initiated with *sec*-BuLi and allowed to proceed at -78 °C in THF. After 4 h, a small portion of the reaction medium was removed and quenched with degassed methanol to determine the degree of polymerization of the PS block. Afterward, the purified 4VP was added into the solution and stirred for another 16 h at -78 °C. The polymerization was terminated with a mixture of degassed methanol and acetic acid (99%, Sigma-Aldrich). Finally, after removal of THF under reduced pressure, the polymer solution was precipitated in Millipore water and the polymer was dried at 40 °C for several days under vacuum to remove the residual solvents and water trace.

The number average molar mass (M_n) and dispersity index (\mathcal{D}) of the PS precursor and the diblock copolymers were measured by gel permeation chromatography (GPC) (Waters 2410 refractive-index detector, *N,N*-dimethylacetamide as eluent) at 50 °C which was calibrated against PS standards. The composition of the block copolymer was determined by ¹H nuclear magnetic resonance spectroscopy (¹H NMR) (in deuterated chloroform) on a Bruker advance 300 NMR spectrometer. Using the composition and the molecular weight of the PS precursor

the total molecular weight of the block copolymer was calculated. All chemicals used in this study were purchased either from Sigma-Aldrich or from Merck.

9.2. Preparation of PS-*b*-P4VP polymer solution

The block copolymer solutions were prepared by dissolving a certain concentration of PS-*b*-P4VP block copolymer in solvent(s); all measurements were done in wt% and the solvents were mixed in weight ratio (wt/wt). Depending on the polymer concentration, the solutions were stirred for 24-72 h at room temperature until they appeared homogeneous, and they were then allowed to rest for some hours prior to use.

9.3. Preparation of bulk films

For the investigation of the bulk morphology of the PS-*b*-P4VP diblock copolymers films were prepared from solution.¹¹⁸ The solutions were prepared by stirring 160 mg of block copolymer in 2.5 mL of chloroform for 24 h. The homogeneous solutions were transferred into polytetrafluoroethylene molds and kept for slow drying. In order to equilibrate the sample, *i.e.*, to remove the solvent effect and air bubbles trapped in the samples; the films were further annealed at temperatures below and above the glass transition temperature of both blocks under vacuum. The temperature was gradually increased to 140 °C near the glass transition of P4VP block and finally the samples were annealed for 4 h at 170 °C. The sections from the same films were used for characterization by SAXS and TEM.

9.4. Flat sheet membrane fabrication

The flat sheet membranes were cast either on glass plates or on non-woven substrate using a doctor blade with gap height 200 μm and different evaporation times. All the experiments were conducted in fume hoods at a temperature around 21-25 °C and a relative humidity from 30-50 %.

9.5. Outside-in hollow fiber membrane fabrication *via* spinning

The outside-in HFM were fabricated by traditional dry-jet wet spinning process as discussed in Section 1.3.7.^{77, 228} The spinning set-up consists of one double orifice spinneret mounted in a spinneret holder for extrusion of polymer solution and bore fluid (water), syringes, two high-precision pumps and precipitation baths. As shown in Figure 9.1, the used double orifice spinnerets have outer diameters of 0.32 and 1.3 mm for bore fluid and polymer solution, respectively. The metal thickness between the two orifices is 0.1 mm. The glass syringes with and without Luer-lock tips were used for filling the polymer solution, which were connected to spinneret holder *via* transparent polyethylene tubes. The micro-precision pumps are used for precise control on flow rates of polymer solution and bore fluid. The pumps and the glass syringes were connected by tubes filled with water. In order to get rid of air bubbles, the syringes were filled one day before the experiments and well-packed afterwards to avoid solvent evaporation. All the spinning experiments were conducted in fume hoods at a temperature around 21-25 °C and a relative humidity from 30-50 %. The spun fibers were collected in a rotating precipitation bath.

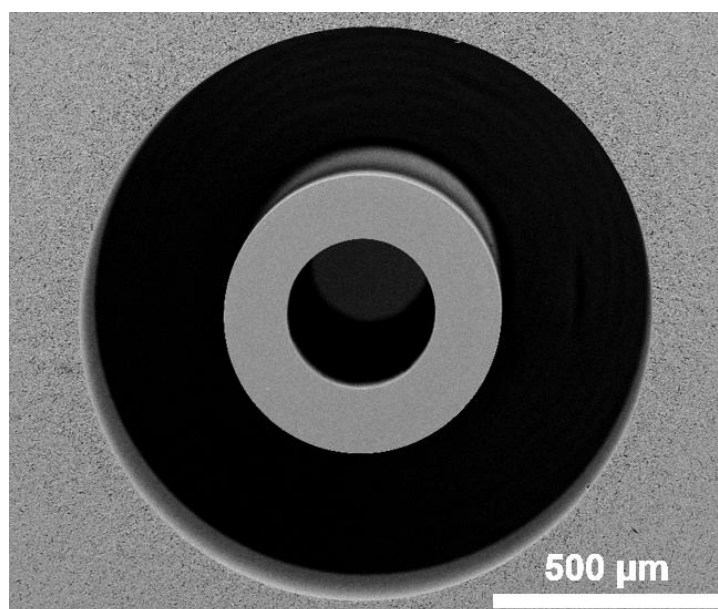


Figure 9.1. The SEM micrograph of the spinneret exit or the extrusion side in bottom of the spinneret, which shows the concentric arrangement of orifices in a double orifice spinneret, used for outside-in isoporous HFM fabrication.

9.6. Small-angle X-ray scattering

With the exception of the bulk films, the SAXS experiments were performed at the microfocus end station of the beamline P03, PETRA III, Deutsches Elektronen-Synchrotron (DESY), in Hamburg, Germany.²²⁷ The X-ray beam having 12.981 keV energy was used to have a good transmission through the block copolymer solution in the shell around the bore fluid. The beam was focused to $28 \times 14 \mu\text{m}^2$ (horizontal \times vertical) by using an assembly of parabolic beryllium compound refractive lenses. The exposure time was 0.2 s with a total number of 20 frames for each measurement resulting in a total acquisition time of 4 s. The used sample-to-detector distance of 8.91 m allowed a q -range from 0.04 to 1.1 nm^{-1} to capture all occurring structural changes in the range of 5.7-157 nm. We used the Pilatus 1M fast-readout detector.

A. SAXS from bulk films

SAXS experiments on equilibrated films were performed on a Bruker Nanostar, Karlsruhe, Germany. The lab source is equipped with a copper anode providing an X-ray beam with an energy of 8 keV. The set-up utilizes a VANTEC-2000 detector with a pixel size of $68 \mu\text{m}$. The sample to detector distance was 1.5 m providing a q -range from 0.06 to 2.2 nm^{-1} .

B. SAXS from Solutions

For investigation of structure in block copolymer solutions, the solutions were filled into quartz capillaries and sealed by epoxy glue some hours before the measurements. The capillaries had a wall thickness of $10 \mu\text{m}$ and a diameter of 2 mm.

C. *In situ* synchrotron SAXS during hollow fiber spinning

For the experiments, the standard spinning set-up for outside-in HFM fabrication was used as schematized in Figures 1.10 and 4.1 and as discussed in Section 9.5. The spinning system comprising of a spinneret fixed in the holder and the syringes was fixed to a remote controlled micro-precision stage, which was used to move the set-up in the plane perpendicular to the X-ray beam in order to change the air gap distance with respect to the beam passing through the extruded fiber. To control the polymer solution and bore fluid flow rates, the micro-precision pumps were mounted outside the synchrotron hutch. As the experiment needed a precipitation

bath, a hanging stage was used being fixed to the available granite bridge. The vertical distance, between the positions of spinneret holder on the x-y stage from the beam, corresponds to a certain L_a providing a certain evaporation time for the as-spun fiber. While, the horizontal moving was used to scan across the fiber with a step size of 30 to 100 μm .

The fibers were thoroughly scanned at different L_a from the nozzle for various block copolymer solutions and spinning parameters, Q_p and Q_w . Simultaneously, the spun fibers were collected in a rotating precipitation bath which was located ca. 50 mm below the beam providing a total air gap, $L = L_a + 50$ mm, where L_a was varied from 1 to 80 mm; so, there was always an additional effect of gravity and strain in the fiber during SAXS measurements. Background measurements were carried out in between by moving the HF out of the beam. However, in order to correlate the SAXS curves and HFM morphology influenced by spinning parameters and solution characteristics, the HF spinings were repeated in the lab. In the repeated HF spinning for morphological investigations by SEM, the structures in as-spun fibers were quenched at particular L_a (so, $L = L_a$). We note that scanning along the fiber by keeping a constant air gap was not possible. Constructing a set-up where the air gap could be kept constant while scanning along the fiber would have been too heavy for the available micro-precision motor stages. Therefore, the water bath was fixed at the bottom of the beamline and only the spinning system was motorized.

For the data integration, masking and normalization the software package DAWN was used.²³³ The two-dimensional images were averaged azimuthally to obtain a trace of intensity vs. the scattering wave vector q ($q = 4\pi \sin(2\theta/2)/\lambda$, where 2θ is the scattering angle and λ is the wavelength of the X-rays). In a further step, the patterns were averaged radially in a certain q -regime which was chosen to include the occurring structure factor. The resulting curves showing the intensity vs. the azimuthal angle allow investigating whether orientation effects are occurring or not. In the case of no orientation a constant intensity is observed whereas for orientation effects two maxima with in a distance of 180° can be seen. For background corrections, frames showing only air scattering were subtracted from the averaged data. The fitting of the correlation peaks and background subtraction were done using MATLAB. All the data for a distinct horizontal scan were compared. No significant variation along the cross-section of the fiber could be seen. Thus, the data at one horizontal height was averaged.

9.7. Inside-out hollow fiber membrane fabrication *via* spinning

The inside-out HFM were fabricated by a modified dry-jet wet spinning process, as detailed in Section 5.1. A triple orifice spinneret having outer diameters of 0.32 mm, 1.3mm and 1.8 mm for bore fluid, polymer solution and water, respectively was used for fabrication of inside-out HFM. The die gaps for polymer solution and water are 0.34 and 0.15 mm, respectively.

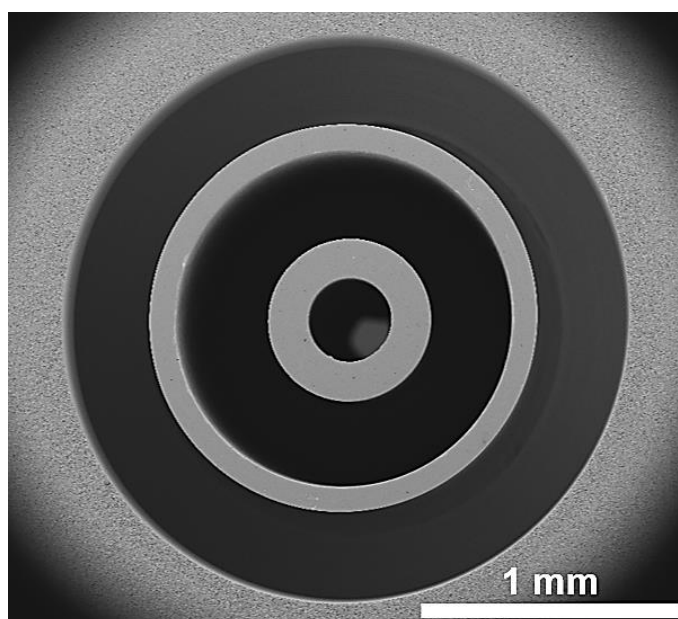


Figure 9.2. The SEM micrograph of the spinneret exit, which shows the arrangement of concentric orifices in a triple orifice spinneret, used for inside-out isoporous HFM fabrication.

9.8. Module design for coating experiments

As a prerequisite for performing coating experiments in the lumen of support membranes, the modules were designed as required in the experiments. The module consists of a transparent PVC U tube having an outer diameter of 6 mm and a thickness of 1 mm that were purchased from Kwerk GmbH, Germany. These tubes were pierced at every 2-3 cm distance, using a bore of 2.4 mm diameter in order to speed up the exchange of solvent(s) by non-solvent, to take away the water filtered through the coated membrane, and to avoid floating of the modules in the precipitation bath. To stabilize the support fibers, both ends of PVC modules were sealed

with epoxy resin, a picture is shown in Figure 9.3. The effective length was varied in the range of 8-20 cm and a typical preparation procedure started with modules containing one support membrane.



Figure 9.3. Scheme of a module holding the substrate HFM.

9.9. Morphological characterization

A. Scanning electron microscopy

To obtain information about the morphology of flat sheet membranes and HFM, SEM investigations were carried out on either a LEO Gemini 1550 VP or a Merlin (both from Zeiss, Oberkochen, Germany), at an acceleration voltage of 1-10 kV. The surface samples were prepared by cutting the membranes and fixing on the sample holder. For the investigation of the inner surface, the samples were prepared by cutting the fibers on the length, and both halves were placed on a sample holder. The cross-section samples were prepared under cryogenic conditions to preserve their microscopic morphology. All the samples were sputtered with ca. 2 nm of platinum as a conductive layer. Secondary electron In-Lens and HE-SE2 detectors were used for imaging the membrane morphology and topography.

The energy selective backscattered electrons (EsB) detector was used for quickly distinguishing different phases of composite HFM by energy specific separation of backscattered electrons (BSE). *E.g.*, in the compositional contrast of the coated block copolymer layer and PES support HFM, PES provides brighter BSE intensity as compared to the block copolymer layer due to the greater atomic number (sulfur).

a. Analysis of SEM micrographs using ImagiC

To obtain the average pore diameter (D_p) and pore density per unit area, the SEM micrographs were analyzed by IMS V15Q4 (Imagic Bildverarbeitung AG, Glattbrugg, Switzerland). The analysis of a SEM micrograph is shown in Figure 9.4, where first, the SEM micrograph is binarized prior to the analysis to find edges of the pores and then the pore area and diameter is

calculated by covering up the area of darker domains. By determining the number and area of pores in the measured area pore density and surface porosity can be calculated, respectively.

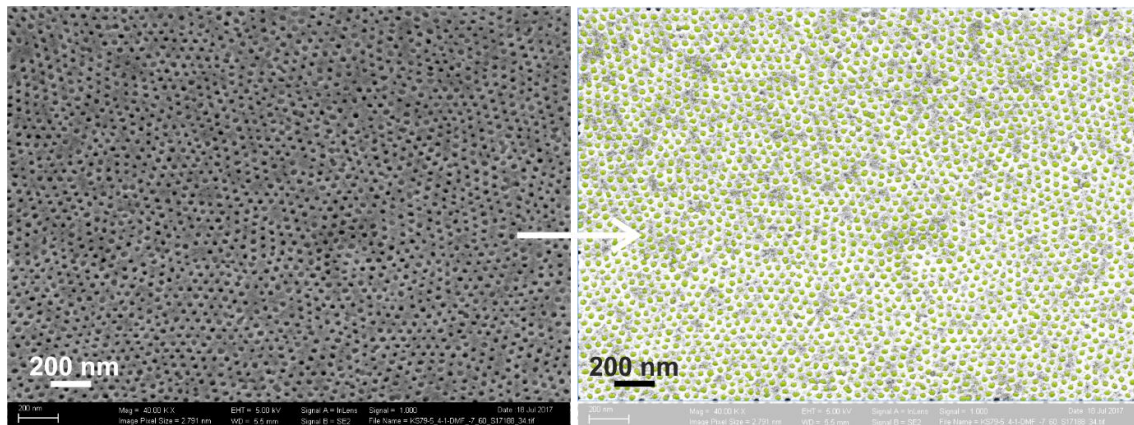


Figure 9.4. Analysis of SEM micrograph using ImagiC.

b. Analysis of SEM micrographs using analySIS

To obtain the D_p and the average center-to-center distance between pores (d_{c-c}), the SEM micrographs were analyzed by analySIS (Olympus Soft Imaging Solutions GmbH, Münster, Germany), see Figure 9.5. To find the edges of the pores the SEM micrographs were binarized prior to the analysis; the brighter area corresponds to pore area; d_{c-c} is an average of distances to next neighboring pore.

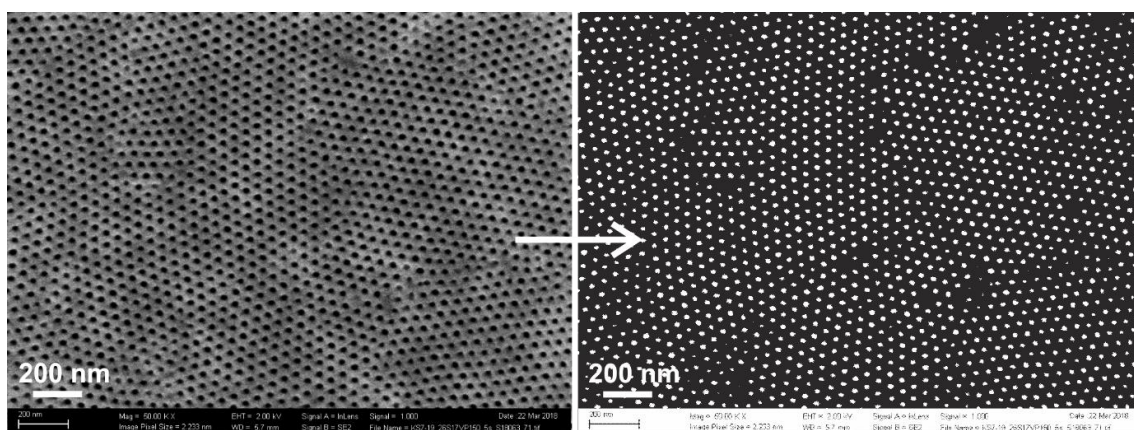


Figure 9.5. Analysis of SEM micrograph using analySIS.

c. Analysis of SEM micrographs by DigitalMicrograph

The SEM micrographs were also analyzed by DigitalMicrograph (Gatan Microscopy Suite Software, Gatan Inc., CA USA) by performing an autocorrelation analysis on the pore distribution. This provides a visual impression of average periodic arrangements of pores with information about D_p and d_{c-c} . As shown in Figure 9.6, D_p is calculated by the diameter of the central bright spot and d_{c-c} is calculated by taking the average of distances between the central bright spot to all nearest bright spots (located in first ring).

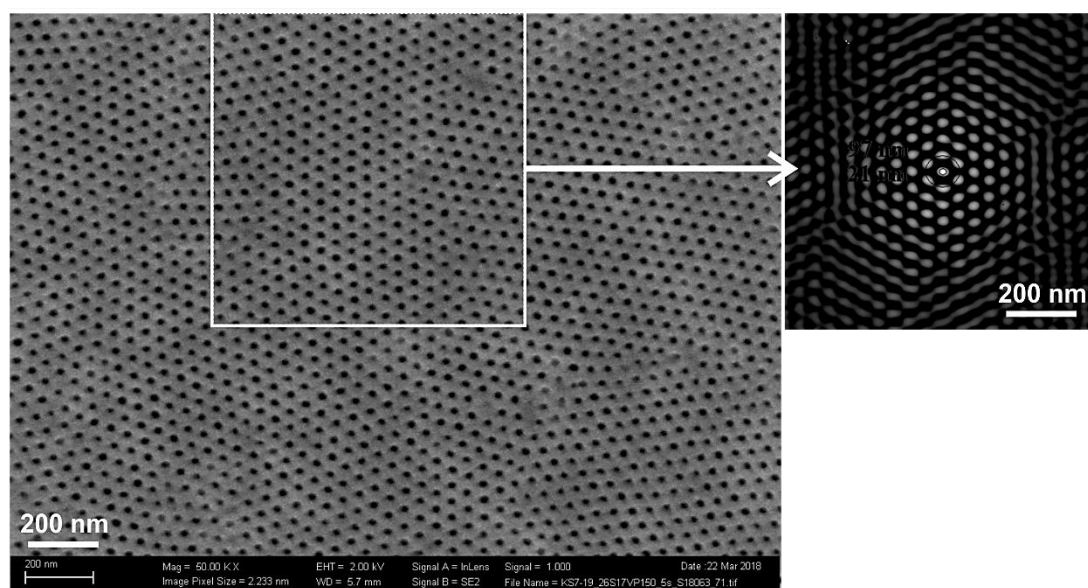


Figure 9.6. Analysis of SEM micrographs by DigitalMicrograph.

B. Transmission electron microscopy

TEM characterizations were performed on a Tecnai G² F20 (FEI, Eindhoven, The Netherlands) operated at 120 kV in bright-field mode. The samples were embedded in an epoxy resin. A Leica Ultramicrotome EM UCT (Leica Microsystems, Wetzlar, Germany) equipped with a diamond knife (Diatome AG, Biel, Switzerland) was used for ultrathin sectioning of the samples with a thickness of roughly 50 nm, which were stained with iodine (I₂) vapor for 1 h (selective for P4VP).

The TEM micrographs of bulk films were analyzed by DigitalMicrograph to obtain average centre-to-centre distance.

9.10. Membrane characterizations

As part of this PhD work, the automated water flux machine and new modules were designed and developed with the help of Joachim Koll, Carsten Scholles and Berthold Wendland, at the Institute of Polymer Research, Helmholtz-Zentrum Geesthacht. For cross-flow retention experiments, the already available machine used for flat sheet membranes was modified to make it applicable for HFM module configuration.

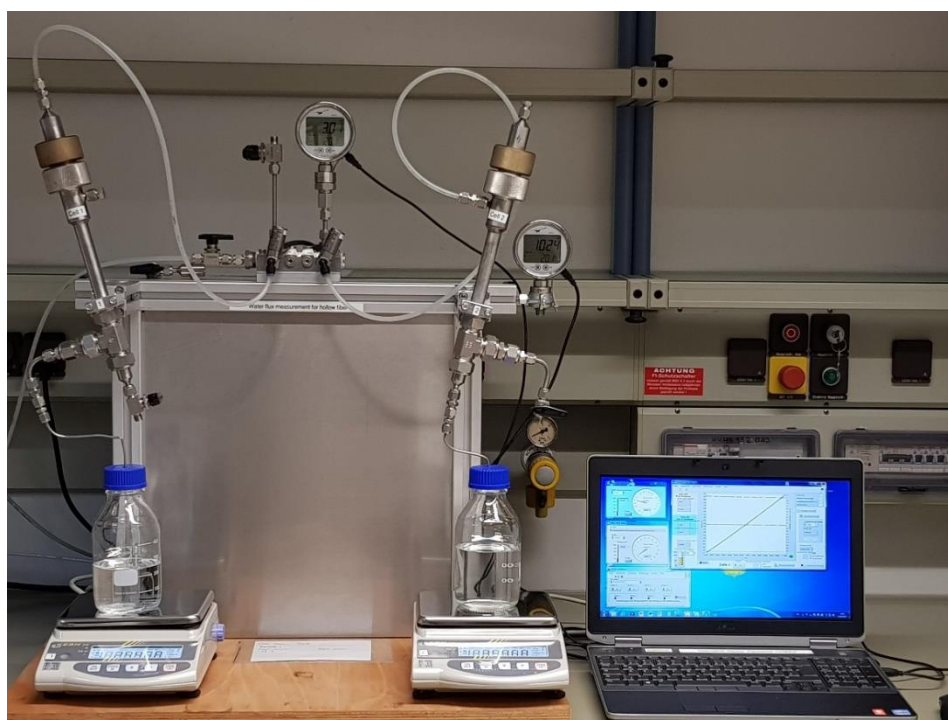


Figure 9.7. Picture of homemade automatic water flux device.

A. Water flux measurements

The membrane modules for the filtration experiments were containing one HFM of an effective length 4-15 cm dried at room temperature. These studies were conducted by employing demineralized water. The water flux measurements were conducted in dead-end mode by using compressed nitrogen to apply the 2 bar transmembrane pressure, at room temperature, using the above shown home-made automatic testing device. To ensure the reproducibility of the results, all experiments were performed at least in triplicate by using three individual single fiber modules. The water flux (J_v) is calculated as follows,

$$J_v = \frac{\Delta V}{A \cdot \Delta t \cdot \Delta p} \quad (3)$$

Where, ΔV is the volume of collected water between two mass measurements, A is the active surface area of membrane, Δt is the time between two mass measurements, and Δp is the transmembrane pressure.

B. Retention experiments

The molecular weight cutoff (MWCO) (minimum molecular weight of the solute with 90% rejection) was checked using PEG (PSS Polymer Standards Service GmbH, Germany) of M_w ranging from 100 to 500 kDa. The retention experiments were conducted in both dead-end and cross-flow modes using aqueous solution of 0.01 wt% of PEG. First, pure water flux was measured for 1 h at 2 bar transmembrane pressure then the feed solution was supplied in the same configuration at 1 bar transmembrane pressure and a feed sample (5 mL) was collected. After 1 h, 5 mL permeate was collected to check the rejection from membrane. The membranes were rinsed thoroughly using water after each solute rejection test.

The retention values were calculated as follows:

$$R\% = \left(1 - \frac{C_p}{C_f}\right) \times 100\% \quad (6)$$

Where, C_p and C_f are concentrations of PEG in permeate and feed, respectively. These concentrations were measured by GPC. The measurements were performed at 35 °C in bidistilled water with 0.5 g/L sodium azide using PSS acrylate copolymer SUPREMA Pre, 100 Å and 3000 Å columns (particle size 10 µm), at a flow rate of 0.5 mL min⁻¹ (VWR-Hitachi 2130 pump). A Waters 410 refractive index detector having a PEG/PEO calibration was used.

Safety Hazards

Table 11: Safety instructions and hazardousness of used chemicals and materials.

Material	GHS-Symbol	H-Phrases	P-Phrases
<i>N,N</i> -Dimethylformamide	GHS02, GHS07, GHS08	H226, H312 + H332, H319, H360D	P201, P280, P305 + P351 + P338, P308 + P313
Tetrahydrofuran	GHS02, GHS07, GHS08	H225, H302, H319, H335, H351	P210, P280, P301 + P312 + P330, P305 + P351 + P338, P370 + P378, P403 + P235
<i>1,4</i> -Dioxane	GHS02, GHS07, GHS08	H225, H319, H335, H351	P201, P210, P233, P261, P280, P370 + P378
Chloroform	GHS06, GHS08	H302, H315, H319, H331, H336, H351, H361d, H372	P201, P260, P264, P280, P304 + P340 + P311, P403 + P233
<i>N</i> -Methyl-2-pyrrolidone	GHS07, GHS08	H315, H319, H335, H360D	P201, P280, P305 + P351 + P338, P308 + P313
Acetone	GHS02, GHS07	H225, H319, H336	P210, P233, P261, P280, P303 + P361 + P353, P370 + P378
Hydrogen peroxide, 30% w/w	GHS05	H318, H412	P280, P305 + P351 + P338 + P310
γ -Butyrolactane	GHS05, GHS07	H302, H318, H336	P261, P208, P305 + P351 + P338
MgAc ₂	-	-	-
Block copolymer	-	-	-
Polyether sulfone	-	-	-

References

1. H. Strathmann, *AIChE Journal*, 2001, **47**, 1077-1087.
2. S. T. Meissner, *BioScience*, 2016, **66**, 174-176.
3. W. J. Koros and C. Zhang, *Nature Materials*, 2017, **16**, 289.
4. W. J. Koros and R. Mahajan, *Journal of Membrane Science*, 2000, **175**, 181-196.
5. B. D. Freeman and I. Pinnau, *Polymer Membranes for Gas and Vapor Separation*, American Chemical Society, 1999.
6. R. Baker, *Membrane Technology and Applications, 2nd Edition*, John Wiley & Sons, 2004.
7. H. Strathmann, *Introduction to Membrane Science and Technology*, Wiley, 2011.
8. G. M. Geise, H.-S. Lee, D. J. Miller, B. D. Freeman, J. E. McGrath and D. R. Paul, *J. Polym. Sci., Part B: Polym. Phys.*, 2010, **48**, 1685-1718.
9. Y. Zhang, N. E. Almodovar-Arbelo, J. L. Weidman, D. S. Corti, B. W. Boudouris and W. A. Phillip, *npj Clean Water*, 2018, **1**, 2.
10. M. Elimelech and W. A. Phillip, *Science (Washington, DC, U. S.)*, 2011, **333**, 712-717.
11. R. W. Baker, *Industrial & Engineering Chemistry Research*, 2002, **41**, 1393-1411.
12. M. A. Shannon, P. W. Bohn, M. Elimelech, J. G. Georgiadis, B. J. Marinas and A. M. Mayes, *Nature (London, U. K.)*, 2008, **452**, 301-310.
13. A. Saxena, B. P. Tripathi, M. Kumar and V. K. Shahi, *Adv. Colloid Interface Sci.*, 2009, **145**, 1-22.
14. P. Bernardo, E. Drioli and G. Golemme, *Industrial & Engineering Chemistry Research*, 2009, **48**, 4638-4663.
15. M. M. Pendergast and E. M. V. Hoek, *Energy Environ. Sci.*, 2011, **4**, 1946-1971.
16. I. Sadeghi, P. Kaner and A. Asatekin, *Chemistry of Materials*, 2018, **30**, 7328-7354.
17. P. S. Goh and A. F. Ismail, *Desalination*, 2018, **434**, 60-80.
18. M. C. Orilall and U. Wiesner, *Chemical Society Reviews*, 2011, **40**, 520-535.
19. M. Freemantle, *Chemical & Engineering News Archive*, 2005, **83**, 49-57.
20. M. Ulbricht, *Polymer*, 2006, **47**, 2217-2262.
21. B. D. Freeman and I. Pinnau, in *Polymer Membranes for Gas and Vapor Separation*, American Chemical Society, 1999, vol. 733, ch. 1, pp. 1-27.
22. M. S. Silverstein, N. R. Cameron and M. A. Hillmyer, *Porous Polymers*, John Wiley & Sons, Inc., 2011.
23. Z. Cui, E. Drioli and Y. M. Lee, *Progress in Polymer Science*, 2014, **39**, 164-198.
24. P. C. Hiemenz and T. P. Lodge, *Polymer Chemistry*, CRC Press, 2007.
25. H. P. Hsieh, R. R. Bhave and H. L. Fleming, *Journal of Membrane Science*, 1988, **39**, 221-241.
26. S. Elangovan, B. Nair, T. Small, B. Heck, I. Bay, M. Timper, J. Hartvigsen and M. Wilson, in *Inorganic Membranes for Energy and Environmental Applications*, ed. A. C. Bose, Springer New York, New York, NY, 2009, pp. 67-81.
27. B. Morreale, J. Ciferno, B. Howard, M. Ciocco, J. Marano, O. Iyoha and R. Enick, in *Inorganic Membranes for Energy and Environmental Applications*, ed. A. C. Bose, Springer New York, New York, NY, 2009, pp. 173-201.

28. B. R. Lanning, O. Ishteiwy, J. D. Way, D. Edlund and K. Coulter, in *Inorganic Membranes for Energy and Environmental Applications*, ed. A. C. Bose, Springer New York, New York, NY, 2009, pp. 203-219.
29. M. V. Mundschau, in *Inorganic Membranes for Energy and Environmental Applications*, ed. A. C. Bose, Springer New York, New York, NY, 2009, pp. 125-153.
30. W. Yang and Y. Li, in *Inorganic Membranes for Energy and Environmental Applications*, ed. A. C. Bose, Springer New York, New York, NY, 2009, pp. 275-286.
31. B. N. Nair, Y. Ando and H. Taguchi, in *Inorganic Membranes for Energy and Environmental Applications*, ed. A. C. Bose, Springer New York, New York, NY, 2009, pp. 287-298.
32. H. Verweij, *Current Opinion in Chemical Engineering*, 2012, **1**, 156-162.
33. E. Drioli, A. I. Stankiewicz and F. Macedonio, *Journal of Membrane Science*, 2011, **380**, 1-8.
34. J. H. Petropoulos, *Journal of Membrane Science*, 1990, **52**, 305-323.
35. J. Vital and J. M. Sousa, in *Handbook of Membrane Reactors*, ed. A. Basile, Woodhead Publishing, 2013, vol. 1, pp. 3-41.
36. M. A. Hillmyer, *Adv. Polym. Sci.*, 2005, **190**, 137-181.
37. J. S. Vrentas and C. M. Vrentas, *Chemical Engineering Science*, 2002, **57**, 4199-4208.
38. I. Pinnau and B. D. Freeman, in *Membrane Formation and Modification*, American Chemical Society, 1999, vol. 744, ch. 1, pp. 1-22.
39. W. Zhang, J. Luo, L. Ding and M. Y. Jaffrin, *Industrial & Engineering Chemistry Research*, 2015, **54**, 2843-2861.
40. H. Strathmann, K. Kock, P. Amar and R. W. Baker, *Desalination*, 1975, **16**, 179-203.
41. H. Strathmann and K. Kock, *Desalination*, 1977, **21**, 241-255.
42. L. Keshavarz, M. A. Khansary and S. Shirazian, *Polymer*, 2015, **73**, 1-8.
43. G. R. Guillen, Y. Pan, M. Li and E. M. V. Hoek, *Industrial & Engineering Chemistry Research*, 2011, **50**, 3798-3817.
44. H. Chae Park, Y. Po Kim, H. Yong Kim and Y. Soo Kang, *Journal of Membrane Science*, 1999, **156**, 169-178.
45. Y. S. Su, C. Y. Kuo, D. M. Wang, J. Y. Lai, A. Deratani, C. Pochat and D. Bouyer, *Journal of Membrane Science*, 2009, **338**, 17-28.
46. L. Gao, B. Tang and P. Wu, *Journal of Membrane Science*, 2009, **326**, 168-177.
47. J. F. Kim, J. H. Kim, Y. M. Lee and E. Drioli, *AIChE Journal*, 2016, **62**, 461-490.
48. D. R. Lloyd, K. E. Kinzer and H. S. Tseng, *Journal of Membrane Science*, 1990, **52**, 239-261.
49. E. Danesh, S. R. Ghaffarian and P. Molla-Abbasi, *Sensors and Actuators B: Chemical*, 2011, **155**, 562-567.
50. R. Thomas, E. Guillen-Burrieza and H. A. Arafat, *Journal of Membrane Science*, 2014, **452**, 470-480.
51. S. Loeb and S. Sourirajan, in *Saline Water Conversion—II*, AMERICAN CHEMICAL SOCIETY, 1963, vol. 38, ch. 9, pp. 117-132.
52. S. Loeb, in *Synthetic Membranes:*, AMERICAN CHEMICAL SOCIETY, 1981, vol. 153, ch. 1, pp. 1-9.
53. J. T. Jung, J. F. Kim, H. H. Wang, E. di Nicolo, E. Drioli and Y. M. Lee, *Journal of Membrane Science*, 2016, **514**, 250-263.
54. J. T. Jung, H. H. Wang, J. F. Kim, J. Lee, J. S. Kim, E. Drioli and Y. M. Lee, *Journal of Membrane Science*, 2018, **559**, 117-126.
55. H. H. Wang, J. T. Jung, J. F. Kim, S. Kim, E. Drioli and Y. M. Lee, *Journal of Membrane Science*, 2019, **574**, 44-54.
56. B. Ericsson and B. Hallmans, *Desalination*, 1994, **98**, 3-16.

57. R. Singh, in *Hybrid Membrane Systems for Water Purification*, ed. R. Singh, Elsevier Science, Amsterdam, 2005, pp. 57-130.
58. R. Singh, in *Hybrid Membrane Systems for Water Purification*, ed. R. Singh, Elsevier Science, Amsterdam, 2005, pp. 1-56.
59. W. J. Koros, Y. H. Ma and T. Shimidzu, *Journal*, 1996, **68**, 1479.
60. X. Shi, G. Tal, N. P. Hankins and V. Gitis, *Journal of Water Process Engineering*, 2014, **1**, 121-138.
61. H. Susanto, A. Roihadin, N. Aryanti, D. D. Anggoro and M. Ulbricht, *Mater. Sci. Eng., C*, 2012, **32**, 1759-1766.
62. K. P. Lee, T. C. Arnot and D. Mattia, *Journal of Membrane Science*, 2011, **370**, 1-22.
63. S. S. Shenvi, A. M. Isloor and A. F. Ismail, *Desalination*, 2015, **368**, 10-26.
64. P. M. Whelan and M. J. Hodgson, *Essential Principles of Physics*, John Murray, 1978.
65. S. Whitaker, *Transport in Porous Media*, 1986, **1**, 3-25.
66. S. P. Sutera and R. Skalak, *Annual Review of Fluid Mechanics*, 1993, **25**, 1-20.
67. J. Pfitzner, *Anaesthesia*, 1976, **31**, 273-275.
68. B. S. Lalia, V. Kochkodan, R. Hashaikeh and N. Hilal, *Desalination*, 2013, **326**, 77-95.
69. W. F. Pickard, *Progress in Biophysics and Molecular Biology*, 1981, **37**, 181-229.
70. J. Cai, B. Yu, M. Zou and L. Luo, *Energy & Fuels*, 2010, **24**, 1860-1867.
71. J. Cai and B. Yu, *Transport in Porous Media*, 2011, **89**, 251-263.
72. J. Cai, E. Perfect, C.-L. Cheng and X. Hu, *Langmuir*, 2014, **30**, 5142-5151.
73. R. Liu, Y. Jiang, B. Li and L. Yu, *Microfluidics and Nanofluidics*, 2016, **20**, 120.
74. H. I. M. a. B. J. Lipps, in *Encyclopedia of Polymer Science and Technology*, Wiley, 1971, vol. 15, p. 258.
75. V. Calabrò and A. Basile, in *Advanced Membrane Science and Technology for Sustainable Energy and Environmental Applications*, eds. A. Basile and S. P. Nunes, Woodhead Publishing, 2011, pp. 3-21.
76. T.-S. N. Chung, John Wiley & Sons, Inc., 2008, DOI: 10.1002/9780470276280.ch31, pp. 821-839.
77. N. Peng, N. Widjojo, P. Sukitpaneenit, M. M. Teoh, G. G. Lipscomb, T.-S. Chung and J.-Y. Lai, *Prog. Polym. Sci.*, 2012, **37**, 1401-1424.
78. K. R. Manoj, A. Silvana and D. Hanming, *Journal*, 2011.
79. S. Bonyadi, T. S. Chung and W. B. Krantz, *Journal of Membrane Science*, 2007, **299**, 200-210.
80. L. Leibler, *Macromolecules*, 1980, **13**, 1602-1617.
81. F. S. Bates and G. H. Fredrickson, *Annu. Rev. Phys. Chem.*, 1990, **41**, 525-557.
82. M. W. Matsen and F. S. Bates, *The Journal of Chemical Physics*, 1997, **106**, 2436-2448.
83. I. Hamley, *The Physics of Block Copolymers*, Oxford University Press, 1998.
84. N. Hadjichristidis, *Block Copolymers: Synthetic Strategies, Physical Properties, and Applications*, John Wiley & Sons, 2002.
85. N. Hadjichristidis, H. Iatrou, M. Pitsikalis and J. Mays, *Progress in Polymer Science*, 2006, **31**, 1068-1132.
86. J. Jennings, G. He, S. M. Howdle and P. B. Zetterlund, *Chem. Soc. Rev.*, 2016, **45**, 5055-5084.
87. F. S. Bates, M. A. Hillmyer, T. P. Lodge, C. M. Bates, K. T. Delaney and G. H. Fredrickson, *Science (Washington, DC, U. S.)*, 2012, **336**, 434-440.
88. M. Pitsikalis, S. Pispas, J. W. Mays and N. Hadjichristidis, *Adv. Polym. Sci.*, 1998, **135**, 1-137.

89. T. Ozturk, A. Kiliclioglu, B. Savas and B. Hazer, *J. Macromol. Sci., Part A: Pure Appl. Chem.*, 2018, DOI: 10.1080/10601325.2018.1481344.
90. X. Yan, J. Li and T. Ren, *e-Polym.*, 2018, **18**, 559-568.
91. I. Terzic, N. L. Meereboer and K. Loos, *Polym. Chem.*, 2018, **9**, 3714-3720.
92. G. Saravanakumar, H. Park, J. Kim, D. Park, S. Pramanick, D. H. Kim and W. J. Kim, *Biomacromolecules*, 2018, **19**, 2202-2213.
93. N. Ye, L. Zhang, X. Gong, X. Li, H. Li and L. Lei, *Cailiao Daobao*, 2014, **28**, 131-135.
94. A. Walther and A. H. E. Müller, *Chemical Reviews*, 2013, **113**, 5194-5261.
95. F. H. Schacher, P. A. Rupar and I. Manners, *Angewandte Chemie International Edition*, 2012, **51**, 7898-7921.
96. J. Bang, U. Jeong, D. Y. Ryu, T. P. Russell and C. J. Hawker, *Adv. Mater. (Weinheim, Ger.)*, 2009, **21**, 4769-4792.
97. I. I. I. T. H. Epps and R. K. O'Reilly, *Chemical Science*, 2016, **7**, 1674-1689.
98. M. R. Bockstaller, R. A. Mickiewicz and E. L. Thomas, *Advanced Materials*, 2005, **17**, 1331-1349.
99. V. Abetz, K. Kremer, M. Müller and G. Reiter, *Macromolecular Chemistry and Physics*, **0**, 1800334.
100. Y. Mai and A. Eisenberg, *Chemical Society Reviews*, 2012, **41**, 5969-5985.
101. D. E. Discher and F. Ahmed, *Annual Review of Biomedical Engineering*, 2006, **8**, 323-341.
102. F. S. Bates and G. H. Fredrickson, *Phys. Today*, 1999, **52**, 32-38.
103. V. Abetz and A. Boschetti-de-Fierro, in *Polymer Science: A Comprehensive Reference*, eds. K. Matyjaszewski and M. Möller, Elsevier, Amsterdam, 2012, pp. 3-44.
104. M. S. Silverstein, N. R. Cameron, M. A. Hillmyer and Editors, *Porous Polymers*, John Wiley & Sons, Inc., 2011.
105. F. Stephan and P. Thomas, *Angewandte Chemie International Edition*, 2002, **41**, 688-714.
106. Q. Yang and K. Loos, *Polymer Chemistry*, 2017, **8**, 641-654.
107. T. Harada, F. S. Bates and T. P. Lodge, *Macromolecules*, 2003, **36**, 5440-5442.
108. C.-I. Huang and T. P. Lodge, *Macromolecules*, 1998, **31**, 3556-3565.
109. N. A. Lynd, F. T. Oyerokun, D. L. O'Donoghue, D. L. Handlin, Jr. and G. H. Fredrickson, *Macromolecules (Washington, DC, U. S.)*, 2010, **43**, 3479-3486.
110. V. Abetz, *Macromol. Rapid Commun.*, 2015, **36**, 10-22.
111. V. Abetz and T. Goldacker, *Macromolecular Rapid Communications*, 2000, **21**, 16-34.
112. W. A. Phillip, M. A. Hillmyer and E. L. Cussler, *Macromolecules (Washington, DC, U. S.)*, 2010, **43**, 7763-7770.
113. W. Sun, Z. Wang, X. Yao, L. Guo, X. Chen and Y. Wang, *J. Membr. Sci.*, 2014, **466**, 229-237.
114. Y. Wang, *Acc. Chem. Res.*, 2016, **49**, 1401-1408.
115. L. Guo, Z. Zhong and Y. Wang, *Adv. Mater. Interfaces*, 2016, **3**, n/a.
116. U. Breiner, U. Krappe, E. L. Thomas and R. Stadler, *Macromolecules*, 1998, **31**, 135-141.
117. T. Goldacker and V. Abetz, *Macromolecular Rapid Communications*, 1999, **20**, 415-418.
118. M. Radjabian, C. Abetz, B. Fischer, A. Meyer, B. Lademann and V. Abetz, *Macromolecular Chemistry and Physics*, 2017, **218**, 1600587.

119. T. I. Loebling, P. Hiekkataipale, A. Hanisch, F. Bennet, H. Schmalz, O. Ikkala, A. H. Groeschel and A. H. E. Mueller, *Polymer*, 2015, **72**, 479-489.
120. B. Nandan and A. Horechyy, *ACS Appl. Mater. Interfaces*, 2015, **7**, 12539-12558.
121. F. S. Bates, 1999.
122. S. B. Darling, *Energy & Environmental Science*, 2009, **2**, 1266-1273.
123. H.-Y. Hsueh, H.-Y. Chen, M.-S. She, C.-K. Chen, R.-M. Ho, S. Gwo, H. Hasegawa and E. L. Thomas, *Nano Letters*, 2010, **10**, 4994-5000.
124. J. G. Son, J. Gwyther, J.-B. Chang, K. K. Berggren, I. Manners and C. A. Ross, *Nano Letters*, 2011, **11**, 2849-2855.
125. I. Vukovic, G. t. Brinke and K. Loos, *Polymer*, 2013, **54**, 2591-2605.
126. S. W. Robbins, H. Sai, F. J. Di Salvo, S. M. Gruner and U. Wiesner, *ACS Nano*, 2014, **8**, 8217-8223.
127. E. J. W. Crossland, M. Kamperman, M. Nedelcu, C. Ducati, U. Wiesner, D. M. Smilgies, G. E. S. Toombes, M. A. Hillmyer, S. Ludwigs, U. Steiner and H. J. Snaith, *Nano Letters*, 2009, **9**, 2807-2812.
128. I. Vukovic, S. Punzhin, Z. Vukovic, P. Onck, J. T. M. De Hosson, G. ten Brinke and K. Loos, *ACS Nano*, 2011, **5**, 6339-6348.
129. J.-F. Lutz, J.-M. Lehn, E. W. Meijer and K. Matyjaszewski, *Nature Reviews Materials*, 2016, **1**, 16024.
130. J. Schöbel, C. Hils, A. Weckwerth, M. Schlenk, C. Bojer, M. C. A. Stuart, J. Breu, S. Förster, A. Greiner, M. Karg and H. Schmalz, *Nanoscale*, 2018, **10**, 18257-18268.
131. Q. Li, A. X. Zhu, X. Wang and L. Zhu, 2018.
132. R. K. O'Reilly, C. J. Hawker and K. L. Wooley, *Chemical Society Reviews*, 2006, **35**, 1068-1083.
133. J. Du and R. K. O'Reilly, *Chemical Society Reviews*, 2011, **40**, 2402-2416.
134. K. Kataoka, A. Harada and Y. Nagasaki, *Advanced Drug Delivery Reviews*, 2001, **47**, 113-131.
135. G. Gaucher, M.-H. Dufresne, V. P. Sant, N. Kang, D. Maysinger and J.-C. Leroux, *Journal of Controlled Release*, 2005, **109**, 169-188.
136. K. Mitra, S. K. Hira, S. Singh, N. K. Vishwakarma, S. Vishwakarma, U. Gupta, P. P. Manna and B. Ray, *ChemistrySelect*, 2018, **3**, 8833-8843.
137. H. Li, L. Sui and Y. Niu, *J. Mater. Sci.*, 2018, **53**, 12718-12730.
138. M. Pei, X. Jia and P. Liu, *Mater. Des.*, 2018, **155**, 288-296.
139. K.-V. Peinemann, V. Abetz and P. F. W. Simon, *Nat. Mater.*, 2007, **6**, 992-996.
140. P. Gao, A. Hunter, S. Benavides, M. J. Summe, F. Gao and W. A. Phillip, *ACS Appl. Mater. Interfaces*, 2016, **8**, 3386-3395.
141. L. Wan, S. Ji, C.-C. Liu, G. S. W. Craig and P. F. Nealey, *Soft Matter*, 2016, **12**, 2914-2922.
142. G. Kim and M. Libera, *Macromolecules*, 1998, **31**, 2569-2577.
143. J. Hahn, J. I. Clodt, C. Abetz, V. Filiz and V. Abetz, *ACS Appl. Mater. Interfaces*, 2015, **7**, 21130-21137.
144. A. Modi, A. Karim and M. Tsige, *Macromolecules (Washington, DC, U. S.)*, 2018, **51**, 7186-7196.
145. C. Jin, B. C. Olsen, E. J. Lubber and J. M. Buriak, *Chemistry of Materials*, 2017, **29**, 176-188.
146. H. Ogawa, M. Takenaka, T. Miyazaki, A. Fujiwara, B. Lee, K. Shimokita, E. Nishibori and M. Takata, *Macromolecules*, 2016, **49**, 3471-3477.
147. X. Gu, I. Gunkel, A. Hexemer, W. Gu and T. P. Russell, *Advanced Materials*, 2014, **26**, 273-281.
148. I. W. Hamley, *Progress in Polymer Science*, 2009, **34**, 1161-1210.

149. T. E. Gartner, T. Kubo, Y. Seo, M. Tansky, L. M. Hall, B. S. Sumerlin and T. H. Epps, *Macromolecules*, 2017, **50**, 7169-7176.
150. M. Luo and T. H. Epps, *Macromolecules*, 2013, **46**, 7567-7579.
151. C. M. Bates, M. J. Maher, D. W. Janes, C. J. Ellison and C. G. Willson, *Macromolecules*, 2014, **47**, 2-12.
152. K. E. B. Doncom, L. D. Blackman, D. B. Wright, M. I. Gibson and R. K. O'Reilly, *Chemical Society Reviews*, 2017, **46**, 4119-4134.
153. DE102006045282B4, 2008.
154. D. A. Olson, L. Chen and M. A. Hillmyer, *Chemistry of Materials*, 2008, **20**, 869-890.
155. S. H. Kim, M. J. Misner, T. Xu, M. Kimura and T. P. Russell, *Advanced Materials*, 2004, **16**, 226-231.
156. S. H. Kim, M. J. Misner and T. P. Russell, *Advanced Materials*, 2004, **16**, 2119-2123.
157. J. Rzyayev and M. A. Hillmyer, *Journal of the American Chemical Society*, 2005, **127**, 13373-13379.
158. J. Rzyayev and M. A. Hillmyer, *Macromolecules*, 2005, **38**, 3-5.
159. T. S. Bailey, J. Rzyayev and M. A. Hillmyer, *Macromolecules*, 2006, **39**, 8772-8781.
160. F. Guo, K. Jankova, L. Schulte, M. E. Vigild and S. Ndoni, *Macromolecules*, 2008, **41**, 1486-1493.
161. J. He, J.-Y. Wang, J. Xu, R. Tangirala, D. Shin, T. P. Russell, X. Li and J. Wang, *Advanced Materials*, 2007, **19**, 4370-4374.
162. U. Jeong, D. Y. Ryu, D. H. Kho, J. K. Kim, J. T. Goldbach, D. H. Kim and T. P. Russell, *Advanced Materials*, 2004, **16**, 533-536.
163. J. He, R. Tangirala, T. Emrick, T. P. Russell, A. Böker, X. Li and J. Wang, *Advanced Materials*, 2007, **19**, 381-385.
164. W. A. Phillip, B. O'Neill, M. Rodwogin, M. A. Hillmyer and E. L. Cussler, *ACS Appl. Mater. Interfaces*, 2010, **2**, 847-853.
165. X. Gu, I. Gunkel, A. Hexemer and T. P. Russell, *Macromolecules*, 2016, **49**, 3373-3381.
166. T. Thurn-Albrecht, R. Steiner, J. DeRouchey, C. M. Stafford, E. Huang, M. Bal, M. Tuominen, C. J. Hawker and T. P. Russell, *Advanced Materials*, 2000, **12**, 787-791.
167. C. Liedel, C. W. Pester, M. Ruppel, V. S. Urban and A. Böker, *Macromolecular Chemistry and Physics*, 2012, **213**, 259-269.
168. S. Y. Yang, I. Ryu, H. Y. Kim, J. K. Kim, S. K. Jang and T. P. Russell, *Adv. Mater. (Weinheim, Ger.)*, 2006, **18**, 709-712.
169. S. Rangou, K. Buhr, V. Filiz, J. I. Clodt, B. Lademann, J. Hahn, A. Jung and V. Abetz, *J. Membr. Sci.*, 2014, **451**, 266-275.
170. M. Radjabian, J. Koll, K. Buhr, U. Vainio, C. Abetz, U. A. Handge and V. Abetz, *Polymer*, 2014, **55**, 2986-2997.
171. J. I. Clodt, B. Bajer, K. Buhr, J. Hahn, V. Filiz and V. Abetz, *J. Membr. Sci.*, 2015, **495**, 334-340.
172. C. Stegelmeier, A. Exner, S. Hauschild, V. Filiz, J. Perlich, S. V. Roth, V. Abetz and S. Foerster, *Macromolecules (Washington, DC, U. S.)*, 2015, **48**, 1524-1530.
173. M. Radjabian and V. Abetz, *Advanced Materials*, 2015, **27**, 352-355.
174. C. Stegelmeier, V. Filiz, V. Abetz, J. Perlich, A. Fery, P. Ruckdeschel, S. Rosenfeldt and S. Förster, *Macromolecules*, 2014, **47**, 5566-5577.
175. J. Hahn, V. Filiz, S. Rangou, B. Lademann, K. Buhr, J. I. Clodt, A. Jung, C. Abetz and V. Abetz, *Macromolecular Materials and Engineering*, 2013, **298**, 1315-1321.
176. S. Saleem, S. Rangou, C. Abetz, B. Lademann, V. Filiz and V. Abetz, *Polymers*, 2017, **9**, 216.

177. J. Hahn, V. Filiz, S. Rangou, J. Clodt, A. Jung, K. Buhr, C. Abetz and V. Abetz, *Journal of Polymer Science Part B: Polymer Physics*, 2013, **51**, 281-290.
178. H. Ahn, S. Park, S.-W. Kim, P. J. Yoo, D. Y. Ryu and T. P. Russell, *ACS Nano*, 2014, **8**, 11745-11752.
179. S. Schöttner, H.-J. Schaffrath and M. Gallei, *Macromolecules*, 2016, **49**, 7286-7295.
180. J. Wang, M. M. Rahman, C. Abetz, S. Rangou, Z. Zhang and V. Abetz, *Macromolecular Rapid Communications*, 2018, **39**, 1800435.
181. A. Jung, V. Filiz, S. Rangou, K. Buhr, P. Merten, J. Hahn, J. Clodt, C. Abetz and V. Abetz, *Macromolecular Rapid Communications*, 2013, **34**, 610-615.
182. R. M. Dorin, D. S. Marques, H. Sai, U. Vainio, W. A. Phillip, K.-V. Peinemann, S. P. Nunes and U. Wiesner, *ACS Macro Lett.*, 2012, **1**, 614-617.
183. W. A. Phillip, R. Mika Dorin, J. Werner, E. M. V. Hoek, U. Wiesner and M. Elimelech, *Nano Lett.*, 2011, **11**, 2892-2900.
184. J. L. Weidman, R. A. Mulvenna, B. W. Boudouris and W. A. Phillip, *J. Am. Chem. Soc.*, 2016, **138**, 7030– 7039
185. J. L. Weidman, R. Mulvenna, Y. Zhang, B. W. Boudouris and W. A. Phillip, 2016.
186. M. Radjabian, C. Abetz, B. Fischer, A. Meyer and V. Abetz, *ACS Applied Materials & Interfaces*, 2017, **9**, 31224-31234.
187. Y. Gu and U. Wiesner, *Macromolecules (Washington, DC, U. S.)*, 2015, **48**, 6153-6159.
188. J. I. Clodt, S. Rangou, A. Schröder, K. Buhr, J. Hahn, A. Jung, V. Filiz and V. Abetz, *Macromolecular Rapid Communications*, 2013, **34**, 190-194.
189. M. Gallei, S. Rangou, V. Filiz, K. Buhr, S. Bolmer, C. Abetz and V. Abetz, *Journal*, 2013, **214**, 1037-1046.
190. S. P. Nunes, A. R. Behzad, B. Hooghan, R. Sougrat, M. Karunakaran, N. Pradeep, U. Vainio and K.-V. Peinemann, *ACS Nano*, 2011, **5**, 3516-3522.
191. Y. M. Li, Q. Zhang, J. R. Álvarez-Palacio, I. F. Hakem, Y. Gu, M. R. Bockstaller and U. Wiesner, *Polymer*, 2017, **126**, 368-375.
192. E. J. Vriezেকolk, E. de Weerd, W. M. de Vos and K. Nijmeijer, *J. Polym. Sci., Part B: Polym. Phys.*, 2014, **52**, 1568-1579.
193. Y. M. Li, D. Srinivasan, P. Vaidya, Y. Gu and U. Wiesner, *Macromolecular Rapid Communications*, 2016, **37**, 1689-1693.
194. Y. Zhang, R. A. Mulvenna, B. W. Boudouris and W. A. Phillip, *Journal of Materials Chemistry A*, 2017, **5**, 3358-3370.
195. Y. Sageshima, S. Arai, A. Noro and Y. Matsushita, *Langmuir*, 2012, **28**, 17524-17529.
196. J. Lee, J. Kwak, C. Choi, S. H. Han and J. K. Kim, *Macromolecules*, 2017, **50**, 9373-9379.
197. D.-W. Sun and M. Müller, *Macromolecules*, 2018, **51**, 275-281.
198. Y. Chen, Q. Xu, Y. Jin, X. Qian, R. Ma, J. Liu and D. Yang, *Soft Matter*, 2018, **14**, 6635-6647.
199. V. Mishra, G. H. Fredrickson and E. J. Kramer, *ACS Nano*, 2012, **6**, 2629-2641.
200. D. S. Marques, R. M. Dorin, U. Wiesner, D.-M. Smilgies, A. R. Behzad, U. Vainio, K.-V. Peinemann and S. P. Nunes, *Polymer*, 2014, **55**, 1327-1332.
201. Y. Gu, R. M. Dorin, K. W. Tan, D.-M. Smilgies and U. Wiesner, *Macromolecules (Washington, DC, U. S.)*, 2016, **49**, 4195-4201.
202. W.-L. Hung, D.-M. Wang, J.-Y. Lai and S.-C. Chou, *J. Membr. Sci.*, 2016, **505**, 70-81.
203. K. Sankhala, J. Koll, M. Radjabian, U. A. Handge and V. Abetz, *Advanced Materials Interfaces*, 2017, **4**, 1600991.

204. P. K. Pranzas, A. Knöchel, K. Kneifel, H. Kamusewitz, T. Weigel, R. Gehrke, S. S. Funari and R. Willumeit, *Analytical and Bioanalytical Chemistry*, 2003, **376**, 602-607.
205. R. Hilke, N. Pradeep, P. Madhavan, U. Vainio, A. R. Behzad, R. Sougrat, S. P. Nunes and K.-V. Peinemann, *ACS Appl. Mater. Interfaces*, 2013, **5**, 7001-7006.
206. T. Bucher, V. Filiz, C. Abetz and V. Abetz, *Membranes*, 2018, **8**, 57.
207. N. Noor, J. Koll, M. Radjabian, C. Abetz and V. Abetz, *Macromol. Rapid Commun.*, 2016, **37**, 414-419.
208. T. S. Chung, J. J. Qin and J. Gu, *Chem. Eng. Sci.*, 1999, **55**, 1077-1091.
209. Y. Liu, T. Liu, Y. Su, H. Yuan, T. Hayakawa and X. Wang, *J. Membr. Sci.*, 2016, **506**, 1-10.
210. Y. Zhang, R. A. Mulvenna, S. Qu, B. W. Boudouris and W. A. Phillip, *ACS Macro Letters*, 2017, **6**, 726-732.
211. S. Dami, C. Abetz, B. Fischer, M. Radjabian, P. Georgopoulos and V. Abetz, *Polymer*, 2017, **126**, 376-385.
212. L. Oss-Ronen, J. Schmidt, V. Abetz, A. Radulescu, Y. Cohen and Y. Talmon, *Macromolecules (Washington, DC, U. S.)*, 2012, **45**, 9631-9642.
213. D. S. Marques, U. Vainio, N. M. Chaparro, V. M. Calo, A. R. Behzad, J. W. Pitera, K.-V. Peinemann and S. P. Nunes, *Soft Matter*, 2013, **9**, 5557-5564.
214. S. P. Nunes, M. Karunakaran, N. Pradeep, A. R. Behzad, B. Hooghan, R. Sougrat, H.-Z. He and K.-V. Peinemann, *Langmuir*, 2011, **27**, 10184-10190.
215. R. M. Dorin, D. S. Marques, H. Sai, U. Vainio, W. A. Phillip, K.-V. Peinemann, S. P. Nunes and U. Wiesner, *ACS Macro Letters*, 2012, **1**, 614-617.
216. M. Lawrence and Y. Jiang, in *Bio-aggregates Based Building Materials : State-of-the-Art Report of the RILEM Technical Committee 236-BBM*, eds. S. Amziane and F. Collet, Springer Netherlands, Dordrecht, 2017, pp. 39-71.
217. C. M. Bates and F. S. Bates, *Macromolecules*, 2017, **50**, 3-22.
218. E. A. Jackson and M. A. Hillmyer, *ACS Nano*, 2010, **4**, 3548-3553.
219. J. I. Clodt, V. Filiz, S. Rangou, K. Buhr, C. Abetz, D. Hoeche, J. Hahn, A. Jung and V. Abetz, *Adv. Funct. Mater.*, 2013, **23**, 731-738.
220. M. Cetintas, J. de Grooth, A. H. Hofman, H. M. van der Kooij, K. Loos, W. M. de Vos and M. Kamperman, *Polym. Chem.*, 2017, **8**, 2235-2243.
221. C. Höhme, J. Hahn, B. Lademann, A. Meyer, B. Bajer, C. Abetz, V. Filiz and V. Abetz, *European Polymer Journal*, 2016, **85**, 72-81.
222. T.-S. N. Chung, 2008.
223. B. Freeman, *Angewandte Chemie International Edition*, 2012, **51**, 9485-9485.
224. J. Hahn, J. I. Clodt, V. Filiz and V. Abetz, *RSC Adv.*, 2014, **4**, 10252-10260.
225. G. Jeon, S. Y. Yang and J. K. Kim, *J. Mater. Chem.*, 2012, **22**, 14814-14834.
226. Q. Zhang, Y. Gu, Y. M. Li, P. A. Beaucage, T. Kao and U. Wiesner, *Chemistry of Materials*, 2016, **28**, 3870-3876.
227. A. Buffet, A. Rothkirch, R. Doehrmann, V. Koerstgens, M. M. Abul Kashem, J. Perlich, G. Herzog, M. Schwartzkopf, R. Gehrke, P. Mueller-Buschbaum and S. V. Roth, *J. Synchrotron Radiat.*, 2012, **19**, 647-653.
228. M. Radjabian, J. Koll, K. Buhr, U. A. Handge and V. Abetz, *Polymer*, 2013, **54**, 1803-1812.
229. J. Qin and T.-S. Chung, *J. Membr. Sci.*, 1999, **157**, 35-51.
230. N. Widjojo and T.-S. Chung, *Ind. Eng. Chem. Res.*, 2006, **45**, 7618-7626.
231. S. Dami, C. Abetz, B. Fischer, M. Radjabian, P. Georgopoulos and V. Abetz, *Polymer*, 2017, **126**, 376-385.

232. J. Kestin, M. Sokolov and W. A. Wakeham, *Journal of Physical and Chemical Reference Data*, 1978, **7**, 941-948.
233. M. Basham, J. Filik, M. T. Wharmby, P. C. Y. Chang, B. El Kassaby, M. Gerring, J. Aishima, K. Levik, B. C. A. Pulford, I. Sikharulidze, D. Sneddon, M. Webber, S. S. Dhesi, F. Maccherozzi, O. Svensson, S. Brockhauser, G. N aray and A. W. Ashton, *Journal of Synchrotron Radiation*, 2015, **22**, 853-858.

Acknowledgment

I would first like to show my foremost gratitude to my advisor and *Doktorvater* Prof. Dr. Volker Abetz for believing in me and providing the freedom to explore a very interesting topic at the Institute of Polymer Research, Helmholtz-Zentrum Geesthacht. I am eternally grateful for all the scientific discussions, help in solving research problems, and contributing to the success of my research efforts. His words of wisdom motivated me throughout this doctoral studies and will stay with me for lifetime. I am also grateful for the numerous opportunities he has provided me to participate in several meetings and international conferences. I also thank him for being the first evaluator of this thesis.

I thank Prof. Dr. Horst Weller for kindly agreeing to invest his time to be the second evaluator of this thesis.

I gratefully acknowledge the financial support from Helmholtz-Zentrum Geesthacht.

I am thankful to BASF SE for providing the opportunity to work in a project and the block copolymers; I specially thank Dr. Konrard Knoll, Dr. Claudia Staudt and Dr. Natalia Widjojo for discussions and their contribution during the research project.

I gratefully acknowledge the facility of SAXS measurements at P03 beamline of light source PETRA III at DESY, a member of the Helmholtz Association (HGF).

Cut Membrane Technology GmbH is acknowledged for kindly providing the PES2 support HFM.

Although it is impossible to list all persons that helped me through this time at Helmholtz-Zentrum Geesthacht, I owe special thanks to several individuals that strongly influenced during my Ph.D. studies.

I begin with Joachim Koll for the strongest support during this journey. I sincerely thank him for his restless efforts, always ready to help, numerous discussions and fulfilling all the technical requirements in the work and being a good friend. Nelé had been a stress-buster.

I would like to thank PD Dr. Ulrich A. Handge for his supervision as the head of the department of material characterization and processing at HZG, and the scientific discussions we had.

My sincere thanks goes to Clarissa Abetz, for her support with microscopical investigations, her input for improvements and discussions. I want to thank Anke-Lisa Metze for introducing me to SEM and helping with morphological characterizations. I am thankful to Dr. Maryam Radjabian for interesting scientific discussions and care. My special gratitude goes to Dr. Florian Wieland for always being so helpful and without his support my dream of doing SAXS experiments would not have become true. I am grateful to Brigitte Lademann for synthesizing the block copolymers used in this study, Maren Brinkmann and Barbara Bajer for GPC measurements, Silvio Neumann for NMR characterizations, Heiko Notzke for help with designing the tools and Thorsten Wolff for working on the cover picture. In addition, I thank Karabi Halder for improving the social life and Ilona Zillich for her help with administrative processes.

I thank Dr. Kapil Arya for reviewing the thesis, Fynn Weigelt and Jiali Wang for their help. A big thank you goes to all my former and present coworkers at HZG who managed to make this experience memorable. So in no particular order, Sergey Shishatskiy, Carsten Scholles, Berthold Wendland, Ivonne Ternes, Jelena Lillepaerg, Sarah Saleem, Muntazim Khan, Lara Grunig, Elvin Aliyev, Zhenzhen Zhang, Alberto Tena, Prokopios Georgopoulos, Mónica de la Viuda, Sofia Dami, Evgeni Sperling, Thomas Bucher, Kristian Buhr, Meiling Wu, Christian Höhme, David Meis, Nazia Noor, and many more for being supportive and all the good times.

I would like to thank Dr. Matthias Schwarzkopf for help with setting up the beamline P03 at DESY, Hilmar Burmester, Jens Brehling and Dirk Jan Siemers for their support.

Last but not the least, very special thanks to my beloved grandparents, parents, Yogesh, my teachers, family and friends, for their strong support, motivation and encouragement which has always been a driving force for me.

Declaration on Oath

I hereby declare on oath, that I have written the present dissertation by my own and have not used other than the acknowledged resources and aids. The submitted written version corresponds to the version on the electronic storage medium. I hereby declare that I have not previously applied or pursued for a doctorate (Ph.D. studies).

(Kirti Sankhala)
Hamburg, 27/03/2019

Affidavit

I declare under penalty of perjury, that the present dissertation was prepared independently and solely by me under the specified tools.

(Kirti Sankhala)
Hamburg, 27/03/2019

Curriculum Vitae

Kirti Sankhala

kirti.sankhala@hzg.de; kirtisankhala309@gmail.com

Educational qualification

Since 10/2018 **Research Associate**, Institute of Polymer Research, HZG, Germany

04/2015 - 09/2018 **Ph.D. Student**, Institute of Polymer Research, HZG, Germany
Thesis: “Structure Formation in Isoporous Block Copolymer Membranes by Controlled Evaporation-Induced Self-Assembly”
Date of disputation: 26.07.2019

07/2012 - 07/2014 **Master of Science (M.Sc.)** in Applied Physics (Grade: A)
Malaviya National Institute of Technology (MNIT) Jaipur, Rajasthan, India
Thesis: “Synthesis & Characterization of Cobalt Doped Tin Dioxide Nanoparticles for Gas Sensors”

07/2009 - 05/2012 **Bachelor of Science (B.Sc.)** in Physics, Chemistry and Mathematics (Grade: First Class)
Jai Narayan Vyas University, Jodhpur, Rajasthan, India